SUBSURFACE CHARACTERIZATION OF FLEXIBLE PAVEMENTS

CONSTRUCTED OVER EXPANSIVE SOIL SUBGRADES AND SELECTION OF

SUITABLE REHABILITATION ALTERNATIVES

by

Kazi Moinul Islam

A thesis

submitted in partial fulfillment

of the requirements for the degree of

Master of Science in Civil Engineering

Boise State University

August 2017

BOISE STATE UNIVERSITY GRADUATE COLLEGE

DEFENSE COMMITTEE AND FINAL READING APPROVALS

of the thesis submitted by

Kazi Moinul Islam

Thesis Title: Subsurface Characterization of Flexible Pavements Constructed over Expansive Soil Subgrades and Selection of Suitable Rehabilitation Alternatives

Date of Final Oral Examination: 18 July 2017

The following individuals read and discussed the thesis submitted by student Kazi Moinul Islam and they evaluated his presentation and response to questions during the final oral examination. They found that the student passed the final oral examination.

Debakanta Mishra, Ph.D.	Co-Chair, Supervisory Committee
Bhaskar Chittoori, Ph.D.	Co-Chair, Supervisory Committee
Arvin Farid, Ph.D.	Member, Supervisory Committee

The final reading approval of the thesis was granted by Debakanta Mishra, Ph.D., Chair of the Supervisory Committee. The thesis was approved by the Graduate College.

DEDICATION

This thesis is dedicated to the memory of my father.

ACKNOWLEDGEMENTS

Finally, I would like to thank my family for their enormous patience, comprehension, and love.

ABSTRACT

Expansive soils present significant engineering challenges, with annual costs associated with repairing structures constructed over expansive soils estimated to run into several billion dollars. Volume changes in expansive soil deposits induced by fluctuations in the moisture content can result in severe damage to overlying structures. A flexible pavement section near the Western Border of Idaho has experienced recurrent damage due to volume changes in the underlying expansive soil layer; traditional stabilization methods have provided partial success over the years. The main objective of this research effort was to characterize the problematic soil layer contributing to the recurrent pavement damage and propose suitable rehabilitation alternatives.

An extensive laboratory test matrix was carried out to characterize soil samples collected from underneath the problematic pavement section. Laboratory tests showed that the problematic expansive soil deposit was often at depths greater than 6 ft. (183 cm) from the pavement surface. Potential Vertical Rise (PVR) values calculated for ten boreholes strategically placed along the problematic pavement section closely matched with the surface roughness profile observed in the field. Liquidity Index (LI) calculations indicated that the active-zone extended to a depth of least 11 ft. (335 cm) from the pavement surface, and therefore, most of the heaving likely originates from soil layers as deep as 11 ft. (335 cm) from the pavement surface. Clay mineralogy tests indicated the presence of high amounts of Montmorillonite that can lead to significant volume changes. Moreover, high sulfate contents were detected in soil samples obtained from several of

the boreholes, indicating a potential for sulfate-induced heaving upon chemical stabilization using calcium-based stabilizers. Based on findings from the laboratory testing, it was concluded that chemical stabilization or shallow treatment alternatives are not likely to be successful in mitigating the recurrent differential heave problems.

A mechanical stabilization approach using geocells was proposed as a likely rehabilitation alternative for this pavement section. By dissipating the heave-induced stresses over a wider area, this reinforcement configuration was hypothesized to significantly reduce the differential heave. Finite-element models of the pavement section comprising six alternative geocell-reinforced configurations were prepared using the commercially available package, ABAQUS®. Moisture swelling and suction properties for the expansive soil deposit were established in the laboratory and were used in the numerical model to simulate the swelling behavior. Results from the numerical modeling effort established that placing two layers of geocell within the unbound granular base layer led to the highest reduction (~60%) in the differential heave. Placing a single layer of geocell, on the other hand, reduced the differential heave magnitude by approximately 50%. A single layer of geocell was therefore recommended for implementation to achieve the optimal balance between pavement performance and construction costs.

TABLE OF CONTENTS

xi

LIST OF TABLES

xiv

LIST OF FIGURES

xvi

xvii

xviii

xix

CHAPTER 1:   INTRODUCTION

1.1   Introduction

Expansive soil is a term describing soils that have a potential for swelling due to an increase in moisture content (Nelson and Miller, 1992). Wray (1995) defined an expansive soil as "*a clay soil that has the ability to change in volume when the moisture content of the soil changes.*" Expansive soils are commonly found throughout many regions of the world, particularly in arid and semiarid areas in Australia, Canada, China, India, Israel, South Africa, and the United States (Nelson and Miller, 1992). In these countries, the annual rainfall is less than the evaporation rate, so there is usually a moisture deficiency in the soil. There is an observed pattern of short periods of rainfall followed by long dry periods (drought) in semi-arid regions, which result in seasonal cycles of swelling and shrinkage (Nelson and Miller, 1992). These soils typically exhibit moderate to high plasticity, low to medium strength, and shrink-swell characteristics (Holtz and Gibbs, 1956; Aitchison, 1973; Chen, 1988).

A study sponsored by the National Science Foundation (NSF) reported that the damage to structures, particularly to lightly loaded engineering structures, caused by expansive soils is more than any other natural disaster, including earthquakes and floods (Jones and Holtz, 1973). In the United States, the total annual cost of damage from these soils is $2.3 billion (Gromko, 1974). Petry and Armstrong (1989) noted that it was more economical to perform initial stabilization of these problematic soils before/during construction of the overlying structures rather than performing remedial treatments later

on with existing structures around. The problem of damage to structures constructed over expansive soil deposits is prevalent across the world. Pavements represent a common example of lightly-loaded structures that are adversely affected by underlying expansive soil deposits.

The performance of a pavement system depends to a large extent on properties of the underlying soil layer. When the subgrade layer exhibits expansive nature, it affects the performance of the pavement structure and results in a shorter service life. Damages sustained by pavements due to the expansion of the underlying subgrade layer can be in the form of distortion and cracking in both flexible (asphalt) and rigid (concrete) pavements, as well as heave-related bumps; both of these lead to ride discomfort. Cracks developed in pavements further allow moisture intrusion into subsoils, which further weakens the underlying layers. Figure 1.1 shows photographs of pavement sections damaged due to volume change in underlying expansive soil deposits. Overall, the magnitude and extent of damages to pavement structures can be extensive, impairing the usefulness of the roads and practically making them uncomfortable for drivers; these pavements require frequent maintenance activities.

(a)   (b)

Figure 1.1   Photographs Showing Damage to Pavement Systems due to Volume Change in Underlying Expansive Soil Deposits (Manosuthikij, 2008)

Several rehabilitation approaches such as soil replacement, pre-wetting, moisture control, and lime stabilization have been implemented in the past by practitioners with varying degrees of success. These techniques suffer from certain limitations with respect to their applicability such as: (1) high cost for hauling suitable re-fill materials for soil replacement purposes (Snethen et al., 1975; Chen, 1988); (2) longer time periods required for pre-wetting highly plastic clays (Felt, 1953); (3) difficulties in constructing well-performing moisture barriers (Snethen et al., 1975); and (4) pulverization and mixing problems in case of lime stabilization (Ramana Murty, 1998), etc. Moreover, implementation of these alternatives can prove to be particularly challenging at locations where the expansive soil deposits extend to significant depths below the pavement surface. In such scenarios, mechanical stabilization alternatives may need to be explored.

Since the 1970s, geosynthetics have been increasingly used as construction materials in civil engineering projects such as roads, retaining walls, landfills, etc. Different types of geosynthetic products available in the market are: geogrids, geomembranes, geotextiles, geonets, geocomposites, and geocells (Koerner, 2005). Geosynthetics perform at least one of the following five functions: (1) separation, (2) reinforcement, (3) filtration, (4) drainage, and (5) containment (Kwon, 2007). The performance and design life of pavement structures can often be enhanced through geosynthetics reinforcement. Geocell, a special type of geosynthetics, is a three-dimensional (3D) honeycombed cellular structure that provides confinement to the compacted infill material. Published literature has focused on the use of geocells to increase bearing capacity and reduce settlement in foundations on soft soils (Dash et al., 2001; Sitharam et al., 2005). Bathurst and Jarrett (1988) reported that geocell-reinforced

base layers exhibited higher load-carrying capacity when compared to soft peat

subgrades. Similarly, Bortz (2015) reported that geocells can help reduce the thickness

requirements for HMA and base layers constructed over weak subgrades. Recently, the

Association of American Railroads (AARs) and the *Transportation Technology Center*

Inc. (TTCI) observed that geocellular confinement systems were 14 times more effective

compared to other geosynthetic types and eliminated the need for frequent ballast

tamping and resurfacing activities. Figure 1.2 shows a schematic of track structure

comprising a geocell (also known as geoweb) reinforced subballast layer (AAR/TTCI,
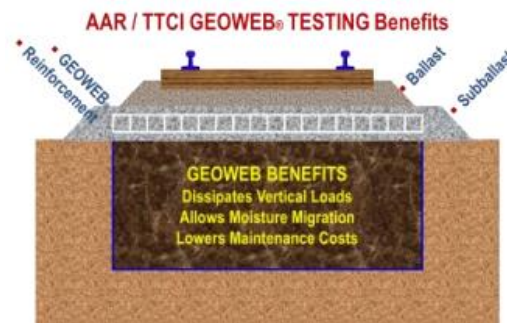
2012).

**Figure 1.2   Schematic of Railroad Track Structure Comprising a Geocell-
Reinforced Subballast Layer (AAR/TTCI, 2012).**

Therefore, geocells represent an economical alternative solution for pavements

and railroads. The use of geocells as a remedial measure to rehabilitate pavement sections

constructed over expansive soil deposits has not been explored in the past.

1.2   Background and Problem Statement

Volumetric changes induced in expansive soils upon fluctuations in the moisture

content lead to the development of cracks in overlying lightly loaded structures such as

pavements. Both flexible and rigid pavements built over expansive soil layers can

undergo significant cracking due to the heaving caused by expansive soil deposits. One approach to mitigate this problem involves preventing the access of moisture to the expansive soil deposits. Jayatilaka and Lytton (1997) reported that vertical moisture barriers with impermeable geomembranes could reduce the moisture variation in expansive subgrade and restrain pavement roughness. Vertical moisture barriers minimize moisture variations by isolating the soil from climatic changes. In wet seasons, moisture barriers prevent access to water, whereas, in dry seasons, the moisture barriers prevent excessive drying of the subgrade soil, especially under pavement shoulders and thus reduce the chances of longitudinal shrinkage cracking (Steinberg, 1992). The main drawback of this approach lies in the high expense and complex construction methods. Another widely used approach involves chemical stabilization of expansive soils using Calcium-based stabilizers like lime and cement. However, this stabilization technique may not be applicable for soil layers exhibiting high sulfate contents due to the formation of high-swelling minerals like Ettringite and Thaumasite. When the problematic soil layer deposits are located at depths greater than 3 ft. (~91 cm) from the pavement surface, traditional shallow stabilization treatments or soil removal and soil replacement may not be feasible. Therefore, remedial measures that can mechanically dissipate the stresses generated due to volume changes in the underlying expansive soil deposits may be more appropriate.

A problematic section of U.S. highway 95 along the Idaho-Oregon border experiencing recurrent differential heaving and pavement damage was selected for detailed investigation in this research effort. Although the recurrent pavement distresses have been attributed to volume changes in the underlying expansive soil deposits, prior

stabilization and remediation approaches have achieved only partial success. Accordingly, this research study focused on identifying the primary mechanisms contributing to the recurrent pavement damage and proposing adequate remedial approaches.

1.3   Research Hypothesis and Objectives

The research questions needed to be answered were:

1.   For the problematic flexible pavement section, where is the problematic soil layer located (with respect to the pavement surface)?

2.   Is it possible to remediate the problem of recurrent pavement damage through conventional soil stabilization approaches?

3.   If conventional stabilization approaches are not feasible, can geosynthetic reinforcement of the pavement help mitigate the differential heaving problem?

4.   If geosynthetic reinforcement is an option, where should it be placed within the pavement structure for optimum performance?

The primary research hypothesis associated with research question numbers (3) and (4) listed above is *"Geosynthetics can be effectively used as remedial measures to mitigate the problem of differential heave in pavement sections constructed over expansive soil deposits."*

The following research tasks were completed in an effort to answer the research questions

1.   Establish the physical, mineralogical, and chemical characteristics of soil samples collected from underneath the problematic pavement section through the completion of an extensive laboratory test matrix.

2.   Numerical modeling of pavement sections incorporating geocell-reinforced to select evaluate its effectiveness as a candidate remedial measure to mitigate the differential heave problem in flexible pavement sections constructed over expansive soil deposits.

1.4   Outline of the Thesis Document

This Master's thesis document comprises five chapters.

Chapter 2 presents a review of published literature on expansive soil behavior and different factors influencing the expansive behavior of soils. Identification and characterization of expansive soils and various remedial measures to mitigate damage to structures overlying expansive soil deposits are also discussed in this chapter.

Chapter 3 presents a detailed background of the problematic pavement section investigated in this research effort. This is followed by a discussion of the laboratory test matrix developed for extensive characterization of soil samples collected from underneath the problematic pavement section. Findings from the laboratory testing effort are then presented, and inferences are drawn concerning the primary mechanisms contributing to the recurrent pavement damage. Finally, underlying principles of potential remedial measures to adequately address the source of the problem are discussed.

Results from laboratory test to establish material properties as inputs for the numerical model are presented. Chapter 4 presents details of the numerical modeling effort undertaken during this research effort. Finally, results from the numerical models are discussed and inferences are drawn concerning the effectiveness of geocell reinforcement as potential rehabilitation measures for pavements experiencing expansive soil-related differential heaving.

Finally, summary and conclusions from this research study, the significance of the findings from laboratory and numerical modeling efforts, and future research needs are addressed in Chapter 5.

CHAPTER 2:   REVIEW OF PUBLISHED LITERATURE

2.1   Introduction

In recent years, several research studies have been conducted to study the swell-shrink behavior of expansive soils. Several alternatives have been developed by researchers and implemented to control the swell-shrink behavior of these soils. The swelling potential of the expansive soil primarily depends on important soil properties, environmental factors such as susceptibility to fluctuations in moisture contents, and stress and surcharge conditions. Each year, expansive soils cause damage to houses, buildings, roads, pipelines, and other pavement structures. This is more than twice the damage from floods, hurricanes, tornadoes, and earthquakes combined (Jones and Holtz, 1973). This chapter presents a literature review on expansive soil behaviors and different factors influencing the expansive behavior of soils. Towards the end of the chapter, detailed review of several remediation strategies for pavement damage occurring due to expansive soils has also been presented.

2.2   Factors Influencing the Expansive Behavior of Soils

The factors affecting the shrink-swell potential of soil can be categorized into three different groups: soil characteristics such as clay mineral, plasticity, soil suction, and dry densities; environmental factors such as climate, groundwater, vegetation, and drainages; and the state of stress (Nelson and Miller, 1992). These intrinsic properties contribute to swelling and shrinkage with a change in moisture content in the ambient

environment and can be used to determine the behavioral characteristics of expansive soils. Brief discussions of these factors are presented in the following subsections.

2.2.1   Clay Mineral

The magnitude of swelling potential is a function of the amount and type of clay mineral present in the soil (Johnson et al., 1975). Clay mineral types that are commonly responsible for volume changes are Smectite, Vermiculites, and some mixed layers of these minerals. Montmorillonite, which falls in the Smectite group of minerals is highly expansive in nature. Kaolinite, on the other hand, is significantly less expansive in nature but can cause volume change when mineral particle sizes are less than few tenths of a micron (Nelson and Miller, 1992). Johnson et al. (1975) showed that mineralogical composition along with environment is responsible for swelling potential of the soil.

2.2.2   Soil Fabric

Clays tend to exhibit higher swelling potential when flocculated; however, the swelling potential reduces when particle arrangements are altered to disperse upon compaction (Johnson et al., 1975; Nelson and Miller, 1992). Fabric and structure are altered by compaction at high moisture content or remolding. Remolding suppresses the structural strength and the strong connections between soil particles that were a result of long and complicated natural events. Thus remolded soil samples swell freely compared to undisturbed soils. Higher the dry density, larger is swelling potential of the soil. This is mainly due to closer particle spacing corresponding to soils compacted to higher densities, which results in greater particle contact and, thereby, leads to significant volume changes (Johnson et al., 1975; Chen, 1988; Nelson and Miller, 1992).

2.2.3   Surcharge Loads

Using surcharge or external load can reduce the amount of swelling by balancing inter-particle repulsive forces. Confining pressure has a significant influence on the swelling potential of clays. Greater the confining pressure, smaller will be the vertical deformation. Overburden pressures exerted due to lightly loaded engineering structures such as pavements are too small to counter excessive swelling pressures applied by underlying expansive soils (Johnson et al., 1975).

2.2.4   Active-Zone

The depth in the soil, which periodic changes of moisture occur, is usually referred to the *active-zone*. The depth of the active-zone varies, depending on location and moisture fluctions. In some clays and clay shales in the Western United States, the depth of the active-zone can be as much as 50 ft. (1524 cm). The active-zone depth can be easily determined by plotting the liquidity index (LI) against the depth of the soil over several seasons as shown in Figure 2.1 (O'Neill and Poormoayed, 1980; Das, 1999). LI is defined as the relative consistency of a cohesive soil in its natural state, which is given by:

$$LI = \frac{w - PL}{LL - PL} \qquad (2.1)$$

where LL = Liquid Limit (%); w = Natural Moisture Content (%); PL = Plastic Limit (%).

Vanapalli and Lu (2012) stated that soil heave is induced due to the change in soil suction within the active-zone. Soil suction is the principal stress-state variable that governs the swelling potential of the clayey soil. In other words, it can be explained a soil suction within the active-zone is an illustration of a state of balance of environmental factors (i.e., soil-atmospheric interactions) and soil-water storages processess (Vanapalli

and Adem, 2013). It is critical to define a zone that could be wetted with time because as

water travels through pores in the soil, different zones are wetted at various times.
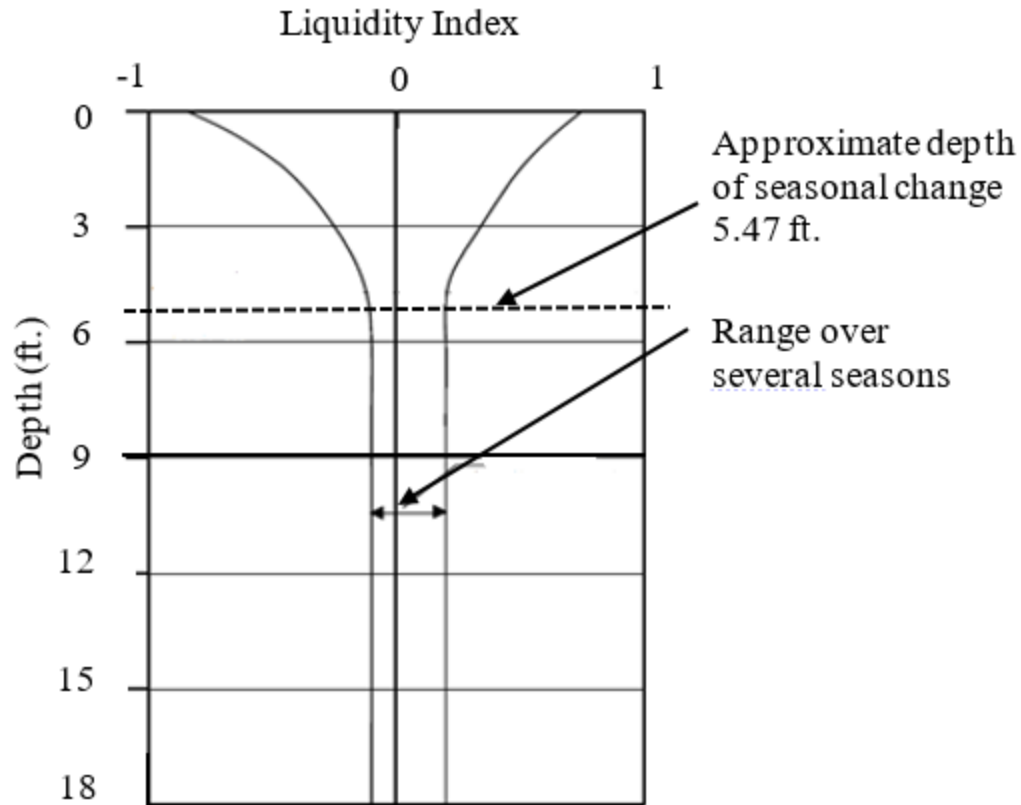
Figure 2.1   Determining Active-Zone using Liquidity Index (Recreated from Source: O'Neill and Poormoayed, 1980; Das, 1999) (1 ft. = 30.5 cm)

2.3   Identification and Characterization of Expansive Soils

Different methods have been developed to identify expansive soils in the

laboratory and field. Various criteria adopted to recognize the presence of expanding-

lattice-type clay minerals in a natural soil can be broadly classified into three categories,

namely (1) index property tests, (2) mineralogical identification, and (3) physical and

mechanical characterization methods. Brief discussions on these methods are presented in

the following subsections.

2.3.1   Index Property Tests for Evaluating Swell Potential

Index property tests can be used for the evaluation of the swelling potential of

expansive soils. The first and still most commonly used index properties correlated with

swell potential are the soil consistency limits. The plasticity index and liquid limit are

useful indices for determining the swelling characteristics of most clays (Holtz and

Gibbs, 1956). Seed and Lundgren (1962) showed that the plasticity index alone could be

used as a preliminary indication of the swelling characteristics of most clays. The relation

between the swelling potential of clays and the liquid limit and plasticity index can be

classified in Table 2.1.

Table 2.1   Classification of swelling soils (Army TM 5-818-7, 1983)

Classification of potential swell	Liquid Limit (LL) (%)	Plasticity Index PI (%)
Low	<30	0-10
Medium	30-50	10-20
High	50-60	20-35
Very High	>60	>35

Some other tests are easy to perform and should be included as routine tests in the

investigation of pavement sites in those areas having expansive soil. Such tests may

include (1) linear shrinkage tests, and (2) colloid content tests, etc. Altmeyer (1955)

provided some values for shrinkage limits and linear shrinkages as a guide to determine

potential expansiveness of clayey soil. These values are presented in Table 2.2.

Table 2.2   Relation between Swelling Potential, Shrinkage Limits and Linear Shrinkages (Source-Altmeyer, 1955; Chen, 1988)

Shrinkage Limit (%)	Linear Shrinkage (%)	Degree of Expansion
<10	>8	Critical
10-12	5-8	Marginal
>12	0-5	Non-critical

Accordingly, Seed and Lundgren (1962) believed that there is no correlation between swelling potential and percentage of clay sizes. For any given clay type, the relationship between the swelling potential and percentage of clay size can be expressed by the equation:

$$S = KC^X \qquad (2.2)$$

where S is the swell potential (%); C is the percentage of clay sizes finer than 0.002 mm; X is an exponent depending on the type of clay, and K is the coefficient depending on the clay type.

Where a hydrometer test determines the number of the clay size particles, the quality of colloid reflected by X and K in the above equation, controls the amount of swell.

2.3.2   Mineralogical Identification and Quantification

Mineralogical identification helps identify elements present in a clay particle. There are several ways to determine the mineralogical composition of a clay particle. Some commonly used methods are X-Ray Diffraction (XRD), Differential Thermal Analysis, Vibrational Spectroscopy, and X-Ray Absorbance Spectroscopy. Quantitative determinations of some clay minerals based on simple comparison of the diffraction peak

heights or areas are uncertain due to many factors like differences in absorption coefficients, particle orientations, crystallinity and other factors (Mitchell and Soga, 2013). As a result, other techniques using chemical mass balance concepts in conjunction with XRD data have been developed that are currently utilized for the clay mineral quantification (Alexaides and Jackson, 1966; Hodgson and Dudeney, 1984; Johnson et al., 1985; Randall et al., 1994).

2.3.3   Physical and Mechanical Characterization Methods

There are several ways very popular and widely practiced to determine swelling potential of the expansive soil. Brief discussions on these methods have been presented in the following subsections.

2.3.3.1 Oedometer Test

Swelling pressure is defined as the pressure in an oedometer test required to prevent soil sample from swelling after being saturated where swelling pressure which is determined by the oedometer test method is one of the important parameters used in determining heave potential (Vanapalli and Lu, 2012). Various loading and surcharge pressures have been used by researchers to represent in-situ conditions. Loading and wetting sequence, surcharge pressure, sample disturbance and apparatus compressibility all should be taken into account while performing oedometer test. The total stress applied to the sample is controlled in the conventional consolidometers. Engineers are widely using oedometer tests; however, environmental factors such as drainage and effects of lateral pressure cannot be simulated while conducting oedometer test (Vanapalli and Adem, 2013). Another disadvantage of this test is that it takes a longer period for achieving equilibrium which makes this tedious and costly. Two types of oedometer tests

commonly practiced are (1) consolidation-swell test, and (2) constant volume or swell pressure test (Nelson and Miller, 1992).

2.3.3.2 Soil Suction Methods

Soil suction is the quantity that can be used to characterize the effect of moisture on volume, and it is a measurement of the energy or stress that holds the soil water in the pores. Surface tension at the air-water interface in an unsaturated soil will lead to negative water pressure in the soil and therefore referred to as matric suction. Matric suction varies with the soil's moisture content. The total suction is expressed as a positive quantity and is defined as the sum of matric and osmotic suction. Researchers used the filter paper test to determine the initial total suction and matric suction of the soil sample. One-dimensional heave and the swelling pressure can be determined using soil suction method as it is based on stress state. In determining heave, soil suction is taken into account through the use of different parameters. Soil suction methods are considered to be reliable and can simulate field conditions (Vanapalli and Adem, 2013).

2.3.3.3 United States Bureau of Reclamation (USBR) Method

This method involves direct correlation of observed volume change with colloidal content, plasticity index, and shrinkage limits. Colloid content is the total percent of particle sizes less than 3.9×10^{-5} in. (0.001 mm) in diameter present in the soil sample. The typical relationship of these properties with swelling potential is presented in Figure 2.2, and the identification criteria of expansive clay are shown in Table 2.3.
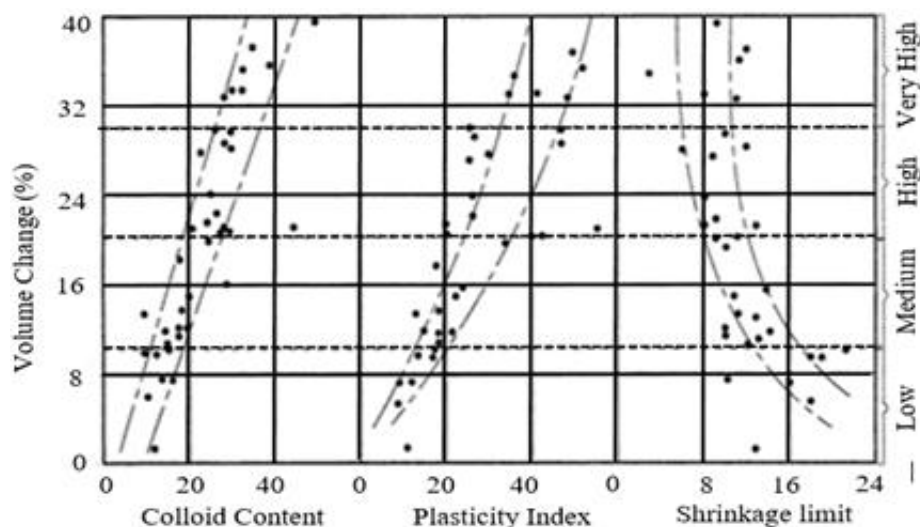
Figure 2.2 Relation of Volume Change to Colloid Content, Plasticity Index, and Shrinkage Limit (Recreated from Source- Chen, 1988; Murthy, 2010)

Table 2.3 Data for Making Estimates of Probable Volume Changes for Expansive Soils (Source: Chen, 1988; Murthy, 2010)

Data from index tests			Probable Expansion, percent total vol. change	Degree of Expansion
Colloid Content, percent minus 3.9 × 10^{-5} in. (0.001 mm)	Plasticity Index (%)	Shrinkage Limit (%)		
>28	>35	<11	>30	Very high
20-13	25-41	7-12	20-30	High
13-23	15-28	10-16	10-30	Medium
<15	<18	>15	<10	Low

2.3.3.4 Potential Volume Change (PVC)

The Potential Volume Change (PVC) method was developed by T.W. Lambe

(1960) for the Federal Housing Administration (FHA). In this approach, a remolded soil

sample is compacted in a fixed ring consolidometer with a compaction effort of 55,000

pcf (~8640 kN/m^3). After compaction, a pressure of 200 psi (~1379 kPa) is applied on to

the sample. Then the sample is wetted and allowed to swell against the proving ring.

Swell index is then calculated by converting pressure in the proving ring to a qualitative volume change using the plot shown in Figure 2.3. PVC test is an indirect method for determining the swelling potential of the expansive soil, and also the test is carried out on remolded samples. So, this test can only be used for identifying the expansive soil, and should not be used as design parameters for undisturbed soil samples (Chen, 1988; Murthy, 2010).
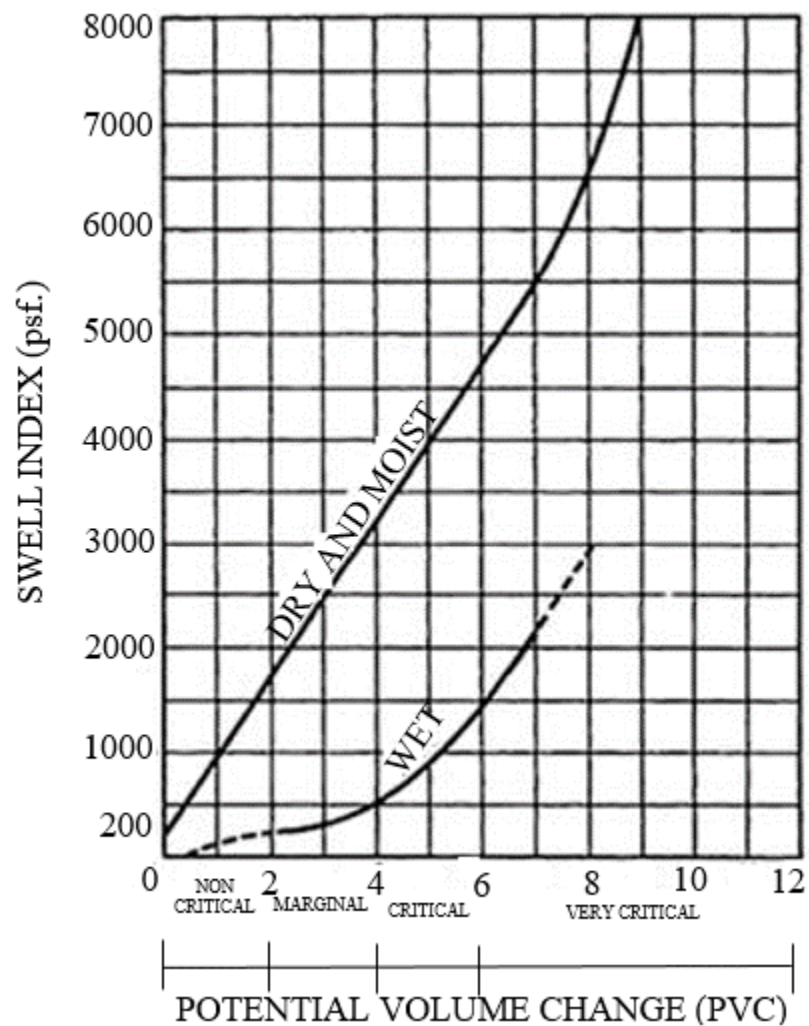
Figure 2.3   Determining PVC from Swell Index (Recreated from Lambe, 1960) (1 psf = 0.05 kPa)

2.4   Methods for Prediction of Swelling Potential

There are three general methods for predicting potential heave, namely, (1) empirical, (2) semi-empirical, and (3) analytical methods (Nelson and Miller, 1992). Most of the methods assume some change in soil moisture content, generally from the in-situ moisture content to an assumed final moisture content (such as saturation). Most semi-empirical methods are only used to predict potential vertical heave, which is commonly referred to as Potential Vertical Rise (PVR). PVR values can easily be used to predict the effects of select fill. Brief discussions on PVR methods have been presented in the following subsections.

2.4.1   Potential Vertical Rise (PVR)

The Potential Vertical Rise (PVR) method, developed by McDowell in 1956 (1956), is widely used across the United States to the estimate the volume change behavior of expansive soils. PVR, expressed in inch (cm). The PVR computed for a given site is currently used in pavement design to determine what depth of the natural soil must be removed and replaced with a more inert soil in place. In order to reduce the computed PVR to 1 in. (2.54 cm), 1.5 in. (3.75 cm), or 2 in. (5 cm) dependent upon the highway facility. There are some recommended values of 1 in. (2.54 cm) for interstate, and U.S. highways, 1.5 in. (3.75 cm) for state highways, and 2 in. (5 cm) for farm-to-market roads (Jayatilaka et al., 1993). A summary of assumptions together with discussions based on PVR are listed below (Lytton, 2004):

1.   Soil at all depths has access to water in capillary moisture conditions.

2.   The vertical swelling strain is one-third of the volume change at all depths.

3.   Remolded and compacted soils adequately represent soils in the field.

4. PVR of 0.5 in. (1.27 cm) produces poor riding quality.

5. Volume change can be predicted by the use of plasticity index alone.

Moreover, there are limitations and drawbacks to this method. For example, this approach does not consider topography, vegetation and drainage effects. It is an overly conservative estimation of swell potentials for low plasticity soils and an underestimation for high PI soils (Lytton, 2004). However, this method has limitations of not considering topography, vegetation and drainage effects, as well as overly conservative estimations of swell potentials. Therefore, Texas Department of Transportation (TxDOT) uses Tex-124-E (TxDOT, 1999) test method to determine the PVR.

2.5 Remediation Strategies for Pavement Damage Occurring due to Expansive Soil

The volumetric change may be more severe and thus become a bigger challenge for expansive soil. The expansion action may result in intolerable differential heaving of pavements. The commonly used remediation methods include (1) mechanical/chemical stabilization, (2) moisture control barriers, and (3) geosynthetics reinforcement. The following sections describe different remediation methods.

2.5.1 Pre-wetting

The objective of pre-wetting is to allow the soil to reach moisture equilibrium prior to placement of pavement. Pre-wetting a site to increase moisture content can eliminate an expansive soil problem if high moisture content can be maintained (Thomas, 1998). The soil is allowed to swell in order to maintain a constant volume, achieving a no heave state, and therefore structure built over it will not be damaged (Chen, 1988). Experience in Southern California indicates that pre-wetting moderately expansive soils

to a condition of 85% saturation at a depth of 30 in. (~76 cm) is often satisfactory, while in the case of highly expansive soils, pre-wetting to as much as 36 in. (~91 cm) may not be sufficient (Chen, 1988).

Although this method has been successful in some projects, a significant problem is associated with this technique. Pre-wetting has greater chances of success during the hot, dry season when soils are in a desiccated state. Clayey soils usually have low permeability and thus the time required for pre-wetting of soil to desired depth will be longer. Therefore, soil mass and depth needed for pre-wetting are usually limited. Also, wetting of deep, expansive layer takes longer time and becomes susceptible to future heave. Another disadvantage is that clayey soil when saturated reduces the bearing capacity. There is a possibility that excess water left in the upper soil can cause swelling in deeper layers at a later date (Chen, 1988).

2.5.2   Surcharge

The expansive behavior of clay can be reduced by loading structure with a surcharge sufficient to counteract swell pressures caused by an increase in moisture content. This method consists of applying sufficient pressure to the expansive soil to reduce the amount of swell. For example, a layer of non-expansive soil or less expansive soil can be placed on top of the expansive soil deposit to apply sufficient downward pressure on the soil layer. The greater the surcharge pressure, the lower will be the percent swell. The surcharge pressure can be calculated by one of the following approaches: (1) constructing an inert embankment to pre-calculated height and (2) replacing soil to a calculated depth with an inert material. The principle is to make a balance between the pavement structure, and the subgrade by eliminating the upward

swelling pressure (Djellali et al., 2012). This can be done applying a surcharge on the

subgrade (see Figure 2.4).
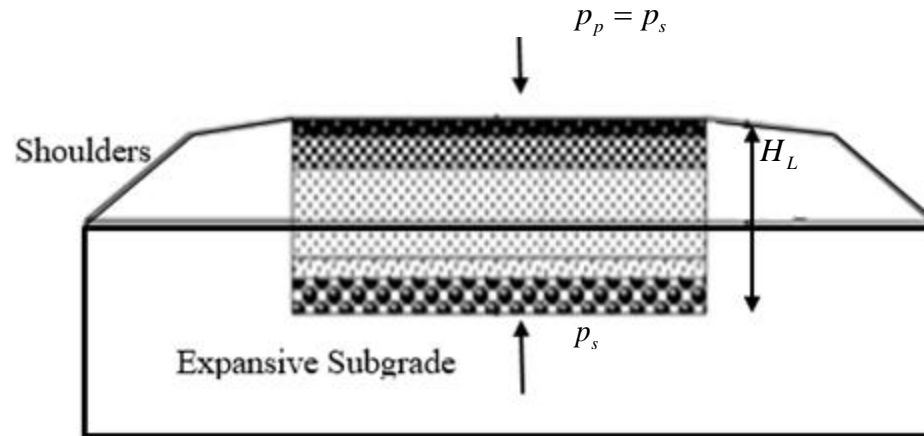
Figure 2.4   Principle of the Stabilization of an Expansive Subgrade (Djellali et al., 2012).

where p_p is the applied vertical pressure, lb/ft^2 (kN/cm^2), p_s is the swelling pressure,

lb/ft^2 (kN/cm^2), H_L is the selected fill thickness, ($in./cm$).

This method is only feasible for soils with low to moderate swelling pressure.

Proper laboratory and field testing are required to determine swelling pressure of the soil

(Nelson & Miller, 1992). However, the vertical stress applied by lightly loaded

engineering structures such as pavements is often lower in magnitude than swell

pressures exerted by expansive soil subgrades. Therefore, the surcharge approach to

counter the swell pressure from subgrade soil is more feasible for structures with heavy

foundations (Johnson et al., 1975).

2.5.3   Chemical Stabilization

Cement and lime stabilization have been widely used to improve the strength of

the expansive soils. The reason for chemical stabilizer popularity is that they are

applicable in a wide range of soil type and are widely available and relatively cheap as

compared to other modes of soil stabilization. Brief discussions on different types of admixture have been presented in the following subsections.

2.5.3.1 Lime

Lime stabilization is widely used to chemically transform the unstable soils so that the soils could be used as sound foundations. Lime stabilization creates some important engineering properties of soils, such as the advantages of providing increased strength; improved resistance to fracture, fatigue, and permanent deformation; improved resilient properties; reduced swelling; and resistance to the damaging effects of moisture. The most substantial improvements in these properties are seen to be in moderate to high plasticity soils, such as heavy clays (Little et al., 2000). Lime stabilizes soils through two important mechanisms, soil modification, and soil stabilization. The rapid physicochemical reactions such as cation exchange and flocculation between lime and clay minerals are referred as soil modification while the long-term soil-lime pozzolanic reactions are referred as soil stabilization (Rao et al., 2008).

2.5.3.2 Cement

Many researchers have indicated that the role of cement as a soil stabilizer is similar to lime due to the presence of calcium in both products (Estabragh et al., 2013). Cement stabilization develops from the cementitious materials between the calcium silicate, aluminate hydration products and the soil particles (Croft, 1967). The addition of cement to clay soil reduces the liquid limit, plasticity index, and swelling potential; and increases the shrinkage limit and shear strength of soil (Nelson and Miller, 1992).

2.5.3.3 Fly Ash

Fly ash is a byproduct of coal-combustion electric-generating plants. There are mainly two types of fly ash, namely (1) Class-F, and (2) Class-C fly ash. Class-F is obtained from the burning of bituminous coal, which contains a very low concentration of calcium product, and thus Class-F does not possess self-cementing characteristics but can be used in the presence of lime and cement. On the other hand, Class-C fly ash is obtained from burning of sub-bituminous coal, which is rich in Calcium Carbonate and thus contains cementing agent Calcium. Usually, Class-C fly ash is used in the presence of lime and cement. But Class-C fly ash can form a cementitious bond similar to Portland cement so in some cases only fly ash can be used (Mackiewicz and Ferguson, 2005)**.** A study carried out by Malhotra and Naval (2013) concluded that the right proportion of fly ash and lime could decrease swelling and shrinkage characteristics of the expansive soil.

2.5.4   Moisture Barriers

The primary factor influencing volume change of expansive soil is fluctuations in the moisture content. In the encapsulation technique, the soil is made isolated from any moisture changes by the use of waterproof membrane (Johnson et al., 1975). The encapsulation technology provides for the complete isolation of expansive soils from all water sources. Encapsulating barriers have been constructed using both asphaltic materials, and more recently, with geomembranes. Encapsulation can only be used with new pavement construction. The barrier could be of two types: horizontal as well as vertical barriers.

Horizontal moisture barriers are installed around rigid paving or flexible paving to prevent excessive intake of moisture from the surrounding. Based on a study by

Browning (1999), horizontal moisture barriers neither produce a smoother ride than the unprotected pavement in the roughness tests nor reduce the moisture variance.

Vertical moisture barriers are installed around the perimeter of a building to prevent water entering under slab soils. Koerner (2005) discusses that moisture barriers are not likely to work as thermos-dynamic processes by themselves lead to moisture fluctuations in the soil. The major drawback of this approach lies in the high expense and complex construction methods. Field trials to evaluate the effect of barrier depth showed that deeper barriers at 8 ft. (~244 cm) outperformed the shallow barriers at 6 ft. (~183 cm) in maintaining a more constant moisture regime, thereby further reducing vertical movements (Gay and Lytton, 1988). However, the deeper the barrier, the more expensive the construction will become. Thus, using vertical moisture barriers has usually only been reserved for major highways.

2.5.5   Geosynthetics Reinforcement

A more innovative, evolving technique being used in pavement design for expansive soils is the use of geosynthetic reinforcements in the base layer or at the interface of the base and subgrade layers. The American Society for Testing and Materials (ASTM) defines geosynthetics as "*a planar product manufactured from a high density polymeric material used with soil, rock, earth, pipelines or other geotechnical engineering related material as an integral part of a man-made project, structure, or system* (ASTM 4439 2004)." Various types of geosynthetics have different functions that can be grouped as separation, reinforcement, filtration, drainage, and containment (Kwon, 2007; Christopher, 2010). Geosynthetics provide a significant improvement in pavement construction and performance. Figure 2.5 illustrates a number of potential

geosynthetic applications in a layered pavement system to improve its performance and the design life of pavement structures. The reinforcement approach shown in Figure 2.5 can be provided by geosynthetic through friction or interlock (geogrids) developed between the aggregate and the geosynthetic interface. These applications include subgrade stabilization, base/subbase, and asphalt reinforcement (Christopher, 2010).
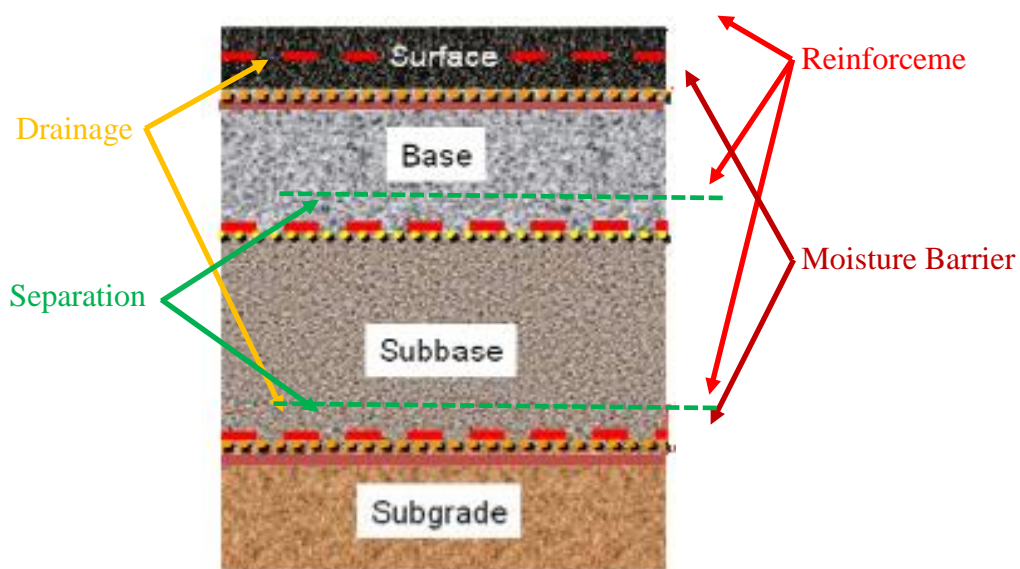
Figure 2.5   Potential Applications of Geosynthetics in Layered Pavement System (Christopher, 2010)

Geosynthetics include geogrids, geomembranes, geotextiles, geonets, geocomposites, and geocells (Koerner, 2005). Among all the geosynthetic types stated above, the effect of geocells inclusion for the case of pavement application is described in the following subsections.

2.5.5.1 Geocell

Geocell is one of the geosynthetic products used primarily for improving soil conditions. In the 1970s, it was originally developed by the U.S. Army Corps of Engineers for quick reinforcement of cohesion less soil in the military field. Like other

geosynthetic products, geocellular confinement systems (geocells) are 3D permeable, honeycomb or web structure and usually made from polymeric materials, such as high-density polyethylene (HDPE). For convenient transportation, most geocell products have a foldable three-dimensional geometry as shown in Figure 2.6 (Webster and Alford,

1977).

Figure 2.6   3D Geocellular Confinement (Webster and Alford, 1977).

Various shapes and sizes of geocell exist (see Figure 2.7), and they can be found in a multitude of materials. This multitude of product specifications allows extreme versatility in its applications to soil reinforcement.
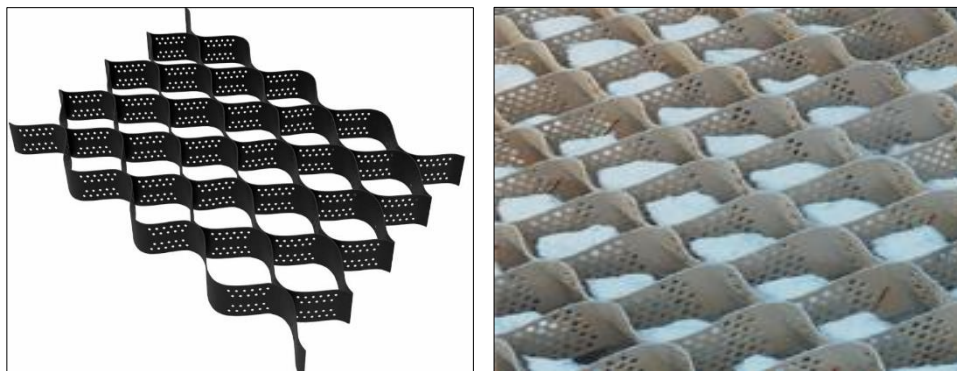
Figure 2.7   Various Geocells: Strataweb (left, copyright: Strata Systems), and Neoweb (right, copyright: PRS Mediterranean).

2.5.5.2 Mechanism of the Geocell Reinforcement

Zhao et al. (2009) reviewed the geocell-reinforced layers under embankments and suggested that the main geocell layer functions in three aspects: (1) lateral resistance

effect, (2) vertical stress dispersion effect, and (3) membrane effect. The reinforcing

mechanism in the geocell provides all round confinement to the materials by virtue of its

interconned cells a result it prevents the lateral spreading of soil on the application of

load (see Figure 2.8a). Because of this better composite material is formed and the

geocell layer behaves as a stiffer mattress that redistributes the footing load over a wider

area, as shown in Figure 2.8b (Dash et al., 2008). The loads from the embankment deflect

the geocell reinforcement thus generate tension force, as shown in Figure 2.8c.

(a) Lateral Resistance Effecet

(b) Vertical Stress Dispersion Effect
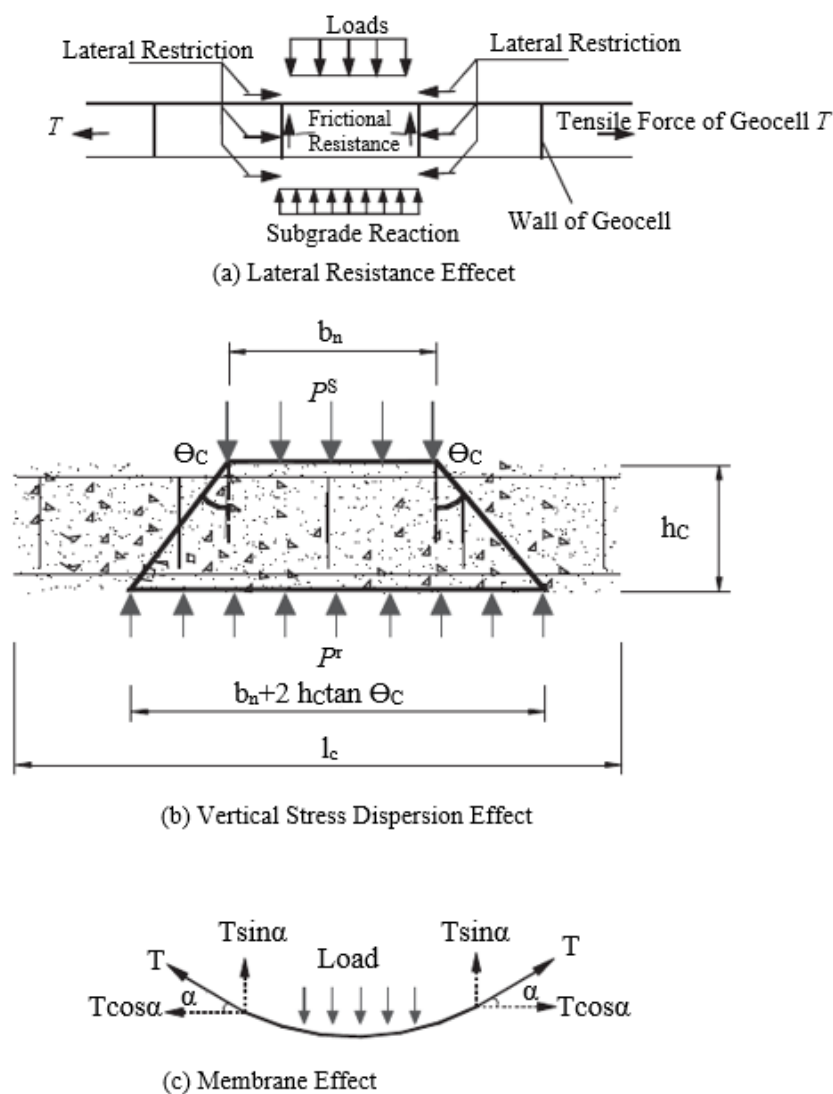
(c) Membrane Effect

Figure 2.8   Possible Reinforcement Functions Provided by Geocell in Roadways (a) Lateral Resistance Effect, (b) Vertical Stress Dispersion Effect, and (c) Membrane Effect (Zhao et al., 2009).

2.5.5.2 Application of the Geoccell Reinforcement

Geocells are widely used for the reinforcement of soft soil. There is a bundle of areas where geocells are applied successfully. These are widely being used for enhancing the bearing capacity and shear strength of soil under the different types of civil engineering structures. Geocells have been now used for different structures like embankments, foundation, paved and unpaved roads, retaining walls, and also for slope stability. Geocells are used to improve the bearing capacity of the foundation and meanwhile reduce the settlement, as shown in Figure 2.9 (a & b). Figure 2.9 (c & d) illustrates the application of geocell-reinforced base course supporting repeated traffic load in both paved and unpaved roads. Besides, geocell can be used for erosion control and earth retaining structures (see Figure 2.9e & f). This suggests that geocell could be beneficial in pavement foundation applications as well.
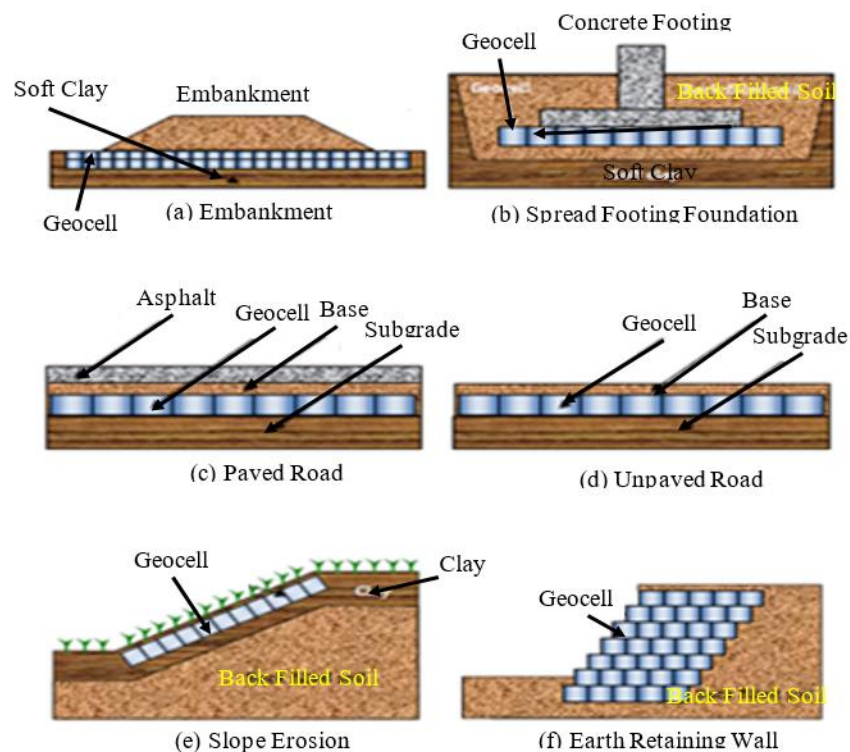
Figure 2.9   Geocell Application (Yang, 2010)

Several studies have shown that utilization of the cellular confinement mechanism significantly improves the strength and stiffness of a granular material; however, a lack of generic design methodology has inhibited its implementation (Han et al., 2008). Leshchinsky (2011) noted that the confinement of the ballast using geocell was quite effective in reducing vertical settlement and lateral spreading. Despite the use of geocell reinforcement in a variety of geotechnical applications for decades, there is a limited study on its use in expansive soil, possibly due to a combination of moisture swelling effects, conservative nature of the field and a lack of design methodology for such an application, specifically for expansive subgrade. A hybrid geosynthetic system uses two or more geosynthetic alternatives to solve a given problem. For example, a hybrid geotextile system was applied in a landfill that contains coal combustion residuals along with other waste products (Ahlberg et al., 2015). Another example that is very relevant to this problem is the use of geogrid and geocell combination to solve expansive soil problem for a railroad application in Israel (Kief, 2015) (see Figure 2.10).
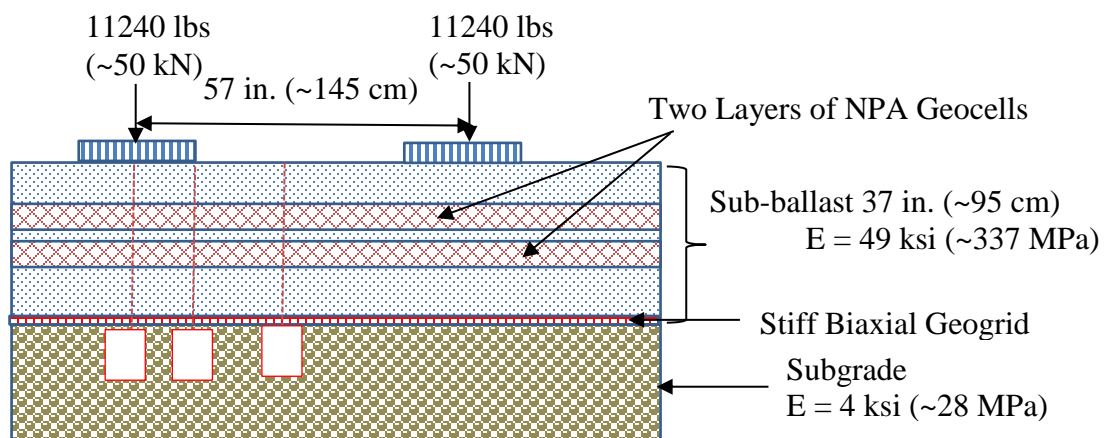
Figure 2.10   Cross Section of Hybrid Geosynthetic Solution Implemented in a Railroad Track Construction in Israel (Recreated from Source: Kief, 2015)

The success of the solution was corroborated through track monitoring measurements, which showed negligible rail head settlements compared to an adjacent parallel unreinforced section. In most cases, projects that have used geosynthetics have employed the use biaxial geogrids and geocells but there are a few cases where geotextiles and glass grids are used. Although guidelines have not been firmly established for this technique, geosynthetics have proven to reduce or even prevent the development of longitudinal cracking of pavement over expansive clays (Zornberg & Gupta, 2009). This technique does not alter the swelling potential expansive clays but the geosynthetics can redistribute the non-uniform uplift load such that points of high stress move from the paved area to the shoulder area (Rhoodi & Zornberg, 2012). Thus, the geosynthetic improves the performance of the pavement and can increase the overall lifetime of the pavement structures (Palmeira, 2009).

2.6   Summary of the Literature Review

Expansive soils cause significant damage to civil engineering structure as discussed throughout this chapter and therefore remedial measures are required to repair the damage caused. However, it is important to establish some factors before embarking on a remedial measure implementation plan. Apparently, to select an appropriate corrective measure an adequate forensic site investigation is required. Key information needed includes (1) cause and extent of damage, (2) soil profile (as it is often difficult to determine whether settlement/heave is the cause of structural distress), and (3) a measure of the expansive potential of the soil. Expansive soils tend to swell and shrink with a change in moisture content. The expansion potential of the soil is governed by its mineralogical composition, the extent of volume change experienced by a soil layer on

the field is also affected by environmental and site-specific factors such as the degree of moisture variation and drainage characteristics. Different methods used for identifying and quantifying the expansive potential of soils were discussed in this chapter. For the quantitative measurement of swelling potential, the oedometer test is widely used and is common in engineering practice. However, it is crucial to stabilizing shrink/swell soils before construction to prevent loss of properties and lives. Though no universal guideline can be applied to all situations involving expansive soil related problems, particular site characteristics and historical performance records accompanied by forensic investigations can often lead to the selection of suitable rehabilitation alternatives.

This chapter presented findings from a review of published literature on topics pertinent to the research objectives. First, an overview of factors affecting the shrink-swell behavior of expansive soil was presented, followed by an overview of clay mineralogy, soil fabric, active-zone, and their properties. The objective was to identify and to quantify of the soil as expansive soil. Subsequently, detailed review of several remediation strategies for pavement damage occurring due to expansive soil was presented. Finally, a brief discussion on geocell reinforcement of the pavement was presented.

The next chapter (Chapter 3) of this thesis document will present a detailed project background of this Master's thesis effort and laboratory findings from an extensive laboratory test matrix.

CHAPTER 3:   PROJECT BACKGROUND AND LABORATORY

CHARACTERIZATION OF EXPANSIVE SOILS SAMPLES

3.1   Introduction

This chapter presents a detailed background of the problematic pavement section investigated within the scope of this Master's thesis effort. This is followed by a discussion of the laboratory test matrix developed for extensive characterization of soil samples collected from the problematic pavement section. Findings from the laboratory testing effort are presented, and inferences are drawn concerning the primary mechanism contributing to the recurrent pavement damage. Finally, underlying principles of potential remedial measures to adequately address the source of the problem are discussed.

3.2   Study Location and Project Description

As mentioned in Chapter 1, the problematic stretch of pavement investigated in this research study is an 18.5-mile (~30-km) long section of U.S. highway 95 just east of the Oregon-Idaho border. Figure 3.1 shows an aerial map of the location highlighting the section under investigation. A summary of the project construction history as extracted from Hardcastle (2003) is given below.

Figure 3.1   Aerial Image Showing Project Location (source: Google Maps)

3.3   Pavement Construction and Maintenance History

Different segments of the problematic pavement section have been subjected to various maintenance/rehabilitation efforts over the last few decades. Figure 3.2 shows a schematic of the problematic highway segment and identifies different segments and corresponding rehabilitation methods. For instance, segments AD (MP 0.0-6.36), and BC (MP 6.36-18.5) were realigned in 1972 and early 1980s, respectively. A chronological list of the different rehabilitation methods implemented has been presented in Table 3.1.

A research study was undertaken by Hardcastle (2003) to investigate the recurrent heaves observed along this stretch of pavement. A series of laboratory tests were performed including conventional geotechnical tests such as Atterberg limits, and 1D swell tests, along with tests such as X-Ray Diffraction (XRD) and Cation Exchange Capacity (CEC) aimed at mineralogical characterization of field-obtained soil samples. Hardcastle (2003) also evaluated different stabilization methods and recommended swell remediation and prevention techniques for existing and new constructions.
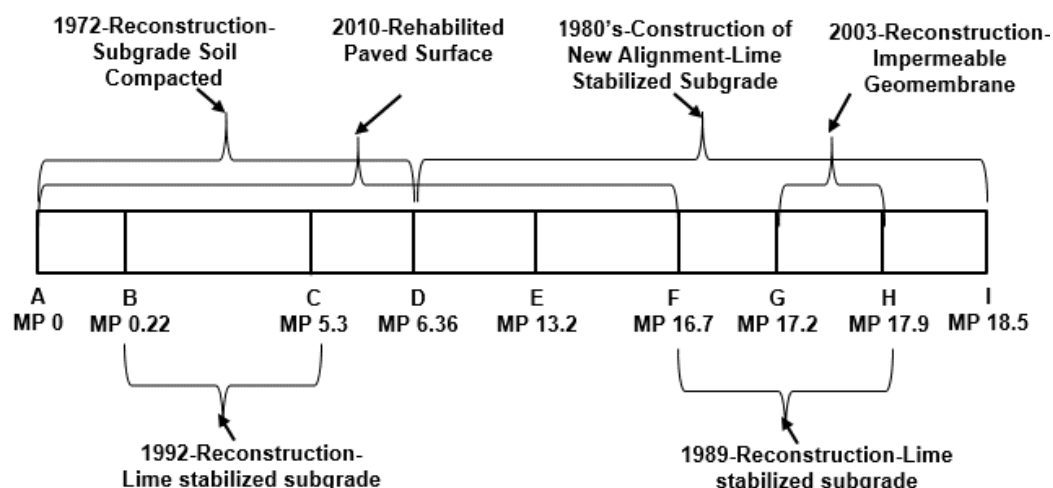
Figure 3.2   **Schematic Representation of the Problematic Pavement Section (1 mile = 1.6 km)**

Table 3.1   **Construction/Reconstruction Activities over the Life of the Project**

Year	Roadway Segment	Activity and Stabilization Effort
1972	AD (MP 0.0 - 6.36)	Reconstruction and subgrade soils compacted wet of optimum moisture content (OMC);
Early 1980's	DI (MP 6.36 - 18.5)	Construction of new alignment and 15 in. (~38 cm) of lime-stabilized subgrade;
1989	FH (MP 16.7 - 17.9)	Reconstruction and15 in. (~38 cm) of lime-stabilized subgrade;
1992	BC (MP 0.22 - 5.3)	Reconstruction and 15 in. (~38 cm). of lime-stabilized subgrade;
2003	GH (MP 17.2 - 17.9)	Reconstruction and impermeable geomembrane;
2010	AF (MP 0.0 - 16.7)	Reconstruction and geogrid reinforcement.

Note that not all soils encountered and sampled by Hardcastle (2003) along this section of U.S. highway 95 showed high expansion potential. Correspondingly, not all locations along this pavement section exhibited heaving-induced distresses. Hardcastle (2003) observed that swelling-related distresses primarily occurred at the transitions

between the cut and fill sections as at Milepost 2.3. Moreover, locations close to the natural ground surface in relatively flat areas underlain by colluvial soils also exhibited significant amounts of distress. The hypothesis was that potentially expansive soil adjacent to the cut sections were used to construct the fill sections at the transition locations. The higher initial suction of the compacted expansive soil and increased exposure to surface water at the grade points could be the primary factors leading to increased pavement distresses at these locations. Finally, recommendations were also made for the base materials to be used in new construction over expansive soils. It was recommended that these materials be well-graded with non-plastic fines having hydraulic conductivities less than 3.28×10^{-7} $ft/s(10^{-6} cm/s)$. If such materials were not available resulting in the use of conventional free-draining base materials, placement of an impervious asphalt or geosynthetic membrane on the surface of the subgrade before
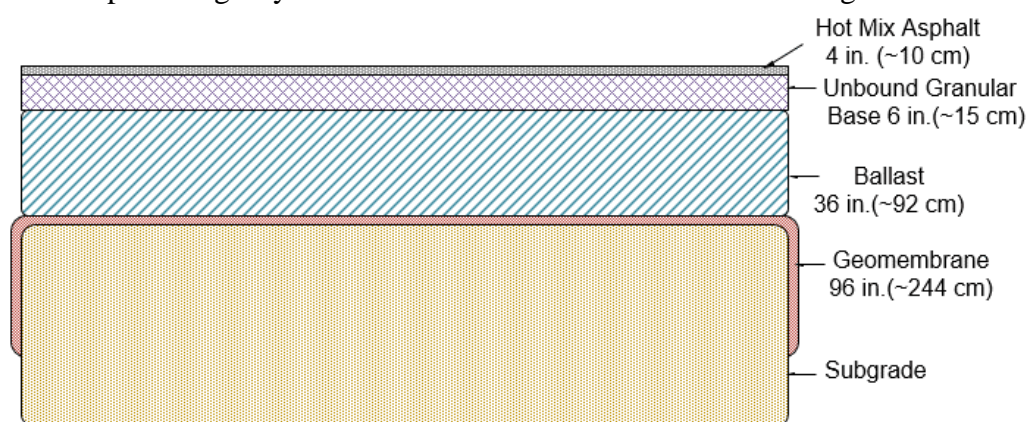
placing any base was recommended (see Figure 3.3)

Figure 3.3   Schematic Representation of Rehabilitated Pavement Section Recommended by Hardcastle (2003)

Idaho Transportation Department (ITD) implemented these recommendations during the reconstruction of this stretch of highway, which resulted in partial success. While most sections performed satisfactorily after treatment, a few sections continued to

exhibit pavement distresses resulting from subgrade heaves. Figure 3.4 shows the severe

distress observed at the site as of May 2015.

Figure 3.4   Problematic Sections of MP 16.3 to MP 18.0 (Picture Taken in May 2015)

3.4   Development of an Extensive Laboratory Test Matrix

The main objective of this research effort was to characterize the problematic soil

layer contributing to the recurrent pavement damage due to volume changes in the

underlying soil layers. The laboratory testing program was designed to determine

properties relating to volume change behaviors of expansive soil samples extracted from

the section of U.S. highway being investigated. Extensive laboratory testing program was

mainly comprised of tests to determine basic soil properties; clay mineralogy; and

physical and mechanical characteristics. Ten boreholes were strategically placed on and

off heave zones along the pavement section, and soil samples were collected for

laboratory testing and characterization. Eight of the ten boreholes were drilled through

heaved zones while the other two were drilled through the non-heave zone to identify any

possible the difference in soil stratigraphy. The relative locations of the boreholes are

shown on a map in Figure 3.5. The boreholes were designated as AH-1 through AH-10 where AH stands for Auger Hole.
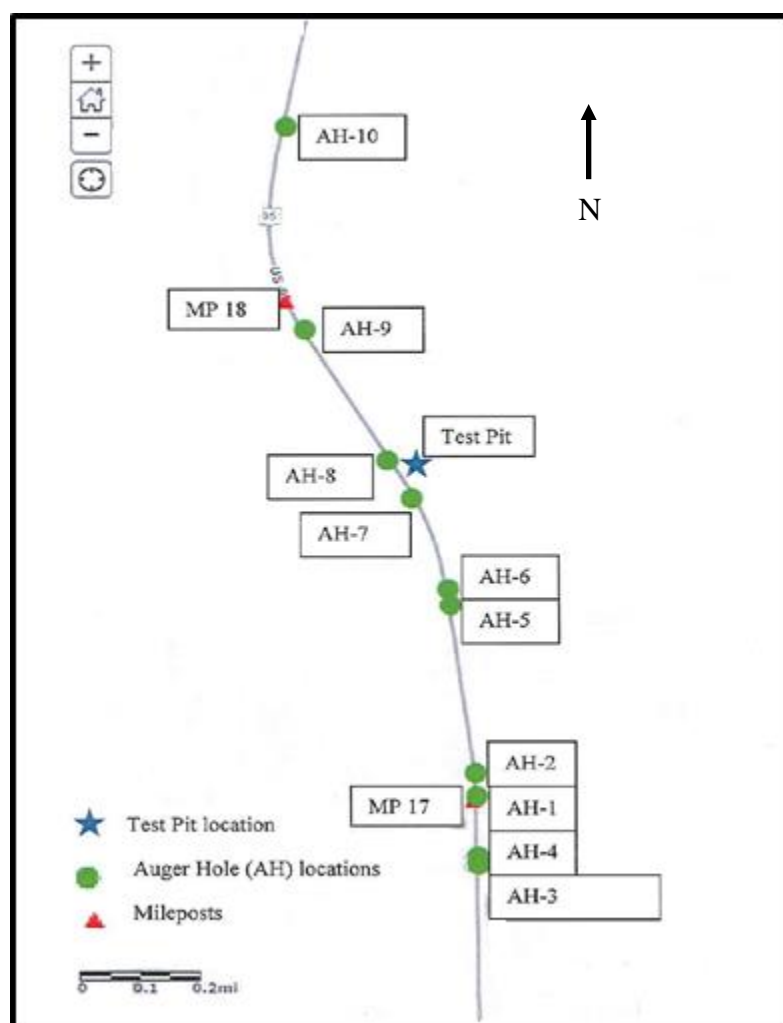
Figure 3.5   Boreholes Locations Map (Courtesy-ITD)

3.5   Drilling and Sample Collection

Drilling and sampling of the subsurface soils in the pavement section of interest performed in collaboration with ITD between May to June 2015. Drilling was performed using dry hollow-stem augers. With this system, the soil sample is retained inside clear Polyvinyl Chloride (PVC) sampler tubes with dimensions of 3.25 in. (~8 cm) inside diameter and 30 in. (~76 cm) length. In addition Standard Penetration Tests (SPT) were

performed, and split-spoon samples were collected at various depths. Figure 3.6 shows

photographs of the drilling and sampling conducted on site. Boreholes were terminated

when strong gravelly layers were encountered which made sampling difficult. Table 3.2

presents a list of the borings with their location specifics and termination depths

measured from the pavement surface. A typical borelog obtained from the drilling efforts

have been shown in Appendix B. Samples collected during drilling were transported to

the laboratory, and stored in a moisture-controlled chamber for testing and

characterization.

(a)   (b)

**Figure 3.6   Drilling and Sample Collections: (a) Full view of Drilling Operation
(b) Plastic Tube Sampler with Soil Sample Inside (Sample Collected in May 2015;
Courtesy-ITD)**

**Table 3.2   List of the Borings with their Location Specifics and Termination
Depths Measured from the Pavement Surface (1 ft. = 30.5 cm)**

S. No.	Location Characteristic	Termination Depth (ft.)	S. No.	Location Characteristic	Termination Depth (ft.)
AH-1	On the heave	26.0	AH-6	Next to heave	14.9
AH-2	Next to heave	20.9	AH-7	On the heave	18.5
AH-3	On the heave	22.5	AH-8	Next to heave	19.5
AH-4	Next to heave	11.7	AH-9	Non-heave zone	16.3
AH-5	On the heave	17.9	AH-10	Non-heave zone	13.0

The laboratory test matrix included: (1) Moisture content tests, (2) Atterberg limits tests, (3) Specific surface area (SSA) tests, (4) Cation exchange capacity (CEC) tests (5) One-dimensional (1D) swell test, and (6) Soluble sulfate content tests. A summary of the laboratory procedures, apparatus used, and results are presented in this chapter.

3.6   Moisture Content Tests

The initial moisture content of the expansive soils controls the amount of swelling. Moisture content tests were performed to establish the field moisture contents within the soil layers at the time of the sampling. These tests were performed per the AASHTO T 265 (2004) test procedure. A total of 169 tests were conducted on samples corresponding to different depths within each borehole. Moisture content values established for various samples collected from AH-1 are presented in Table 3.3. As seen from the table, soil samples from a depth beyond 5 ft. (~150 cm) showed the significantly higher percent of moisture content compared to those from shallow depths. The moisture content in each layer was determined to reach a conclusion regarding possible source of moisture ingress. The moisture movement within the soil was not caused by the suction mechanism as the ground water table (GWT) was at more than 26 ft. (~793 cm) depth from the pavement surface. Therefore, moisture in pavement layer comes from other sources such as infiltration of rain water through the cracks in pavement and percolation from the drainage ditches etc. Similar data for other boreholes have been shown in Appendix B.

Table 3.3   Summary of Moisture Content for AH-1 (1 ft. = 30.5 cm)

S. No.	Sample Depth (ft.)	Moisture Content (%)	S. No.	Sample Depth (ft.)	Moisture Content (%)
1	1.0-2.0	7	6	7.0-9.3	70
2	2.0-2.5	6	7	9.5-11.8	74
3	2.5-4.0	8	8	14.5-16.8	72
4	4.7-5.5	64	9	19.5-21.8	69
5	6.1-6.3	70	10	24.3-24.5	57

3.7   Atterberg Limits Tests

Liquid Limit (LL) values have been linked to the expansive potential of soils. Soils with LL values greater than 60% are considered to be highly expansive (Holtz and Gibbs, 1956). Atterberg limit tests reveal properties related to consistency of the soil and can be used to establish the Liquid Limit (LL), Plastic Limit (PL) and Shrinkage Limit (SL) values. Upon addition of water, the state of soil changes progressively from dry, semisolid, plastic, and finally to liquid. The moisture content at the boundaries of these states are known as Shrinkage Limit (SL), Plastic Limit (PL) and Liquid Limit (LL), respectively (Lambe, 1960). The numerical difference between LL and PL values is known as Plasticity Index (PI) and characterizes the plasticity nature of the soil. Representative soil samples from the ten boreholes drilled in this study were tested for Atterberg limit values following the ASTM D 4318 (1994) test procedure.

A total of sixty eight (68) samples were tested from the ten boreholes to establish the variation in LL and PL values with depth. The LL values ranged from 29% to 164% while the PL values ranged from 20% to 75%. Atterberg limit values established for different samples collected from AH-1 are presented in Table 3.4. As seen from the Table

3.4, soil samples from a depth beyond 9 ft. (~275 cm) showed significantly higher LL and PI values compared to those from shallow depths. Similar data from other boreholes are presented in Appendix B.

Table 3.4   Summary of Atterberg Limits for AH-1 (1 ft. = 30.5 cm)

S. No	Sample Depth (ft.)	Liquid Limit (%)	Plastic Limit (%)	Plasticity Index (%)
1	1.0-2.0	60	35	25
2	2.0-2.5	60	35	25
3	2.5-4.0	60	35	25
4	4.7-5.5	60	35	25
5	6.1-6.3	89	54	35
6	7.0-9.3	89	54	35
7	9.5-11.8	148	54	94
8	14.5-16.8	139	59	80
9	19.5-21.8	138	63	75

3.7.1   Change in Liquid Limit Values with Depth

Figure 3.7 presents liquid limit profiles for AH-1 and AH-2 boreholes. It should be noted that the red dotted line in these plots indicates the cutoff LL between high and low swelling potentials. It can be observed from Figure 3.7 that soils from 2 ft. (~60 cm) to 5 ft. (~150 cm) depth had LL values close to 60 while soil samples obtained from depths greater than 5 ft. (~150 cm) showed LL higher than 60 for AH-1. Similar observations can be made for borehole AH-2 where the LL values were less than 60 up to a depth of 10 ft. (~305 cm) and greater than 60 after that. From these observations, it is clear that soils with higher swell potentials exist at much shallower depth at AH-1 than at

AH-2. This could be one of the reasons for pavement heaving at AH-1 while no heaving was observed at AH-2.
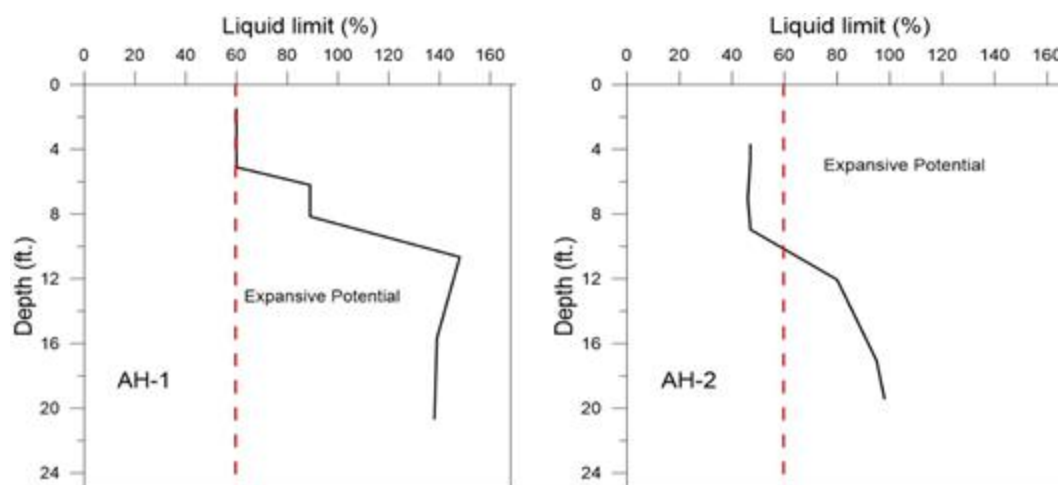
Figure 3.7 **Liquid Limit vs Depth for Boreholes AH-1 (left) and AH-2 (right) (1 ft. = 30.5 cm).**

Similar plots were generated for AH-3 through AH-10 and have been included in Appendix B. Similar phenomenon can be observed at AH-3 and AH-4 where high swelling soils were encountered at shallower depths at AH-3 to compare with AH-4. This again is reflective of the surface swelling observed at these borehole locations. Such contrast was not visible from the LL profiles with depth for AH-5 and AH-6; both soil profiles showed high swelling soils throughout. This is due to the fact that the heave in this area was spread wider than in the other locations, and hence neither borehole was located out of the heave zone. One notable difference between the profiles is that the LL values for AH-5 soils were as high as 160 at shallow depths while the highest LL value for AH-6 was around 90. High expansive soils were observed at depths starting at 6 ft. (~180 cm) and 5 ft. (~150 cm) for boreholes AH-7 and AH-8, respectively. Lastly, the LL profiles for boreholes AH-9 and AH-10, which were located outside the heaving area did not indicate the presence of any soil with high expansion potentials.

3.7.2   Using Liquidity Index (LI) Values to Establish Active-Zone Depths

As already mentioned in Chapter 2, Liquidity Index (LI) values, defined as

$LI = \dfrac{w - PL}{LL - PL}$, have been used by researchers in the past to identify the depth of active-

zones. Figure 3.8 presents typical LI vs. depth plots for AH-1 and AH-2 boreholes.

Similar plots for the remaining boreholes have been included in Appendix B.
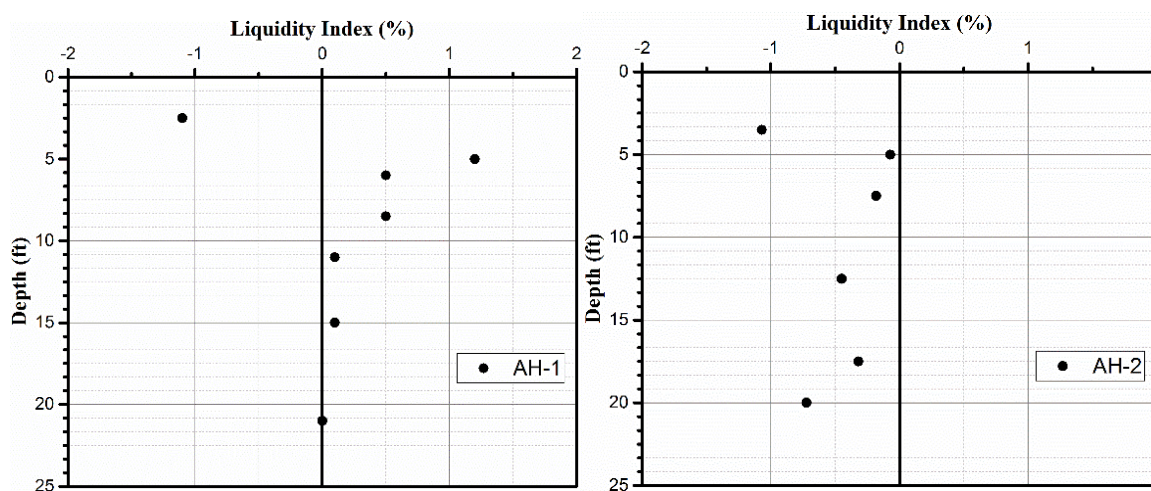
**Figure 3.8   Liquidity Index vs Depth for Boreholes AH-1 (left) and AH-2 (right)
(1 ft. = 30.5 cm)**

A Liquidity Index (LI) value, proposed by O'Neill and Poormoayed (1980), was

used to establish the active-zone depth using LI values from ten boreholes. However, this

profile requires the LI data to be obtained over several seasons. Seasonal variation in

liquidity index (LI) indicates the moisture fluctuation, which leads to shrink-swell

behavior in expansive soils. Based on the data obtained for the ten boreholes, a set of

moisture data were selected over different years (instead of seasons). The moisture data

corresponding to different years was extracted from past studies (Nottingham, 1985 and

1986; Hardcastle, 2003). Figure 3.9 shows that for depths greater than of 11 ft. (~335

cm), there is no significant change in moisture content across different seasons. This

indicates that the active-zone underneath this pavement section extends to a depth of least

11 ft. (~335 cm) from the pavement surface, and therefore most of the heaving likely

originates from the soil layers as deep as 11 ft. (~335 cm) from the pavement surface.

Accordingly, shallow stabilization treatment (often limited to 3 ft. or ~91 cm) may not be

suitable to remediate the recurrent pavement heave.
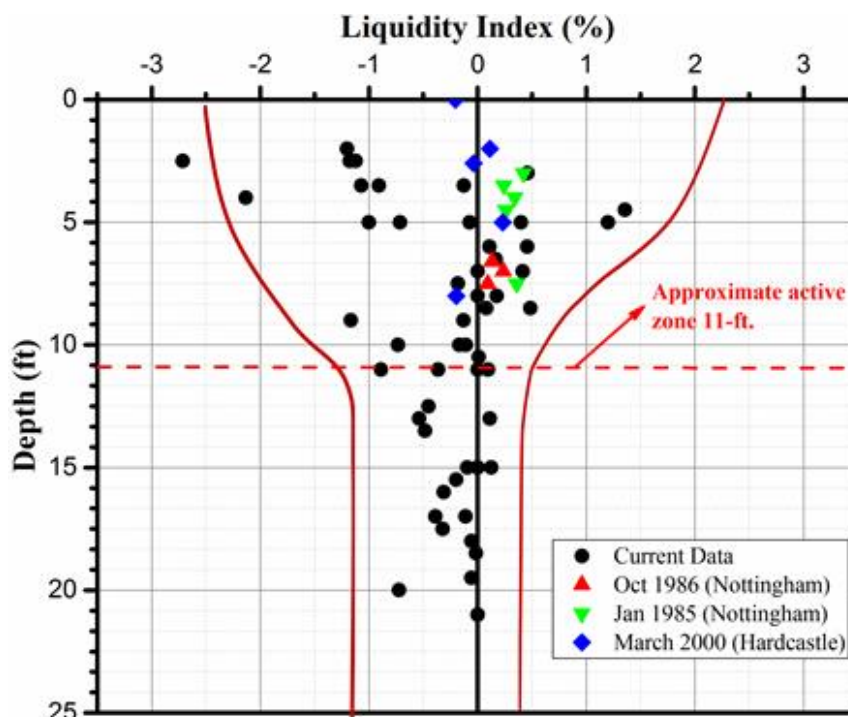
Figure 3.9   Determination of Active-Zone using Liquidity Index Profile (1 ft. = 30.5 cm)

Once the problematic zone was established by using liquidity index profiles, the

next task involved the Potential Vertical Rise Calculations (PVR) to define most

problematic pavement locations.

3.8   Potential Vertical Rise (PVR)

Potential Vertical Rise (PVR) is an index used to quantify the swelling potential

of a particular soil stratum. The PVR approach was developed in Texas Department of

Transportation (TxDOT) procedure Tex-124-E (TxDOT, 1999), and has been

successfully used to identify the swelling potential of soil layer underlying pavements.

The PVR originally developed by McDowell in 1956 (McDowell, 1956), and after that several modifications have undergone. Over the years (Lytton, 1977; Mitchell and Avalle, 1984; Gay, 1994; Jayatilaka, 1999) several other advanced methods to predict the swelling of expansive soil deposits have been developed. PVR tests in this research effort were performed based on the test procedure, TEX-124-E. It represents the simplest and most applicable method to predict the volume change in expansive soil deposits. In this procedure, the natural moisture content and the wet densities of each swelling soil layers are first determined from the core samples collected. The liquid limit (LL) and plasticity index (PI) values of each swelling layer are also used in this analysis to calculate the minimum (dry) and maximum possible moisture (wet) conditions in the respective soil layers. These moisture contents can be obtained by using the following empirical relations

$$\text{Dry moisture condition, } w_d = 0.2 \times LL + 9 \qquad \textbf{(3.1)}$$
$$\text{Wet moisture condition, } w_w = 0.47 \times LL + 2 \qquad \textbf{(3.2)}$$

Then the percentage free swell (swell under no load condition) is calculated using the following formula

$$Free \; swell \; (\%) = Volumetric \; change \; (\%) \times 1.07 + 2.6 \qquad \textbf{(3.3)}$$

Now, the PVR for a particular layer is calculated based on the following function

$$PVR = f \, (LL; PI; moisture \; content; percent \; soil \; binder) \textbf{(3.4)}$$

Once the PVR value for each layer has been calculated, the overall PVR value for the stratum is calculated by taking the cumulative value of the individual contributing layers (see Appendix B). PVR values have been linked to the ability of a soil layer to swell when subjected to moisture fluctuations at given moisture content, density and

loading conditions. The PVR values greater than 1 in. (2.54 cm) are considered to be problematic for U.S. highways, and hence remedial measures need to be adopted in such scenarios (Joyatilaka et al., 1993). Figure 3.10 compares the PVR values calculated for the 10 boreholes drilled during the current study. As shown in the figure, the PVR values of AH-1, AH-3, AH-5, AH-7, and AH-8 are higher than 1 in. (2.54 cm), and therefore the corresponding sections can be considered to be problematic. Borehole numbers AH-9 and AH-10 were located in non-heave zones, and PVR values were less than 1 in. (2.54 cm). The boreholes AH-2, AH-4, AH-6, and AH-8, were located adjacent to heave zone. However, as shown in Figure 3.10, the PVR value corresponding to AH-8 exceeds the threshold value of 1 in. (2.54 cm). This is indicative of high expansion potential. This can be directly related to the fact that the borehole AH-8 was not completely outside the heave zone (see Table 3.2) Figure 3.10 demonstrates that AH-1 recorded the highest PVR among all the boreholes. Supporting data for calculating the PVR is provided in Appendix B.
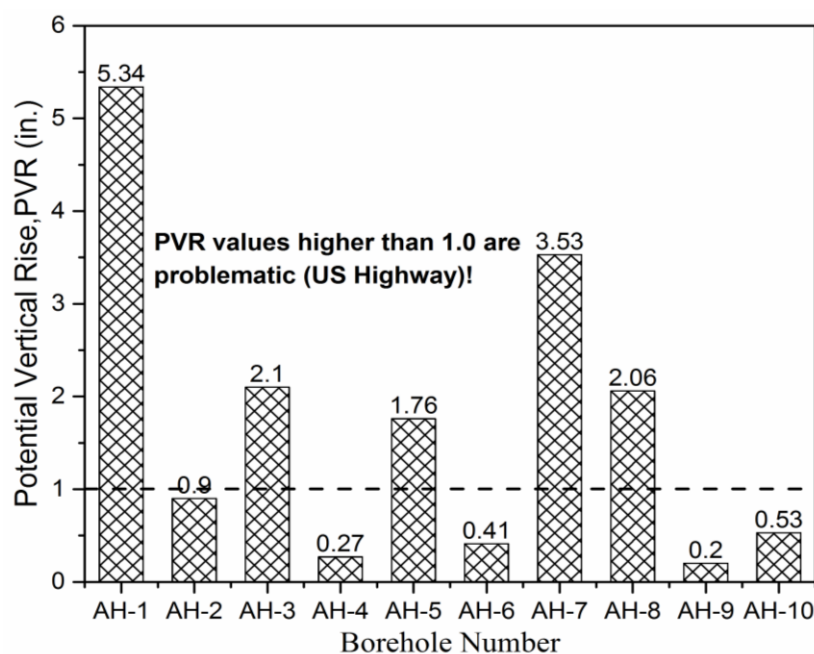
Figure 3.10   PVR Values for the 10 Boreholes (1 in. = 2.54 cm)

The laboratory tests results indicate that subgrade soil corresponding to this problematic section of US-95 is likely to be expansive. Figure 3.11 shows that soil samples from AH-1, AH-2, AH-3, AH-5, AH-6, AH-7 and AH-8 recorded higher LL values beyond the depth at 9 ft. (~275 cm), which corroborate the higher PVR values. This means that PVR values act as representative indicators for the likelihood of pavement surface heave. Primarily PVR assumes a condition that the soil stratum has unlimited access to moisture. But in the field, moisture access to a particular soil stratum depends on site conditions that do not correspond the assume condition for establishing the PVR value. Through PVR value in boreholes can not estimate the actual amount of surface heave, still it helps with the idea of most likely swelling prone locations.
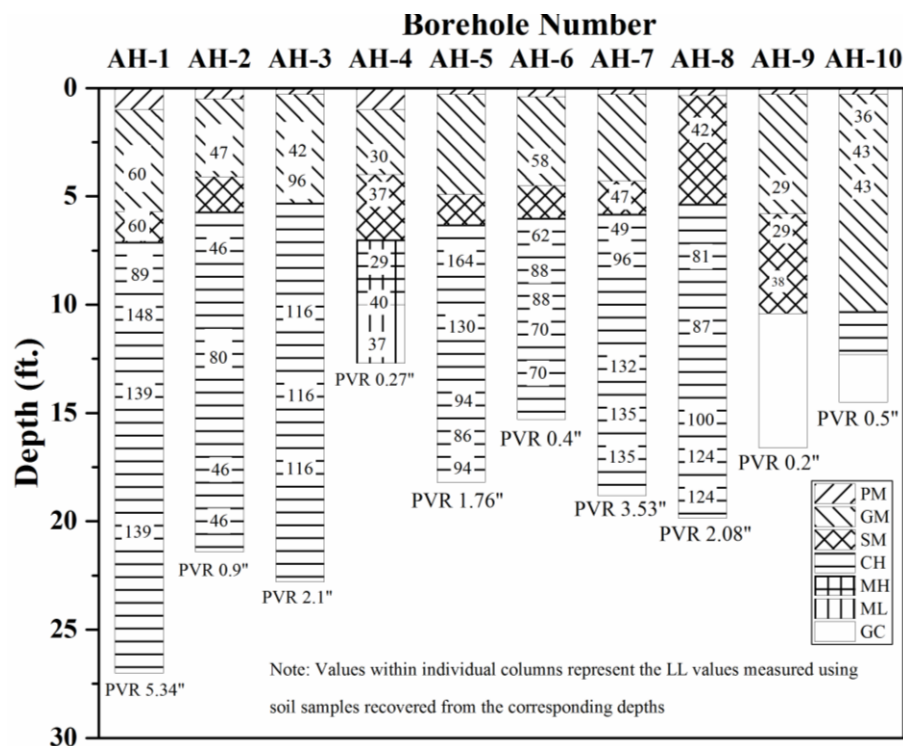
Figure 3.11   Established the Soil Profile, PVR, and LL for the 10 Boreholes (1 ft. = 30.5 cm)

Now, the next task was to evaluate the effectiveness of PVR values in estimating the surface heave by comparing with pavement surface roughness found from International Roughness Index (IRI).

3.9   Evaluating Pavement Surface Roughness using International Roughness Index (IRI) Values

As mentioned, one of the most common approaches to predict the vertical movement in pavements due to volume changes in underlying expansive soil layers involves the use of Potential Vertical Rise (PVR). However, the PVR value is calculated based on index properties of the soil layers and their respective locations within the pavement substructure. Therefore, the PVR value indicates the maximum "rise" that the pavement surface will undergo if the expansive soil layers had unlimited access to moisture. However, this may not be representative of actual conditions in the field. Therefore, it is necessary to evaluate the suitability of the PVR predictions with actual field observations. One common approach to quantifying the surface irregularity of pavement is by the use of the International Roughness Index (IRI). Developed at the International Road Roughness Experiment (IRRE) held in Brazil (Sayers, 1986) under the sponsorship of the World Bank, the IRI values has been adopted as a standard for the FHWA Highway Performance Monitoring System (HPMS) database. The IRI summarizes the longitudinal surface profile along the wheel path and is computed from surface elevation data collected by either a topographic survey or a mechanical profilometer. It is defined by the average rectified slope (ARS), which is a ratio of the accumulated suspension motion to the distance traveled obtained from a mathematical model of a standard quarter car transversing a measured profile at a speed of 50 mph (80

km/h). It is expressed in units of inches per mile (in/mile) or meters per kilometer (m/km).

IRI data for the problematic pavement section was obtained from ITD's automated pavement distress survey records. Exact locations of the boreholes were used to identify particular sections of the pavement where the IRI values could be treated as being representative heaves observed near the borehole locations. IRI information for the pavement section was extracted from the "Pathweb" website, a service provided by "Pathway Services" (pathweb.pathwayservices.com/Idaho). This website interface allows the user to identify exact segments of a particular highway to extract the corresponding IRI information. Figure 3.12 shows a screenshot of the "Pathweb" interface. As seen in Figure 3.12, the interface can generate plots of the IRI values for identified pavement segments. The latitude and longitude values for individual boreholes were used to extract the corresponding IRI values using the "Pathweb" interface. Another source for the IRI values was a spreadsheet obtained from ITD that lists IRI values along a particular pavement section based on latitude and longitude values. As some discrepancy between the two data sources was observed (possibly due to different years of data collection), this study used both data sources to map the IRI values along the section of highway being investigated. Note that IRI= 0 indicates a perfectly flat driving surface; there is no theoretical upper limit to the IRI value.

Figure 3.12   Photograph Showing Pathweb (a) IRI Graph (b) Image Control

Table 3.5 presents the IRI values corresponding to each of the borehole locations, as obtained from the "Pathweb" interface as well as the spreadsheet provided by ITD. From the Table 3.5, it can clearly be seen that AH-9 and AH-10 correspond to significantly lower IRI values when compared to the other eight boreholes. This observation is directly in-line with the PVR trends observed for the ten boreholes. In an effort to compare the PVR values with the pavement surface roughness trends observed in the field, Figure 3.13 shows both the PVR as well as IRI trends for the ten boreholes. As seen in Figure 3.13, the PVR and IRI trends closely match with each other. For example, AH-1 corresponds to the highest PVR and IRI values, whereas the values for AH-9 are the lowest. This clearly indicates that the PVR trends established using the laboratory test results can be matched with actual field-observed surface profile trends to an acceptable limit. Therefore, PVR values for the boreholes can be reasonably assumed to be indicative of actual expansion potential for the soil layers at those locations.

Table 3.5 **Total Summary of IRI Values for the 10 Boreholes (North Bound)**

Borehole No.	Pathweb		Spreadsheet	
Direction: Increasing (North Bound)				
	Left IRI	Right IRI	Left IRI	Right IRI
AH-1	500	470	194	234
AH-2	300	500	304	218
AH-3	390	500	135	131
AH-4	390	500	135	131
AH-5	345	380	227	184
AH-6	345	445	227	184
AH-7	500	500	160	217
AH-8	500	500	200	225
AH-9	115	105	55	59
AH-10	220	240	66	68
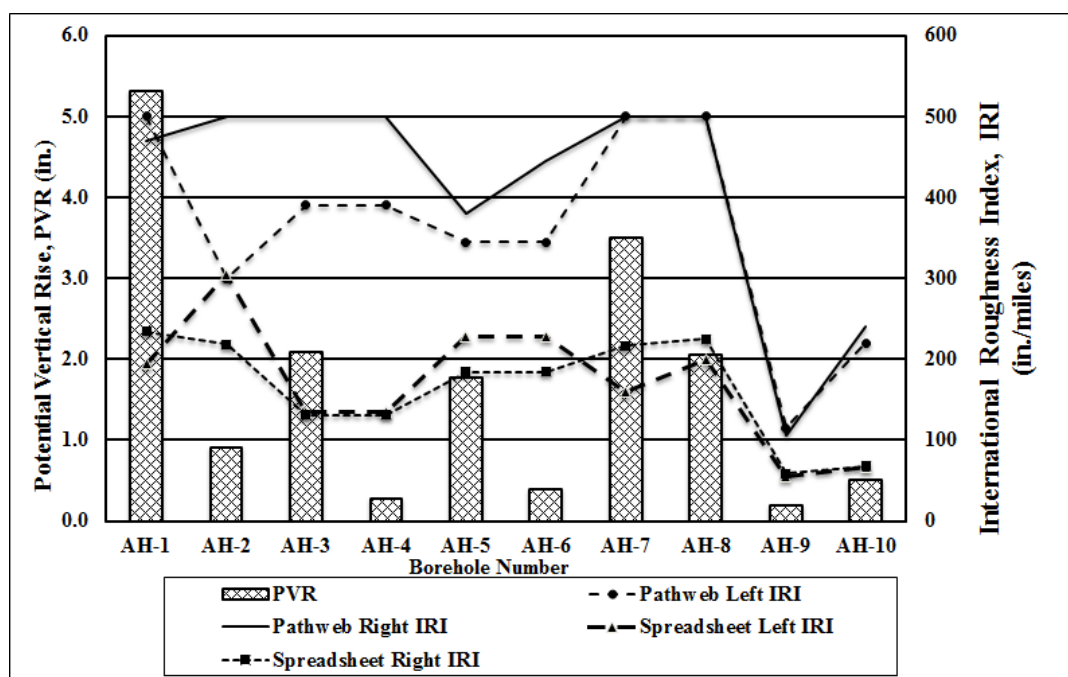
Figure 3.13 **Plot of Potential Vertical Rise (PVR) and International Roughness Index (IRI) Trends along the Problematic Section of US-95 being Investigated (North Bound; 1 in. = 2.54 cm)**

Once the PVR values for the different boreholes along with LL values established at different depths, the next task was to determine the amount of different clay minerals. This was carried out by conducting the chemical tests involving Specific Surface Area (SSA) tests, and Cation Exchange Capacity (CEC) tests.

3.10   Specific Surface Area (SSA) Tests

Specific Surface Area (SSA) of a soil sample is the total surface area contained in a unit mass of soil. This property is primarily dependent on the particle size of the soil. Soils with smaller particle sizes have higher specific surface areas. It should be noted here that soil particles with the high specific surface areas demonstrate high water holding capacity and greater swell potential.

The most commonly used method to establish the SSA of a soil sample comes from the field of agronomy and involves the adsorption of Ethylene Glycol Monoethyl Ether (EGME) (Carter et al., 1986). At the room temperature, EGME has a higher vapor than ethylene glycol, which allows the evaporation to take place more quickly. This method involves saturating prepared soil specimens, equilibrating them in vacuum over a Calcium Chloride – EGME ($CaCl_2$-EGME) solvate, and weighing to find the point when equilibrium is reached. Specific surface is then determined from the mass of retained EGME in comparison to the amount retained by pure montmorillonite clay, which is assumed to have a specific surface area of 4.15×10^6 ft^2/lb (850 m^2/g) (Carter et al., 1986). This test procedure typically takes two days to complete. This method was fully evaluated for geotechnical usage by Cerato and Lutenegger (2002), who concluded that the method is applied to a wide range of mineralogies, and is capable of determining specific surface area ranging from 2.4×10^4 to 4.15×10^6 ft^2/lb (5 to 850 m^2/g). They also

indicated that the procedure gives reliable results. Details of the procedural steps of this

method have been included in Appendix B. Typical SSA values for commonly observed

clay minerals were collected from the literature (see Table 3.6)

Table 3.6   Threshold Values of SSA for Pure Minerals (Cerato and Lutenegger, 2002) (1 ft^2/lb = 2.05× 10^{-4} m^2/g)

Mineral Type	SSA (ft^2/lb)
Illite	3.9×10^5- 6.1×10^5
Kaolinite	2.4×10^4- 2.2×10^5
Montmorillonite	2.9×10^6- 4.1×10^6

A total of sixty four (64) samples were tested from 10 the boreholes to determine

SSA values. The SSA values varied from 2.5×10^5 to 3.6×10^6 ft^2/lb (53 to 773 m^2/g).

SSA values established for different samples collected from AH-1 are presented in Table

3.7. As seen in Table 3.7, soil samples from a depth beyond 5 ft. (~150 cm) showed

significantly higher SSA values compared to those from shallow depths. This indicates

higher expansion potential for soil corresponding to depths greater than 5 ft. (~150 cm)

from the pavement surface. Similar data were established for AH-2 through AH-10, and

have been included in Appendix B.

Table 3.7   Summary of SSA for AH-1 (1 ft. =30.5 cm; 1 ft^2/lb = 2.05× 10^{-4} m^2/g)

S. No.	Sample Depth (ft.)	SSA (ft^2/lb)
1	1.0-2.0	2.5×10^5
2	2.5-4.0	2.1×10^5
3	4.7-5.5	2.7×10^6
4	6.1-6.3	2.9×10^6
5	9.5-11.8	3.5×10^6
6	14.5-16.8	3.6×10^6

3.11   Cation Exchange Capacity (CEC)

The cation exchange capacity (CEC) of soil is a measure of the quantity of readily exchangeable cations neutralizing negative charge in the soil. According to Camberato (2001), CEC refers to a number of negative charges in soil existing on the surfaces of clay and organic matter (see Figure 3.14).
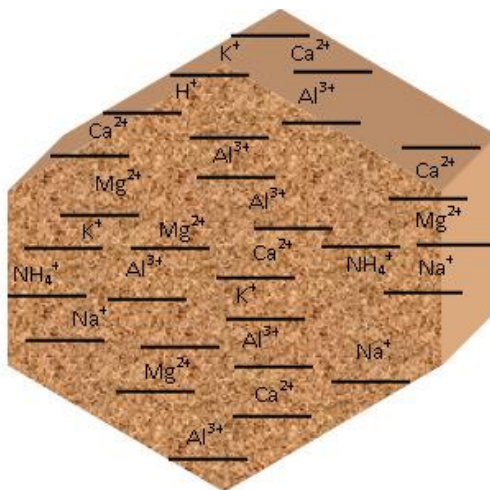
Figure 3.14   Schematic of a Clay Particle with Negative Surface Charge Attracting Various Cations (Camberato, 2001)

The positively charged ions or cations are attracted by negative charges, hence the name *Cation Exchange Capacity*. Soil CEC is normally expressed in units of charge per weight of soil. Two numerically equivalent sets of units are used: meq/0.22 lb (meq/100 g) (milliequivalents of charge per 0.22 lb or (100 g) of dry soil) or cmolc/lb (cmolc/kg) (centimoles of charge per lb (kg) of dry soil). CEC of soil can be defined as the capacity or the ability of the soil to exchange free cations that are available in the exchange locations. One of the most common methods to establish CEC was proposed by Chapman (1965) and has been used in this research.

CEC can be used to determine the mineral composition of the soil specimen with a high CEC value indicating a high amount of expansiveness due to the presence of the

clay mineral Montmorillonite where as a low CEC indicates the presence of non-expansive clay minerals such as Kaolinite and Illite. The isomorphorous substitution in Montmorillonite layer results in charge deficiency in clay particles which is responsible for the swelling behavior of the clay mineral. The method involves the addition of a saturating solution and then removal of the adsorbed cations using an extracting solution. The saturating solution used here is Ammonium Acetate (NH_4OAc) at pH 7. This solution is added to the prepared soil specimen (preparation involves treating for organics with 30% Hydrogen Peroxide (H_2O_2) and set aside for 16 hours after shaking for half hour, to ensure that all the exchange locations are occupied by the ammonium ion (NH^{4+})). Then the solution is filtered through a Buchner funnel and washed with 4 different 25 mL additions of NH_4OAc. This step is to bring out all the cations from the soil sample solution. Now, all the cation places are replaced by the ammonium ion, and excess ammonium is also removed. The CEC of the soil sample can be obtained by measuring a number of ammonium ions. This is done by washing the sample with 8 different 25 mL additions of 1M potassium chloride (KCl) solution. Though potassium ion (K^+) has similar electronegativity, it has higher molecular weight and has the ability to substitute the $NH4^+$ ion. The concentration the $NH4^+$ in the KCl extract gives the CEC of the soil. Details of the procedural steps of this method have been included in Appendix B. A total of sixty four (64) samples were tested from the 10 boreholes to determine CEC values. The CEC values varied from 0.9 to 2.5 meq/0.22 lb (404 to 1150 meq/100 g). CEC values established for different samples collected from AH-1 are presented in Table 3.8. Similar data for AH-2 through AH-10 has been included in Appendix B.

Table 3.8   Summary of CEC for AH-1 (1 ft. = 30.5 cm; 1 meq/0.22 lb=1meq/100 g)

S. No.	Sample Depth (ft.)	CEC, meq/0.22 lb Measured	S. No.	Sample Depth (ft.)	CEC, meq/0.22 lb Measured
1	1.0-2.0	0.90	4	6.1-6.3	1.92
2	2.5-4.0	0.96	5	9.5-11.8	2.0
3	4.7-5.5	622	6	14.5-16.8	2.1

As seen in Table 3.8, the CEC values obtained from laboratory testing were unnaturally high compared to typical CEC numbers for natural soils. This is due to the ammonium electrode used in this test that has interference with potassium from the potassium chloride solutions used in this test. An equation proposed by Yukselen and Kaya (2006), can be used to determine the CEC values from the LL and SSA values.

$$CEC = -0.33 \times LL + 0.44 \times SSA + 8.8 \qquad \textbf{(3.5)}$$

where LL is the Liquid Limit (%); CEC is the Cation Exchange Capacity, $meq/0.22\ lb$ ($meq/100\ g$); SSA is the Specific Surface Area, ft^2/lb (m^2/g). Table 3.9 presents the CEC data for borehole AH-1. For better characterization and understanding, it is desirable to have a comprehensive understanding of the soil mineralogy as well as volume change related characteristics of the soils. Clay minerals which typically cause soil volume changes are montmorillonites and some mixed layer minerals. Illite can be expansive, but generally, do not pose a significant problem. Kaolinite is normally non-expansive (Nelson and Miller, 1992). Table 3.9 also presents the percentage of Montmorillonite (%MM) mineral in the fines fraction of the soil. %MM is an indicator of high swelling nature of the soil. This percentage was obtained by using equation 3.6 which was developed by Chittoori (2008).

$$\%MM = -2.87 + 0.08 \times SSA + 2.66 \times CEC \qquad \textbf{(3.6)}$$

where %*MM* is the percentage by weight of the mineral montmorillonite in the fines

fraction of the soil. As seen in Table 3.9, soil samples from a depth beyond 6 ft. (~183

cm) showed significantly higher percentage of montmorillonite values compared to those

from shallow depths. Similar data from other boreholes are presented in Appendix B.

Table 3.9   Summary of Additional Chemical Testing for AH-1 Borehole

$(1 \text{ ft.} = 30.5 \text{ cm}; 1 \text{ ft}^2/\text{lb} = 2.05 \times 10^{-4} \text{ m}^2/\text{g}; 1 \text{ meq}/100 \text{ g} = 1 \text{ meq}/0.22 \text{ lb})$

S. No.	Sample Depth (ft.)	Liquid Limit (%)	SSA (m²/g)	CEC (meq/100 g) Measured	CEC (meq/100 g) Predicted	%MM in fines fraction (−#200) of the soil
1	2.5-4.0	60	53	411	6	2
2	4.7-5.5	60	43	435	172	78
3	6.1-6.3	89	457	622	184	86
4	9.5-11.8	148	512	875	167	82
5	14.5-16.8	139	517	905	175	85
6	19.5-21.8	138	530	950	150	74

Figure 3.15 shows a graphical representation of % MM vs. depth as established

by testing soil samples collected from the 10 boreholes. It can be observed that soil

samples from a depth beyond 6 ft. (~183 cm) showed significantly higher %MM values

compared to those from shallow depths. The percentage of MM indicated that the

problematic soil areas are located at a greater than 6 ft. (~183 cm) from the pavement

surface, and therefore most of the swelling likely originates from soil layers as deep as 6

ft. (~183 cm) from the pavement surface. Note that even for boreholes (e.g., AH-9 & AH-

10) that did not exhibit high Montmorillonite (%MM) contents, the expansive soil

deposits are often greater than 6 ft. (~183 cm) from the pavement surface.
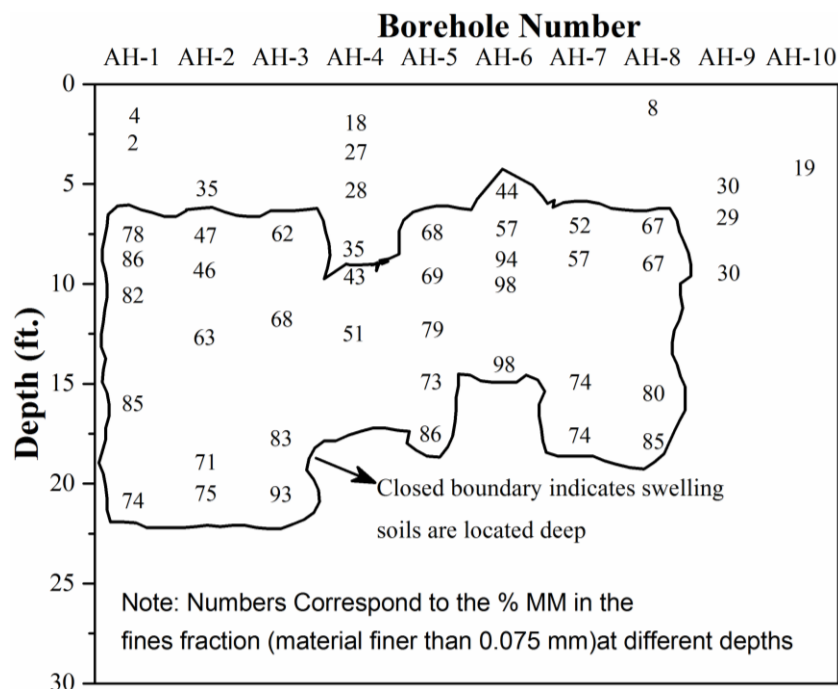
Figure 3.15   Established a Problematic Area of % MM for the 10 Boreholes (1 ft. = 30.5 cm).

After completion of the chemical tests, it is known that the high amount of montmorillonite leads the soil to be expansive in nature. But these approach cannot measure the actual amount of heave. To estimate the amount of heave in the laboratory, 1D swell test was performed.

3.12   1D Swell Test

1D swell tests for the soil specimens were performed in a conventional consolidometer setup in this study. The soil samples obtained from the field were carefully extracted, and placed in the consolidometer. Filter papers were then placed on top and bottom of the soil specimen. A pressure of 1 psi (6.89 kPa) was applied to the soil specimen prior to the start of testing. Once proper seating loading was used, and the LVDT (Linear Variable Differential Transformer) was positioned in place to monitor vertical soil deformation, the soil specimen was subjected to moisture inundation, which resulted in soil swelling with time. Once the soil sample had experienced the maximum

possible swelling, an oedometer test was conducted to establish the swell pressure of the soil. Once the specimen reached a maximum swelling point, loads were added in order to bring back the soil to its original position. The total load applied to the specimen to bring back to its original position was then used to calculate its *swell pressure*. Figure 3.16 presents photographs showing the 1D swell setup for this research.

2.5 in.

(a)   (b)   (c)
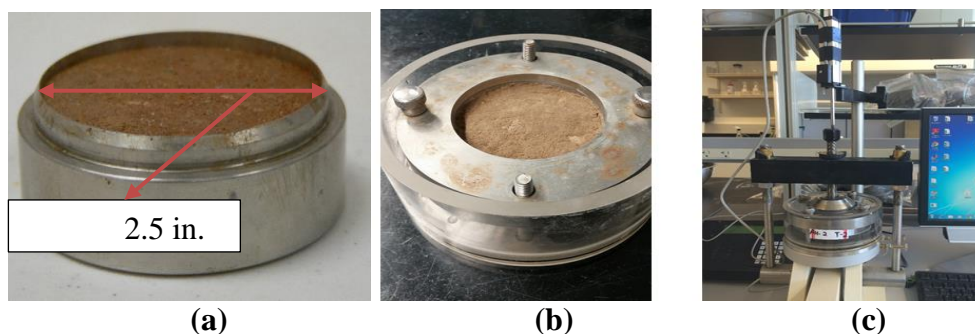
Figure 3.16   Photographs Showing 1D Swell Test Procedure (a) Extracted Soil Sample from the Field (b) Soil Sample in the Consolidation Mold (c) Fully Assembled 1D Swell Test Setup

A total of forty six (46) samples were tested from the ten boreholes to determine the swell pressure values. Swell pressure is defined as the pressure required to keep a soil element at constant volume when boundary conditions are such as to induce a tendency for volume change. Swell pressure is an important parameter for the design of structures interacting with swelling soils. Table 3.10 is a guide for estimating the probable volume change of expansive soils.

Table 3.10   Data for Making Estimate of Probable Volume Change for Expansive Soils (Recreated from Source: Nelson and Miller, 1992) (1 psi = 6.89 kPa)

Swelling Pressure, psi	Degree of Expansion
>138	Very High
34-138	High
20-34	Medium
< 20	Low

Figure 3.17 presents the swell pressure data for the samples that underwent swelling and demonstrates that AH-1 recorded highest swelling pressure 24.4 psi (~168 kPa) while AH-2 experienced swell pressure only 10.4 psi (71.65 kPa). This data showed low to medium swelling in boreholes that recorded high PVR values further corroborating the field observations. The maximum swell pressure (24.4 psi or ~168 kPa) was measured for AH-1, followed by AH-7 (17.4 psi or ~120 kPa), AH-2 (10.4 psi or ~72 kPa) , AH-4 (10.4 psi or ~72 kPa), AH-8 (10.4 psi or ~72 kPa) and AH-5 (3.5 psi or ~24 kPa). Note that no significant swell pressure values were measured for samples from boreholes AH-3, AH-6, AH-9, and AH-10. Only four boreholes (AH-1, AH-2, AH-3, and AH-7) have potential swelling characteristics as the swelling pressure is higher than overburden pressure at these locations as shown in Table 3.11.
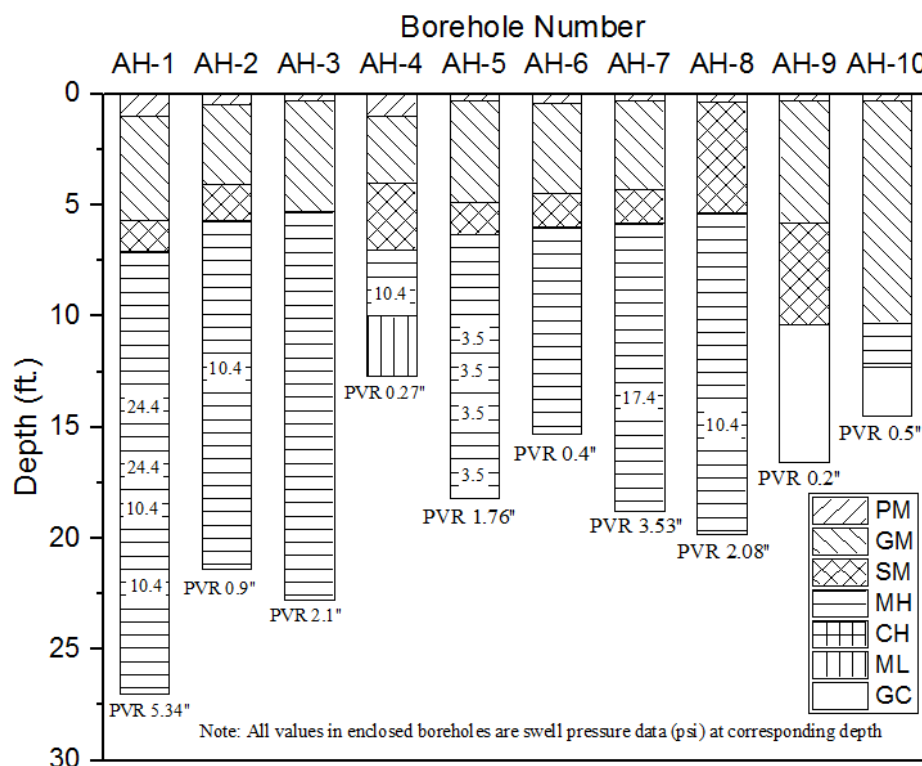
Figure 3.17   Established the Soil Profile, PVR and Swell Pressure for the 10 Boreholes (1 ft. = 30.5 cm; 1 psi = 6.89 kPa)

**Table 3.11   Summary of Swell Pressure and Overburden Pressure for the
Boreholes (1ft. = 30.5 cm; 1 psi = 6.89 kPa)**

Borehole Number	Depth (ft.)	Swell Pressure (psi)	Overburden Pressure (psi)	Swelling Potentiality/Remarks (Y/N)
AH-1	13	24.4	9.8	Y
	16	24.4	12	Y
	18	10.4	13	N
	22	10.4	14	N
AH-2	12	10.4	8.6	Y
AH-4	8	10.4	7.7	Y
AH-5	10	3.5	7.4	N
	13	3.5	8.6	N
	16	3.5	10.8	N
	18	3.5	12	N
AH-7	13	17.4	9.6	Y
AH-8	16	10.4	10.8	N

After establishing the swelling potentiality with the measuring of swelling

pressure exerted by the different boreholes along with the overburden pressure values at

different depths, the next task was to identify the locations having a significant amount of

sulfates presence. By knowing any case having sulfates in soils, the effectiveness of

calcium-based stabilizers was work out with the fact of the probability of forming

Ettringite and Thaumasite minerals. These minerals have a significant amount of swelling

potential.

3.13   Soluble-Sulfate Content

Soluble-sulfate measurement in subgrade soils is an integral part of geotechnical investigations due primarily to sulfate-induced heave distress problems experienced by certain chemically treated sulfate soils. Sulfate measurements can assist engineers in the selection of appropriate soil stabilization methods in construction projects (Puppala et al., 2002). Therefore, it is very important to evaluate sulfate content in a particular soil stratum prior to deciding on the type of chemical stabilization.

There are no ASTM Standards that provide specifications for determining the sulfate content in soils. Current methods, including the University of Texas at Arlington (UTA) method are based on gravimetric procedures and often provide test results with high standard deviations. A modified UTA method, which was developed by addressing the limitations of the earlier methods (Puppala et al., 2002). The AASHTO T-290 method also describes a similar procedure outlined by Puppala et al., (2002).

The test procedure consists of taking 0.022 lbs (10 grams) of dried soil and diluting with 100 mL of distilled water. This solution is shaken on an Eberbach shaker for thirty minutes (see Appendix B). After the shaking, the extraction of the solution is obtained by centrifuging at a speed of roughly 14,000 rpm. The pH values of the solution are controlled within the range of 5 to 7 with the help of Hydrochloric acid. The extracted solution is kept on a hot plate until it starts boiling. Barium Chloride ($BaCl_2$) is then added to the boiling solution to bring out sulfate in the form of Barite ($BaSO_4$). The solution is then placed in an 85°C oven for 12 hours to continue the digestion process in which precipitation takes place to obtain Barite by the gravimetric process. The barite precipitated from this process, is used in the calculations to obtain the soluble sulfate

content in the soil samples. A total of forty two (42) samples were tested from the ten

boreholes to determine the sulfate content in soils. The sulfate content values ranged from

450 to 3366 ppm. Soluble sulfate values established for different samples collected from

AH-1 are presented in Table 3.12. As seen from the Table 3.12, soil samples from a depth

beyond 9 ft. (~275 cm) showed slightly higher sulfate content values compared to those

from shallow depths. Similar data from other boreholes are presented in Appendix B.

Table 3.12   Summary of Soluble Sulfate Test for AH-1 (1 ft. = 30.5 cm)

S. No.	Sample Depth (ft.)	Soluble sulfate content (ppm) in samples	S. No.	Sample Depth (ft.)	Soluble sulfate content (ppm) in samples
1	4.0-4.7	1500	5	11.8-12	1900
2	4.7-5.5	1200	6	14.5-16.8	1900
3	6.1-6.3	1300	7	19.5-21.8	1900
4	9.5-11.8	1900	-	-	-

Soluble-sulfate content values have been linked to the formation of high swelling

minerals like Ettringite and Thaumasite when treated with calcium-based stabilizers such

as lime and cement. Hayes (2007) prescribed some threshold values for soils to be

classified by sulfate contents, and have been listed in Table 3.13.

Table 3.13   Threshold Values for the Classification of Soils by Sulfate Content (Hayes, 2007)

Relative Degree of Sulfate Attack	Sulfate in Water Samples (ppm)
Negligible	0 -150
Positive	150 -1,000
Considerable	1,000 – 2,000
Severe	>2,000

Sulfate content levels greater than 2000 ppm are considered to be indicative of severe sulfate attack related problems (Hayes, 2007). Figure 3.18 shows the variation in sulfate content with depth for soil samples collected for boreholes AH-1 and AH-2. As seen from the figure, soil samples from a depth beyond 5 ft. (~150 cm) showed sulfate content values higher than 2000 ppm for borehole AH-2, therefore classified as "sever" sulfate attack. For borehole AH-1 exhibited sulfate content values up to 1900 ppm of depth 4 ft. (~120 cm) to 12 ft. (~360 cm). According to the Table 3.13, borehole AH-1 classified as "considerable" sulfate attack. From this observation, it is clear that soils with a high chance of sulfate attack were observed at much shallower depth for AH-2 when compared to AH-1. This means the soil at AH-2 is more susceptible to detrimental swelling due to the formation of Ettringite (a swelling mineral) when subjected to stabilization methods such as through the use of lime or cement.
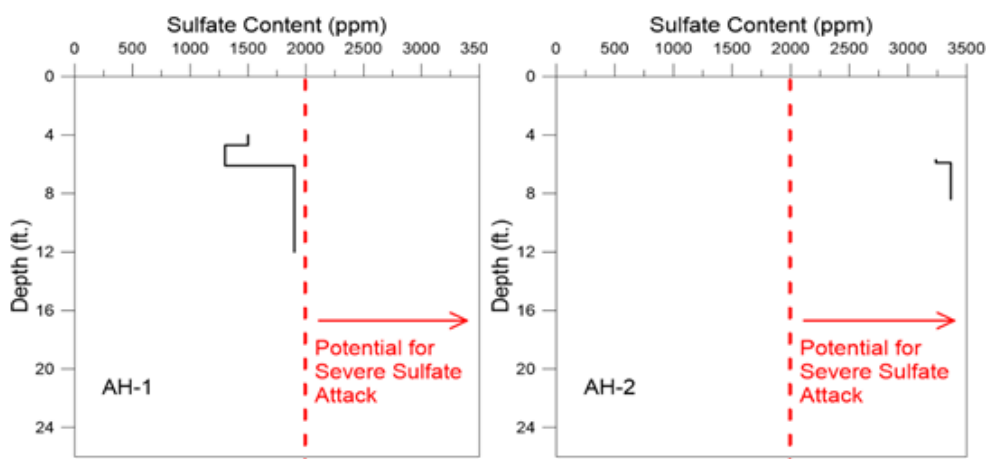
Figure 3.18   Sulfate content vs. Depth for boreholes AH-1 and AH-2

(1 ft. = 30.5 cm)

Similar plots were generated for AH-3 through AH-10, and have been included in Appendix B. Based on the results, the soils corresponding to individual boreholes were ranked in terms of their susceptibility to sulfate attack. Table 3.14 lists the likelihood of

sulfate attack for different boreholes. As seen in Table 3.14, all soils will not pose problems related to the formation of high-swelling minerals upon treatment using calcium-based stabilizers. The test results revealed that soil samples from four boreholes (AH-2, AH-5, AH-7, and AH-8) contained sulfates greater than 2000 ppm and hence may pose problems related to severe sulfate attack. Table 3.14 lists the PVR values for all the ten boreholes along with the corresponding likelihood of sulfate attack, when subjected to stabilization using calcium-based additives.

Table 3.14   Comparisons with PVR and Possible Sulfate Attack (1 in. = 2.54 cm)

Sample ID	Relative Degree of Sulfate Attack	PVR (in.)	Sample ID	Relative Degree of Sulfate Attack	PVR (in.)
AH-1	Considerable	5.34	AH-6	Positive	0.41
AH-2	Severe	0.9	AH-7	Severe	3.53
AH-3	Considerable	2.1	AH-8	Severe	2.06
AH-4	Positive	0.27	AH-9	Positive	0.2
AH-5	Severe	1.76	AH-10	Positive	0.53

As seen in Table 3.14, it can be observed that locations that exhibited high PVR values also corresponded to soil samples with a high likelihood of sulfate attack (e.g., AH-1, AH-2, AH-3, AH-5, AH-7 and AH-8). This means calcium-based stabilization is not suitable for this problematic pavement section. Note that even for boreholes that did not exhibit high sulfate contents, the expansive soil deposits are often at depths greater than 5 ft. (~150 cm) from the pavement surface. Accordingly, even if sulfate related swelling is not an issue, for these locations, chemical stabilization is not economical.

3.14   Inferences Based on Laboratory Test Results

The following inferences can be drawn based on laboratory tests conducted in this study:

1.   Moisture content tests established that the moisture movement within the soil was not caused by the suction mechanism as the ground water table (GWT) was at more than 26 ft. (~793 cm) depth from the pavement surface. Therefore, moisture in pavement layer comes from other sources such as infiltration of rain water through the cracks in pavement and percolation from the drainage ditches etc.

2.   The Atterberg limit values indicated that the soil layers corresponding to most boreholes (except for AH-4, AH-9, and AH-10) likely to be expansive at depths greater than 6 ft. (~183 cm) from the pavement surface. Accordingly, shallow stabilization was ruled out.

3.   Liquidity Index (LI) calculations indicated that the active-zone extended to a depth of at least 11 ft. (~335 cm) from the pavement surface, and therefore, most of the heaving likely originates from soil layers as deep as 11 ft. (~335 cm) from the pavement surface.

4.   The PVR values of AH-1, AH-3, AH-5, AH-7, and AH-8 greater than 1 in. (2.54 cm) are considered to be problematic for a road U.S. highways. Result also demonstrated that AH-1 recorded the highest PVR among all the boreholes.

5.   Investigation of pavement roughness profiles using International Roughness Index (IRI) values corroborated trends predicted form Potential Vertical Rise (PVR) calculations.

6. Clay mineralogy tests indicated the presence of high amounts of Montmorillonite that can lead to significant volume changes.

7. The 1D swell test indicated that only four boreholes (AH-1, AH-2, AH-3, and AH-7) had potential swelling characteristics as the swelling pressure was higher than overburden pressure at these locations.

8. Soluble sulfate content tests indicated that soils from several of the boreholes were susceptible to high levels of sulfate attack. Accordingly, stabilization using Calcium-based additives such as cement or lime may not be feasible.

Based on findings from the laboratory testing, it can be concluded that traditional rehabilitation measures such as chemical stabilization, soil removal and replacement or shallow treatment alternatives (often limited to 3 ft. or ~91 cm) are not likely to be successful in mitigating the recurrent differential heave problems. Due to the fact that expansive soil extends to significant depths below the pavement surface, any installation of moisture barriers (horizontal or vertical) is likely to be very expansive. Therefore, remedial measures that can mechanically dissipate the stresses generated due to volume changes in the underlying expansive soil deposits may be more appropriate. One such alternative is to use a geosynthetic system that is strong enough to support the traffic induced-stressess, and at the same time is flexible enough to subgrade-generated swell pressures.

3.15   Summary

This chapter presented a detailed background of the problematic pavement section. The laboratory test matrix developed for extensive characterization of soil samples collected from the problematic pavement section was presented. Subsequently, a

summary of the laboratory procedures, apparatus used, and results were discussed, and interferences were drawn concerning the mechanisms contributing to the current pavement damage.

The next chapter (Chapter 4) of this document will present the development of candidate remedial measures within the scope of this Master's Thesis.

CHAPTER 4:   DEVELOPMENT OF CANDIDATE REMEDIAL MEASURES

4.1   Introduction

As mentioned in Chapter 3, ten different boreholes were strategically drilled at different locations along the problematic pavement section, and soil samples were collected for extensive laboratory testing. Different physical, mechanical, and chemical tests conducted on the soil samples established that the problematic soil layers were deep within the subgrade, and therefore, traditional rehabilitation measures such as shallow stabilization, or soil removal and replacement are not likely to address the root cause of the problem. Therefore, one potential solution for the heaving problem of this pavement section is to use a flexible mechanical system that nullifies the expansion coming from the underlying clay layers and protects the pavement structure. One such alternative is to use a geosynthetic system that is strong enough to support the pavement structure and flexible enough to dissipate the expansive swelling that results in minimal differential surficial heaving. Several researchers have conducted studies on the potential benefits of geosynthetics in flexible pavement systems through laboratory, field, and finite element methods (Barksdale et al., 1989; Al-Qadi et al., 1997; Berg et al., 2000; Saad et al., 2006; Al-Qadi et al., 2008). The geosynthetic reinforcement system considered in this study involved geocells placed within the granular base layer. Numerical models, using finite-element method (FEM) simulations, have been proven to be more accurate in depicting practical conditions more realistically than theoretical or analytical solutions based on the infinite slab and other idealized assumptions (Kuo and Huang, 2006).

4.2   Finite-Element Modeling of Flexible Pavement Section

In recent decades, the finite-element method has become a popular alternative to traditional analysis methods in geotechnical engineering (Wanstreet, 2007; Bortz, 2015). Proper use of the finite element method in the solution of boundary value problems requires sound knowledge relating to element size, aspect ratio, and material properties. For simulation of swell-related soil movements involving partially saturated soils, various advanced soil models that account for soil matric suction changes, volume changes of soils from moisture content fluctuations, and soil shear strength variations are needed. Such analysis can be more challenging, particularly when the simulation involves a multi-layer system such as a pavement section. Commercially available software, ABAQUS® (Simulia, 2016), has built-in material models that can be used to simulate shrink and swell behaviors of expansive soils by accounting for moisture content and suction related changes. Parameters for these models can be established through commonly used geotechnical tests.

4.3   Establish Material Properties for Input into the Numerical Models

As mentioned in Chapter 3, ten boreholes were strategically placed on and off heave zones along the pavement section, and soil samples were collected for laboratory testing and subsurface characterization. To establish relevant soil parameters to be used as inputs during numerical modeling of the pavement sections, additional soil samples were collected from two boreholes: AH-11 and AH-12. AH-11 was located near AH-1 (laboratory results exhibited highest heave potential), and AH-12 was located close to the pavement section reconstructed in the past incorporating moisture barriers (Hardcastle, 2003). Accordingly, soil samples obtained from the AH-11 and AH-12 boreholes were

tested to establish relevant swell-related parameters. Tests performed on these samples established liquid limit values in excess of 153% and plasticity index values greater than 87%, thus establishing the expansive potential for soil samples from both boreholes. The Optimum Moisture Content (OMC) and Maximum Dry Density (MDD) values for the soil obtained from these two boreholes were established in the laboratory (see Appendix B). Both the boreholes exhibited MDD values of approximately 64 lb/ft^3 (~1021 kN/m^3) and OMC values of ~30%. In addition, two other tests were conducted to establish the soil suction and volumetric strain properties: (1) soil suction, and (2) volumetric swell strain. A summary of the laboratory procedures, apparatus used, and results are presented in the following subsections.

4.2.1   Soil Suction Measurement

The variation of water or moisture affinity for soil is better represented by the soil water characteristic curve (SWCC). The SWCC of a given soil defines the relationship between the water content and soil suction. In engineering practice, soil suction is composed of two components: (1) matric suction, and (2) osmotic suction. Matric suction comes from the capillarity, texture, and surface adsorption forces of the soil. The osmotic suction, on the other hand, reflects the effect of dissolved salts in the pore fluid (Bulut et. al., 2001). In this research, soil suction was determined using the ASTM D 5298 test procedure. This method uses a calibration curve to infer both total suction (matric suction + osmotic suction) and matric suction measurements. This calibration curve is a combination of both wetting and drying curves. Per the ASTM D 5298 test procedure, soil samples were prepared at the constant density and varying moisture contents. Sample dimensions used in this research were 3 in. (~76 mm) diameter and 6 in. (~152 mm) high.

Whatman#42 (diameter 2 in. or 50.8 mm) ashless filter paper was used to determine the suction of the soil. Matric suction was determined by placing a filter paper sandwiched between two protective filter papers and placed between the two halves of the soil sample that was previously cut. This allowed the sandwiched filter paper to be in physical contact with the soil sample and yet not be contaminated with the soil. The two halves of the soil sample were then taped to seal the filter papers inside the soil sample. The taped sample was placed inside a glass jar, and another filter paper was placed on top of the sample. This filter paper was not allowed to touch the soil sample, and hence a 1-in. (25.4-mm) thick Polyvinyl Chloride (PVC) pipe was used as a separator between the soil sample and the filter paper. The glass jar was then sealed and placed inside a temperature-controlled chamber for one week. After equilibrium conditions were achieved, wet filter papers were removed from the samples, and their moisture contents were determined. It should be noted here that filter papers must be handled carefully to avoid external moisture effect. Suction values were then obtained from the calibration curve. The total and matric suction values were determined from the calibration curves for the Whatman#42 filter paper as given in ASTM 5298 test procedure. Figure 4.1 shows photographs of different steps during the process of suction measurement using the filter paper method. SWCCs were established by plotting the moisture contents at which the samples were prepared versus the total and matric suction values determined. Figure 4.2 presents the SWCC curves obtained for both AH-11 and AH-12 Soils.

Figure 4.1 **(a) Matric Suction (left) and Total Suction (right) Measurements**
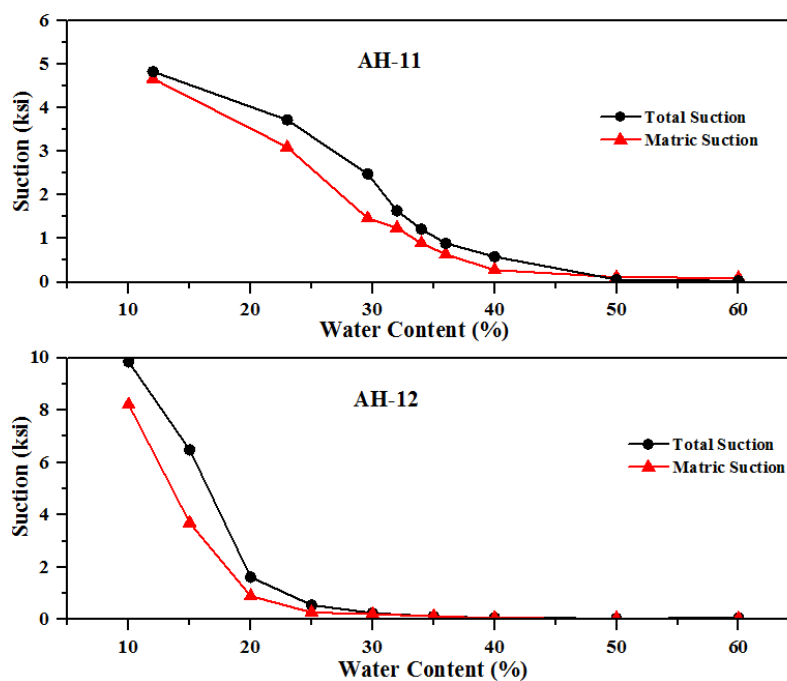
Figure 4.2 **SWCC for Boreholes AH-11 and AH-12 (1 ksi = 6.89 MPa)**

4.2.2   Volumetric Swell Strain Test

Developed by the researchers at The University of Texas at Arlington (UTA), a three-dimensional free swell test provides a reasonable representation of the soil maximum volumetric swell potential (Punthutaecha et al., 2006). This test was conducted to investigate the maximum vertical, radial and volumetric swell potentials of the soils from AH-11 and AH-12.

In this method, 3 in. (~76 mm) diameter and 6 in. (~152 mm) high soil samples were prepared at OMC and MDD conditions. The soil samples were then placed in the oven for 14-20 hours. The dried samples were submerged under water to allow for swelling to occur. Porous stones were placed at the top and bottom of the samples to facilitate water ingress from top and bottom of the soil sample. The soil sample was covered with a latex membrane to avoid surficial erosion. Figure 4.3 shows photographs of this test in progress. Both vertical and radial swell movements were measured at various time by using 'dial gauge' and 'Pi tape' (Figure 4.3), respectively. Vertical and radial swell strains were monitored until there was no further swell and equilibrium conditions were reached. All tests were conducted at room temperature.

In addition, the moisture changes in the sample were also monitored by measuring the sample weight and swell strains at12 hour intervals. It was assumed that the increase in sample weight was primarily due to water absorption and that there was no soil loss during this process.

| (a) | (b) |
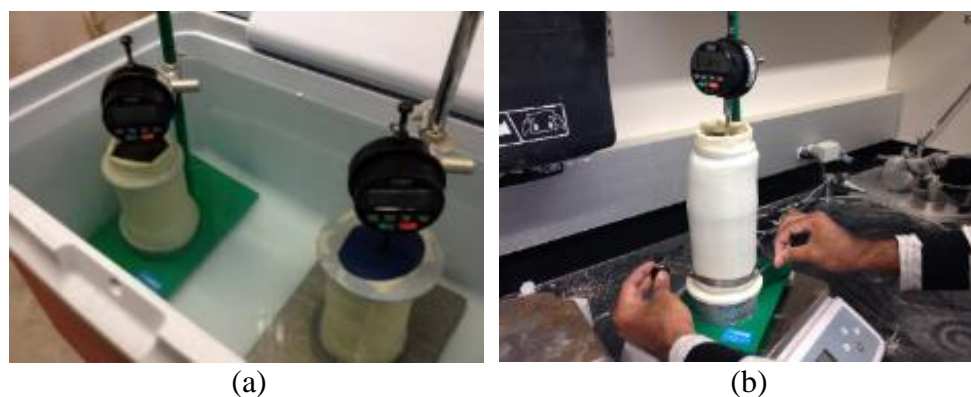
Figure 4.3   (a) Inundation of Soil Sample in Water Bath; (b) Measurement of Radial Swell using "Pi Tape."

Soil samples obtained from AH-11 required approximately 430 hours to reach equilibrium, while AH-12 soil samples reached equilibrium in 140 hours. This indicates

higher permeability for AH-12 soil samples compared to those from AH-11. Typical

swell characteristic graphs are shown in Figure 4.4, which illustrate a maximum 64% and

48% volume increase due to swelling for the AH 11 and AH 12 samples, respectively.

Volumetric swell and suction characteristics established for the two soil types were used

as material inputs during the numerical modeling effort.
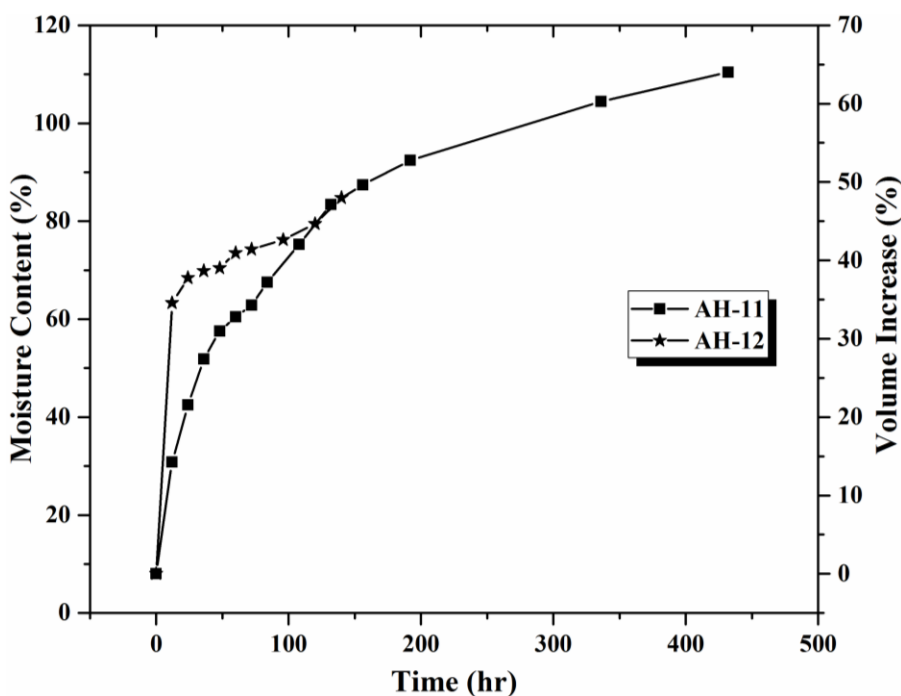
Figure 4.4   Volumetric Swelling of Boreholes AH-11 and AH-12

4.4   Overview of the Model Details

The first steps in the numerical modeling effort involved establishing (1) the

model geometry, (2) material properties, and (3) boundary conditions to adequately

represent the system being analyzed. The model geometry was established through field

visits, boring logs, surveying records, and pavement construction history data. Laboratory

characterization of field-collected soil samples helped establish the material properties to

be used in the numerical models.

4.4.1   Geometry and Cross Section

A typical pavement section comprises a 6-in (~15-cm) thick Hot-Mix Asphalt (HMA) section overlying a 54-in (~137-cm) thick unbound granular base layer overlying the subgrade layer. To overcome infinite boundary effects, Kim et al., (2009) suggested that vertical and horizontal direction should be considered 140 and 20 times the wheel loading radius, respectively. The subgrade was assigned a thickness of 162 in. (~411 cm) after the several analysis because there was not any wheel loading configuration involve in this model. Only shrink-swell behavior was considered defining a finite boundary for the model and eliminating boundary effects. There was also an 18-in (~46-cm) thick lime stabilized soil layer in between the base and subgrade, which was constructed during past stabilization efforts (see Figure 4.5).
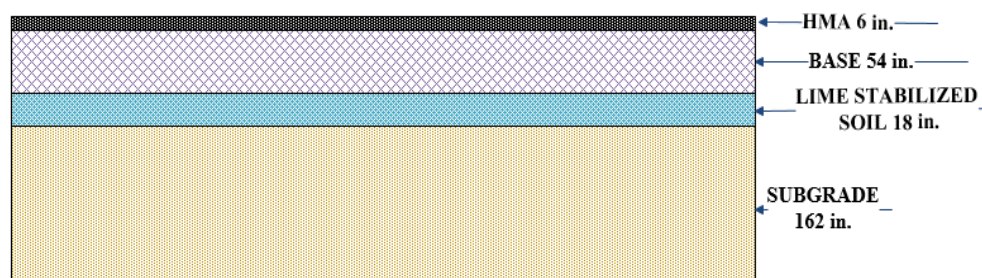
Figure 4.5   Schematic Representation of the Modeled Control Section (1 in. = 2.54 cm)

4.4.2   Selection of 3D Model Geometry

A 266-ft. (~81-m) long and 90.5-ft. (~28-m) wide section was initially modeled. These dimensions included three driving lanes (each lane 144 in. or ~4 m wide), two paved shoulders (138 in. or ~4 m) and clearance for boundary effects as shown in Figure 4.7. The clearance for boundary effects was optimized of 21.5 ft. (~7 m) after several trial analyses. This distance was provided to minimize the effects of boundary conditions on pavement heaving. The length of the pavement was selected to match the distance

between boreholes AH-1 and AH-2 in the field and was separated by a distance of 223 ft.

(~70 m) (see Figure 4.6).
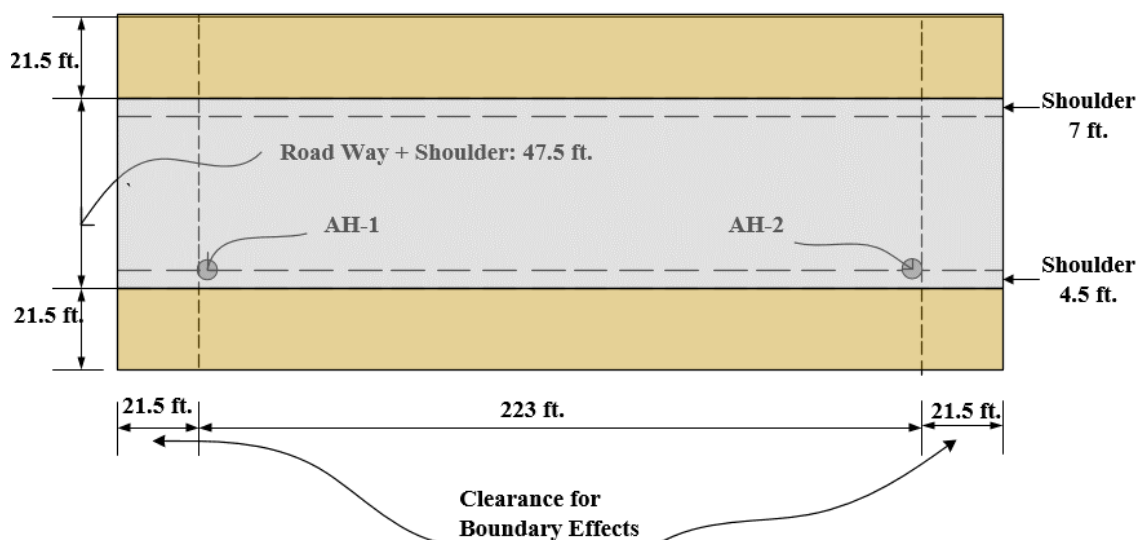
Figure 4.6   Schematic Top View of the Modeled Control Section (1 ft. = 0.305 m)
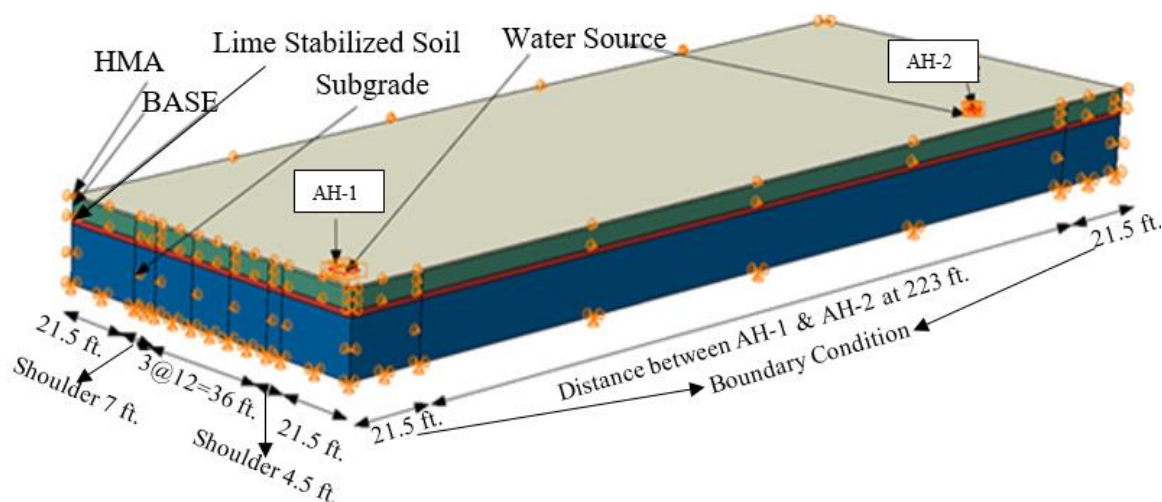
Figure 4.7   Isometric View of the Modeled Control Section (1 ft. = 0.305 m)

4.4.3   Material Properties

Different materials involved in the model were HMA, unbound granular base,

lime stabilized soil, and expansive subgrade. In this study, HMA was modeled as a linear

elastic material while the unbound granular base, lime stabilized soil and the expansive

subgrade were modeled as elastoplastic materials. The soil element, when subjected to

swelling, will undergo volumetric changes caused by absorbing water. This element is not expected to either fail or yield during the swelling period. The resilient modulus of subgrade soils was obtained from laboratory test results which were conducted by Boudreau Engineering, Inc. The material properties used to model each of these materials are listed in Table 4.1. These properties were obtained from various literature and are typical for pavement sections involving geosynthetic treatments.

Table 4.1   Engineering properties of pavement layers used in the model

Properties	HMA	Base	Lime-Stabilized Soil	Expansive Subgrade
Mass Density, ρ lb/ft^3 (kg/m^3)	148 (2390)	137 (2200)	62 (1020)	62 (1020)
Elastic Modulus, E, ksi (MPa)	400 (2756)	43.5 (300)	29 (200)	2.12 (14.6)
Poisson's Ratio, ν	0.3	0.35	0.35	0.4
Internal Angle of Friction, ϕ	-	40	25	10
Angle of Dilation, ψ	-	13	8	3
Cohesion, c', psi (kPa)	-	0.29 (2)	43.5 (300)	10.8 (75)

In the case of the expansive subgrade, two additional material properties were input into the numerical model. These material properties were intended to characterize the *sorption* and *moisture swelling* behaviors. Both of these models help define the volumetric swell behavior in expansive soils and volumetric free swell at different saturation levels. Brief discussions of these two models are presented in the following subsections.

4.4.3.1 Sorption Model

The Sorption model replicates suction changes in the soil matrix with a change in moisture content. The sorption model considers a partially saturated flow condition in a porous medium with a negative value of pore liquid pressure. The degree of saturation usually lies within a certain range depending on pore fluid pressure. This saturation limit will start at the limit where absorption will occur, and end where the exsorption will occur. Figure 4.8 represents this typical range of value s for the degree of saturation where alteration between absorption and exsorption takes place along the scanning curves. The degree of saturation, s value cannot be zero or greater than unity from the definition of the absorption and exsorption behavior of the porous medium (Simulia, 2016).
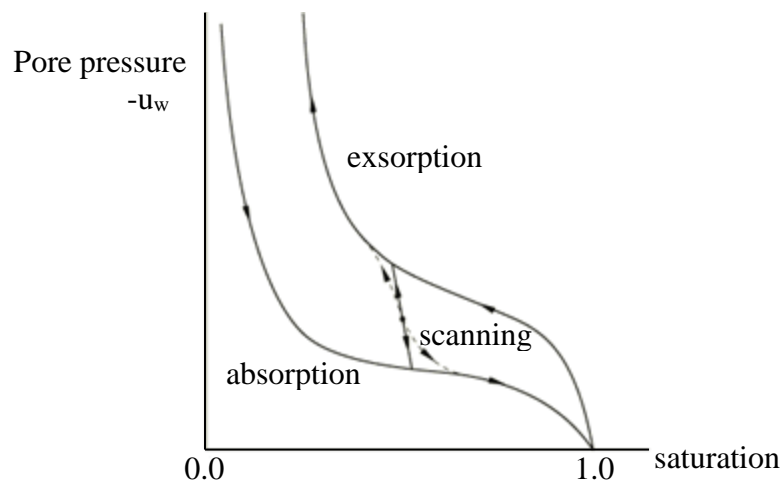
Figure 4.8   Typical Absorption and Exsorption Behaviors (Simulia, 2016)

In ABAQUS, the absorption, exsorption and scanning behaviors need to be defined in the analysis, if the user wants to consider the partial saturation condition in the porous medium. Otherwise, ABAQUS will assume fully saturated flow condition by taking unit value for the degree of saturation as a default. ABAQUS analyzes the partially

saturated flow coupled equation automatically by using its unsymmetric matrix storage

and solution scheme. By software default, the sorption behaviors are defined by

specifying pore pressure values as shown in Table 4.2 which is retrieved from the soil

water characteristic curves (SWCCs) presented in this chapter (Figure 4.2). The material

properties used in the model for expansive subgrade are presented in Table 4.2

Table 4.2   Input Data for Moisture Swelling and Sorption Models

Soil Type	Moisture Swelling		Sorption	
	Strain	Saturation	Pore Pressure, ksi (MPa)	Saturation
AH-11	0	0.09	-4.66 (-32.1)	0.21
	0.14	0.54	-3.09 (-21.3)	0.41
	0.22	0.63	-1.46 (-10.1)	0.52
	0.27	0.69	-1.24 (-8.6)	0.57
	0.31	0.74	-0.89 (-6.15)	0.60
	0.33	0.78	-0.63 (-4.3)	0.64
	0.34	0.83	-0.27 (-1.9)	0.71
	0.37	0.93	-0.11 (-0.8)	0.88
	0.4	1	0	1

4.4.3.2 Moisture Swelling Model

The Moisture-Swelling model defines *the saturation-driven volumetric swelling*

of the soil matrix during partially saturated flow condition and requires volumetric strain

data with changes in moisture content (Simulia, 2016). The soil containing ground water

can be modeled in ABAQUS as a multiphase porous medium. This porous medium

model considers two fluids in the system, one is incompressible wetting liquid, and others

are compressible gases. Both the fluid existing in the partially saturated medium and

wetting liquid are free to move through the medium if driven. Sometimes, the wetting

liquid may be trapped within particles which result in swelling in the process. Negative

pore liquid pressure denotes partial saturation condition in a porous medium and moisture

swelling model developed on the basis of partially saturated flow condition. In the model,

swelling of a porous medium depends on the degree of saturation caused by wetting

liquid in a partially saturated flow condition. In ABAQUS model, swelling behavior of

porous medium is characterized by swelling strain as a function of the degree of

saturation. Figure 4.9 shows the variation of typical volumetric moisture swelling strain

with the degree of saturation (Simulia, 2016)
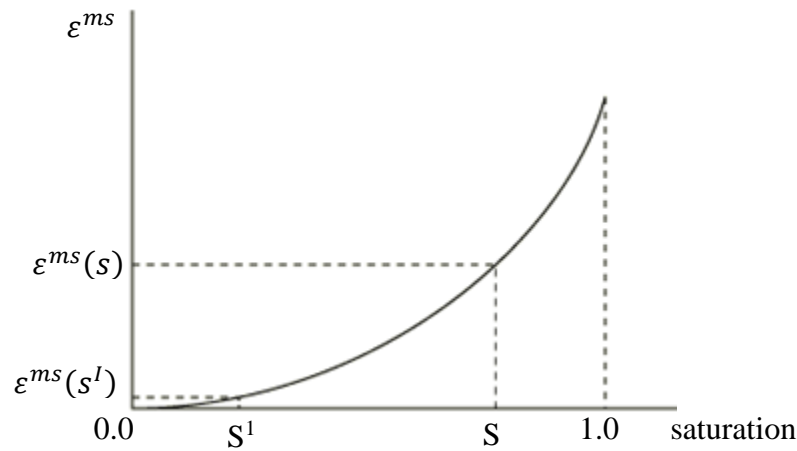
Figure 4.9   Typical Volumetric Moisture Swelling vs. Saturation Curve (Simulia, 2016)

Volumetric swelling strain at particular node in the model is calculated with

reference to volumetric swelling strain obtained at the current and initial saturation level

by using the following equation

$$\varepsilon^{ms}_{ii} = r_{ii} \frac{1}{3}(\varepsilon^{ms}(s) - \varepsilon^{ms}(s^I)) \qquad (4.1)$$

Where $\varepsilon^{ms}(s)$ and $\varepsilon^{ms}(s^I)$ are the volumetric swelling strains at the current and

initial saturations. The ratios r_{ii} are incorporated into the equation to consider an

anisotropic swelling. ABAQUS assumes the isotropic condition if it is not specified by the user i.e model will consider unit r value by default. In the model, the user must define the initial saturation value and the pore fluid pressure that lie within the absorption and exsorption values as discussed in the previous section with Figure 4.8. If this condition is not fulfilled, ABAQUS will adjust the saturation value that will satisfy the pore fluid pressure requirement as discussed above.

4.4.4   Boundary Conditions

The whole pavement section was modeled to simulate the deformations as accurately as possible, while only requiring reasonable computational time. Two types of boundary conditions (BC) were considered in this study: (1) displacement/rotation BC and (2) pore-water pressure BC. The displacement BCs were used to identify the free and fixed directions for the model movement, while pore-water pressure BC was used to specify a source of water for the expansive soil.

Using the displacement BC, the bottom most nodes in the x-z plane of the 3D model were restrained in all three directions, not allowing displacements in any direction. The surface elements in the x-y plane of the model were restricted to move in the z-direction, and the surfaces in the y-z plane were restricted to move in the x-direction (see Figure 4.10). No lateral deformation was allowed on any of the four surfaces, and they were free to move in the vertical direction. The pore-water pressure BC was used at the center of the expansive subgrade layer to have a perpetual source of water. This condition produces the worst-case scenario for the differential heave.
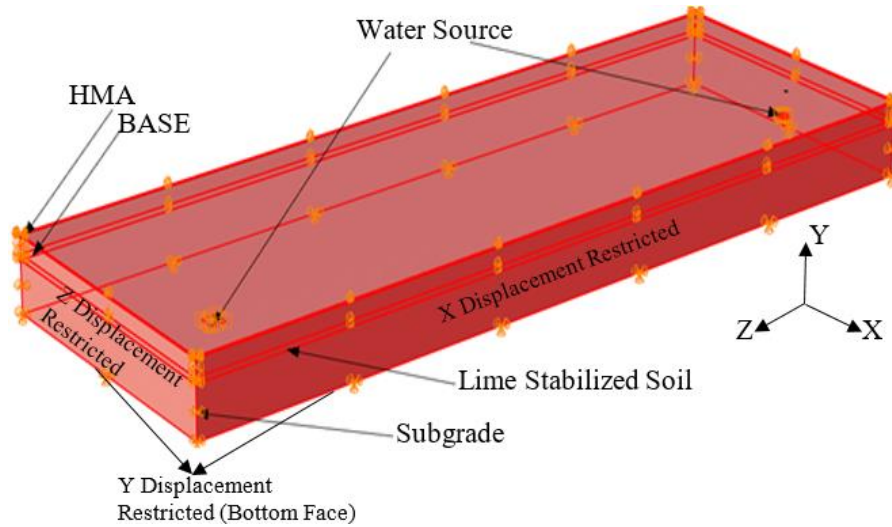
Figure 4.10   3D View of Boundary Conditions

4.4.5   Modeling of Expansive Soil Subgrade

There are two different aspects of the modeling of expansive soil subgrade: (1) representing the layer subgrade, and (2) swell-shrink behavior of soil. This modeling of expansive soil layer would lead to identified differential heaving of the pavement surface. Differential heaving is defined as the difference between the vertical deformations observed on the pavement surface at heaved and non-heaved portions. This differential heaving causes riding discomfort to travelers. The primary objective of numerical modeling of the control section is to match the differential heaving pattern observed in the field. Three possible alternative approaches were considered for the modeling of expansive soil layers.

Firstly, the entire soil subgrade layer was considered as expansive in nature as shown in Figure 4.11, and moisture access was allowed across all boundaries of the subgrade layer. However, this phenomenon would lead to uniform moisture fluctuations across the subgrade layer, thus resulting in uniform volume change throughout the soil deposit. The uniform displacement was observed on entire pavement surface and no differential heaving pattern was seen in Figure 4.12 . As the primary objective behind modeling of the control section was to match the differential heaving pattern observed in the field, this approach was rendered not suitable.
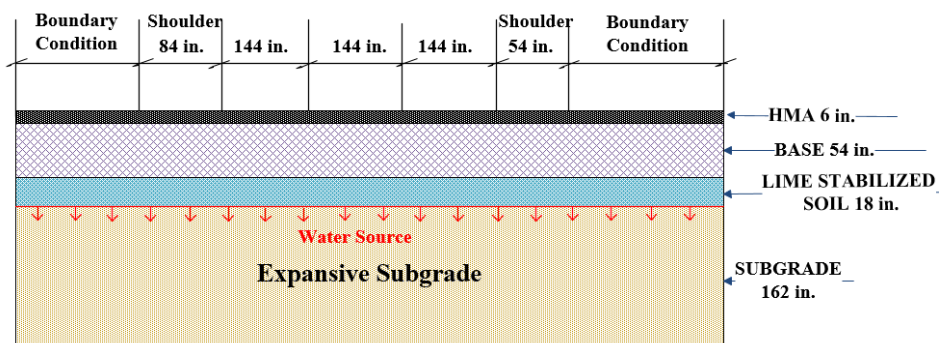
Figure 4.11   Entire Soil Deposit is Expansive in Nature (1 in. = 2.54 cm)
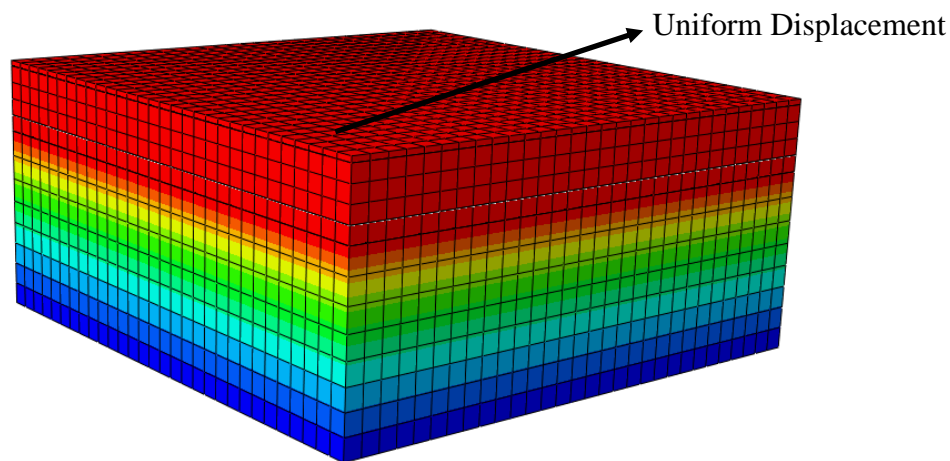
Figure 4.12   Uniform Displacement of the Pavement Section Considering Entire Soil Deposit is Expansive in Nature

The second alternative involved modeling certain portions of the soil stratum as expansive and modeling the rest of the subgrade as non-expansive as shown in Figure 4.13. Allowing moisture access through all boundaries of the subgrade layer would, therefore, lead to volume changes in certain portions, whereas the remaining portions would not undergo any volume change. Although this approach has the potential to simulate differential heave patterns at the pavement surface, the primary challenge is associated with establishing exact locations for the expansive soil segments. Figure 4.14 shows the differential heaving patterns on the pavement surface. As seen in Figure 4.14, only the expansive column has experienced the effect of moisture swelling, and the rest of the non-expansive zones did not show any volume changes. Moreover, such discontinuous patterns in soil properties would most likely not be a realistic representation of actual field conditions.
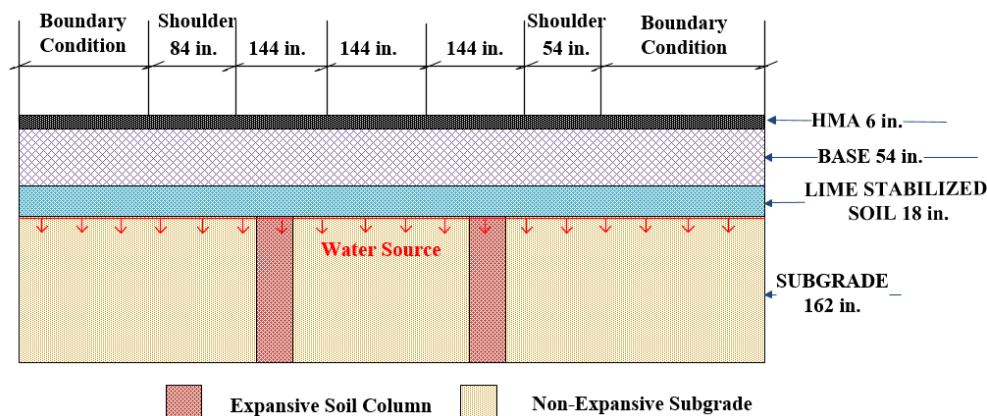
Figure 4.13   Certain Portion of the Soil Stratum are Expansive in Nature
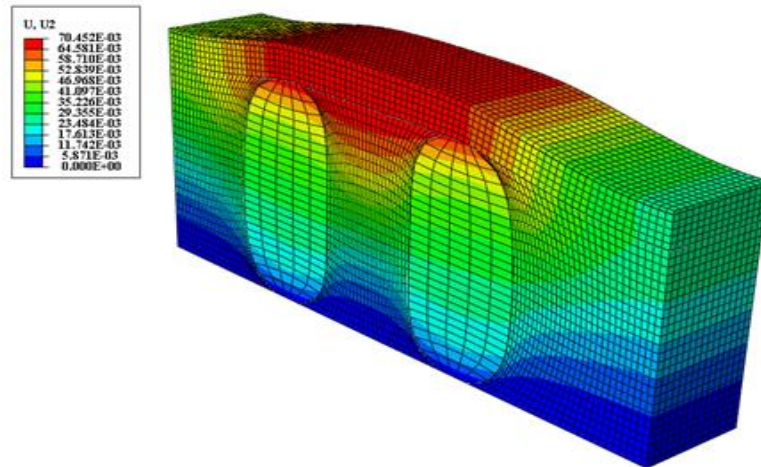
Figure 4.14   Differential Heaving Patterns on the Pavement Surface Considering Certain Portion of the Soil Stratum are Expansive in Nature

As the third alternative, the entire subgrade layer was modeled as expansive in nature, but access to water was limited to selected locations as shown in Figure 4.15. This phenomenon would lead to localized increase in moisture contents, thus resulting in differential heave patterns on the pavement surface. After several trial analyses, the size of the water source was optimized for the calibration of field PVR values. The moisture access was limited to a 5 ft.×5 ft. (152 cm × 152 cm) the region at the interface between the subgrade and the lime-stabilized layers. Figure 4.16 shows the differential heaving patterns on the pavement surface. As seen in Figure 4.16, the maximum heave observed in the middle of the pavement, and minimum heave observed at the edge of the pavement. This means that expansive subgrade and location of moisture have contributed the detrimental effect of swelling. This facilitated the simulation of differential heaving patterns on the pavement surface.
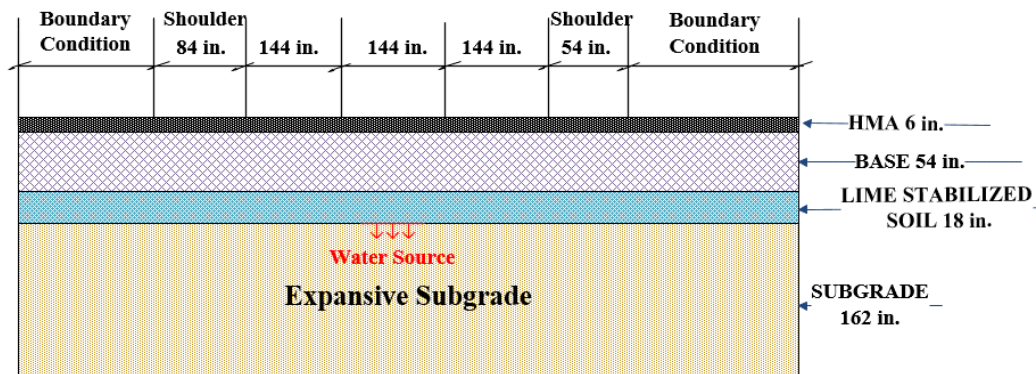
Figure 4.15 Entire Soil Layer is Expansive in Nature, but Access to Water is Limited to Selected Locations (1 in. = 2.54 cm)
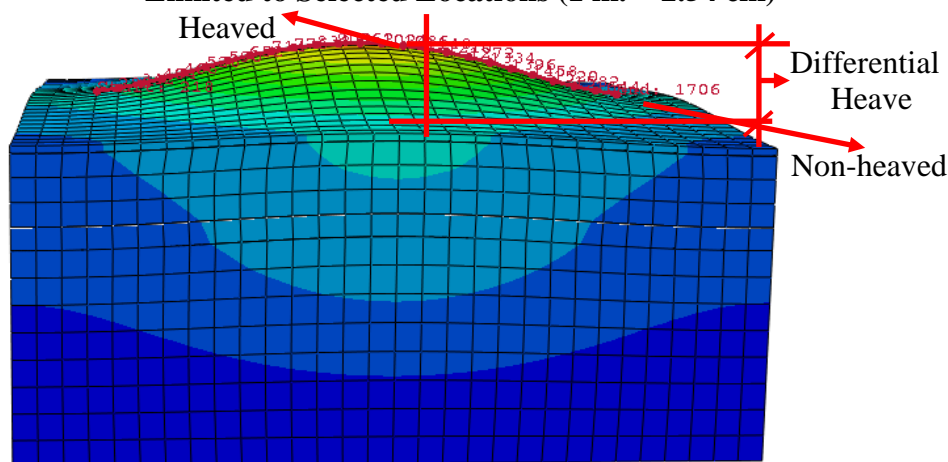
Figure 4.16 Differential Heave of the Pavement Section Considering Entire Layer is Expansive in Nature, and Water is Limited to Selected Locations

Once the expansive layer subgrade along with the location of moisture access established, then next task involved determining the shrink-swell behaviors of expansive soil. These behaviors have already discussed in the previous article 4.4.3.

4.4.6   Element Type and Mesh Size

Meshing criteria are one of the most important features in finite element analysis. The results of analyses can change significantly due to the element's type and size. In this analysis, the mesh size was optimized to produce accurate results, while at the same time maintaining the computational time requirements within reasonable limits. Figure 4.17

illustrates the plot between the element size and computational time requirements. It can be observed from this figure that as the element size decreases, the displacement is increased showing an improvement in the results with the decreasing element size.
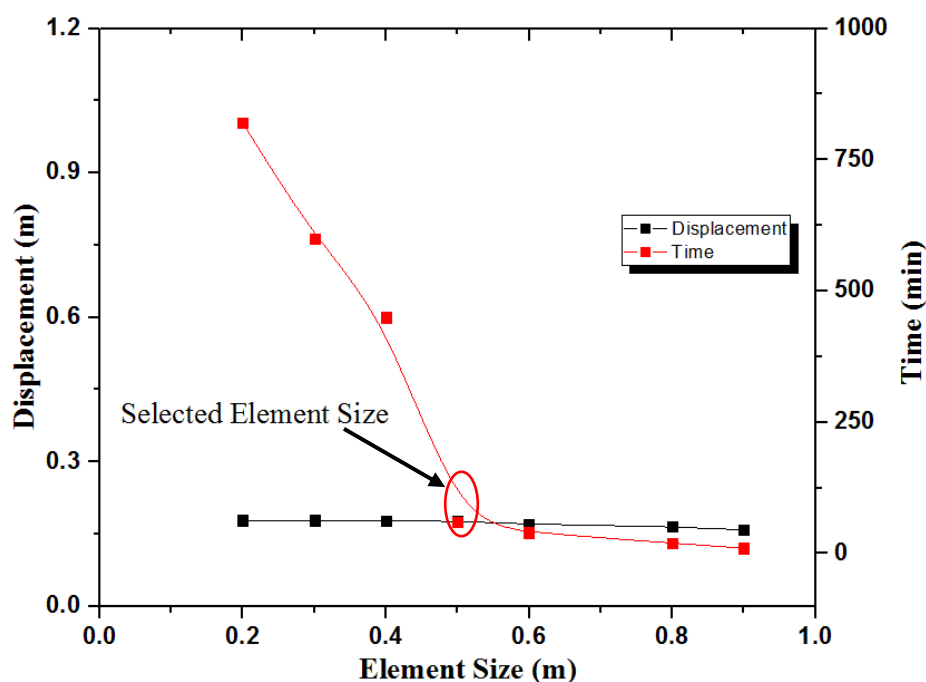
Figure 4.17   Plot Showing Convergence Results (1 m = 39.37 in.)

On reducing the element size from 20 in. (~0.5 m) to 16 in. (~0.4 m), no significant change in the computed displacement values was observed. However, the computational time requirement increased from approximately 60 min to 450 min. Hence, the element size of 20 in. (~0.5 m) was used as the optimum size in the subsequent analyses, to achieve a balance between result accuracy and computational time requirement. Based on the consideration Table 4.3 presents a summary of the element types and the number of elements used for each of the materials used in this study along with the thicknesses.

Table 4.3   Element Details of Different Materials (1 in. = 25.4 mm)

Material Type	Element Type	Number of Elements	Thickness (in.)
Hot Mixed Asphalt (HMA)	C3D8R	5,699	6
Base	C3D8R	9,048	54
Lime Stabilized Soil	C3D8R	4,524	18
Expansive Subgrade	C3D8P	33,522	162

The typical three-dimensional element types C3D8R and C3D8P, which are continuum stress/displacement, three-dimensional, linear hexahedron element types with no pore pressure allowed and with pore pressure allowed, respectively, were assigned in this model for modeling asphalt, base, lime-stabilized soil, and expansive subgrade (see Table 4.3). The C3D8P element type has the ability to replicate partially or fully saturated fluid flow through porous media. Figure 4.18 presents a fully meshed model for the geometry used in this study.
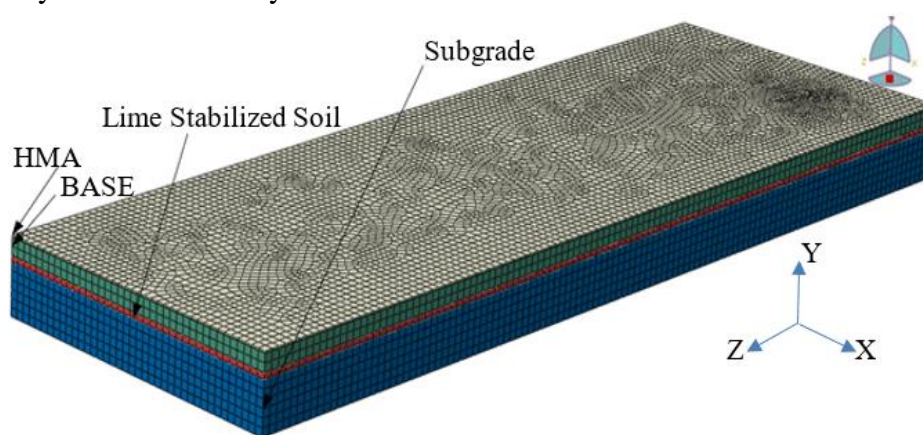
Figure 4.18   Finite Element Mesh for the Control Section

4.4.7   Initial Conditions

Since the swell-shrink behaviors of the soil were the main focus of this research, an element with swell capabilities and sorption properties were used for simulating an expansive subgrade layer. The moisture swelling and sorption model can be used only in the elements that allow for pore pressure. The initial saturation values can be defined as initial conditions otherwise the ABAQUS will consider fully saturated conditions .The initial conditions drive the swelling behavior of expansive soil in the numerical model. Initial conditions are input into the model in the form of an initial void ratio (e_0), initial pore water pressure (U_0) and the initial saturation level (S_0). The amount of swelling the expansive soil experiences depends on its initial saturation level. The lower the saturation value, the higher the swelling, as the expansive soil will swell from this initial saturation value to full saturation (100%). The initial void ratio (1.5) was established from the following relation.

$$e = \frac{G}{\gamma_d} \gamma_w - 1 \qquad (4.2)$$

where G is the Specific Gravity; γ_w is the Unit Weight of Water (pcf or kN/m^3); and γ_d is the Maximum Dry Density (MDD) (pcf or kN/m^3).

The initial conditions used in this analysis are presented in Table 4.4.

Table 4.4   Initial Conditions Specified in the Model

Property	Value
Initial void ratio, e_0	1.5
Initial pore water pressure, U_0 ksi (MPa)	-0.89 (-6.15)
Initial saturation level, S_0	0.6

4.5   Calibration Approach

As mentioned in Chapter 3, the PVR trends established using the laboratory test results can be matched with actual field-observed surface-profile trends to an acceptable limit. Therefore, PVR values for the boreholes can be reasonably assumed to be indicative of actual expansion potential for the soil layers at those locations. A numerical method-based FEM was used to model the pavement section. The results from these numerical model were used to predict swelling behavior experienced by the pavement sections. All these predictions were compared with PVR calculations, and these comparisons were analyzed and discussed. Out of twelve boreholes, AH-1 was located on top of a heave zone while AH-2 was located on a non-heave zone. In order to calibrate the control section, it was decided to match the PVR values from two bore holes (heaved and non-heaved portions) to the heaving observed in the numerical model.

As per laboratory findings, AH-1 demonstrated a PVR of 5.3 in (~135 mm) while the PVR value for AH-2 was 0.9 in (~23 mm). Figure 4.19 presents the deformation contours of the control section modeled using AH-11 soil properties (located near AH-1). Note that AH-12 was located close to the pavement section reconstructed in the past based on Dr. Hardcastle's recommendation (Hardcastle, 2003). As there was no available sample for AH-2, the sorption and moisture swelling data could not be calculated to input in the numerical modeling. Hence to serve the preliminary purpose, AH-11 soil properties were assigned for the entire calibration efforts. Differential heaving on the pavement surface occurs under transient state condition of water infiltration but the PVR value that pavement surface will undergo maximum "rise" if the expansive soil layers had unlimited access to moisture, which is very similar to a steady state condition. Liquidity index

profile shows that seasonal variation in liquidity index value indicates the moisture

fluctuation which leads to shrink-swell behavior in expansive soil. To obtain the LI

profile, the LI data requires over several seasons (a function of time), which leads to the

transient state condition.

It can be observed from Figure 4.19 that the maximum deformation experienced

on the pavement surface at the location corresponding to borehole AH-1 was 5.07 in.

(~129 mm) and that for the location of borehole AH-2, it was 0.72 in. (~18 mm). Figure

4.20 shows the differential nature of the surface heaving observed at the locations

corresponding to AH-1 as compared to AH-2. As indicated in Figure 4.20, the differential

heave predicted by the numerical model (4.35 in. or ~111 mm) closely matched the value

determined as a difference of the PVR values (5.34 in. - 0.9 in. = 4.4 in. or 112 mm)

calculated for these two boreholes. The simulation required approximately 16 hours to

complete.
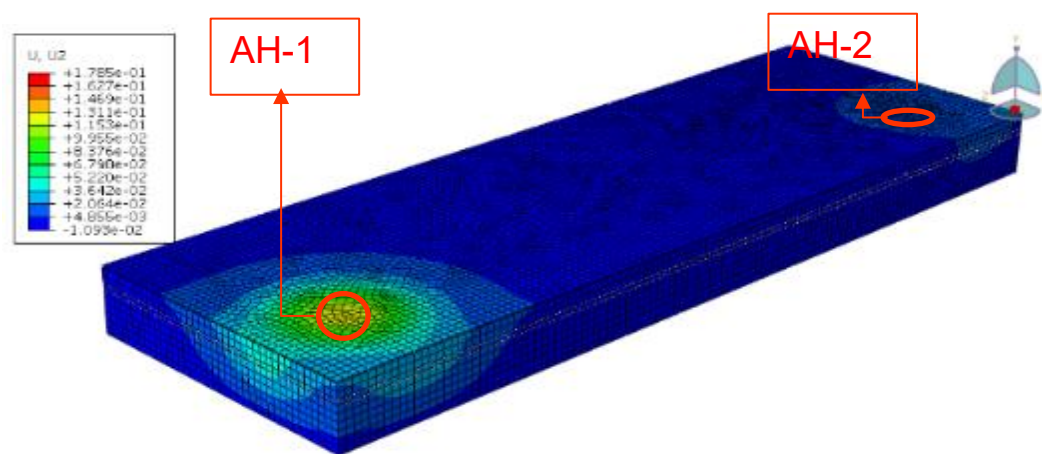
Figure 4.19   Displacement contours for Control Section
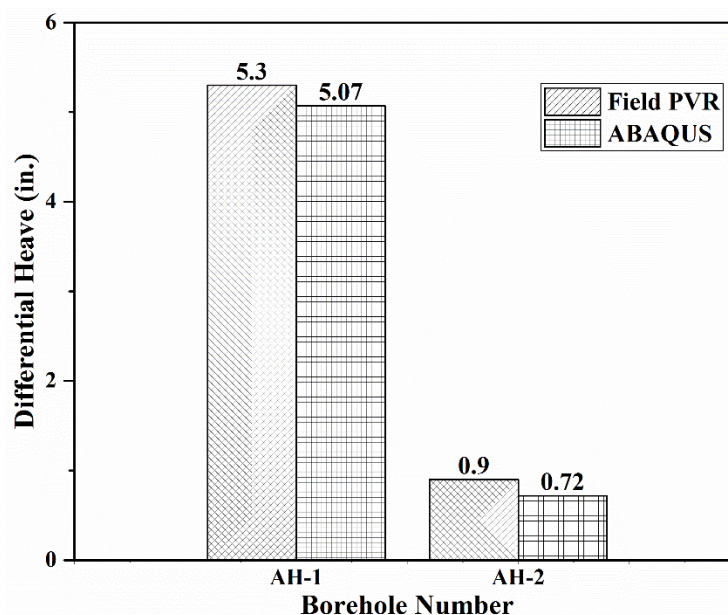
Figure 4.20   Comparisons with PVR and Maximum heave in ABAQUS (1 in. = 25.4 mm)

4.6   Cross Section Selection for the Control Section

After successfully completing the calibration approach and reducing computational time requirements, a 50 ft. $\times$ 50 ft. (~15 m $\times$ ~15 m) cross section of flexible pavement was modeled with a finite element mesh refined to observe important differential heaving behavior due to moisture swelling, both with and without geosynthetic reinforcements in the base layers. The subgrade was modeled as expansive subgrade but only a 5 ft. $\times$ 5 ft. (~1.5 m $\times$ ~1.5 m) the region at top-middle portion area of the expansive subgrade had a continuous water supply. Figure 4.21 presents the isometric view of the pavement control section. An elastic, perfectly plastic material behavior was used to model for the base; lime-stabilized soil, and subgrade. To capture the elasto-plastic behavior of the base, lime-stabilized soil, and subgrade, the Mohr-Coulomb yield criterion was adopted in this analysis. Maximum vertical displacements

were determined to be 6.93 in. (~176 mm) and 0.83 in. (~21 mm) for AH 11 and AH 12

soils, respectively (see Figure 4.22)
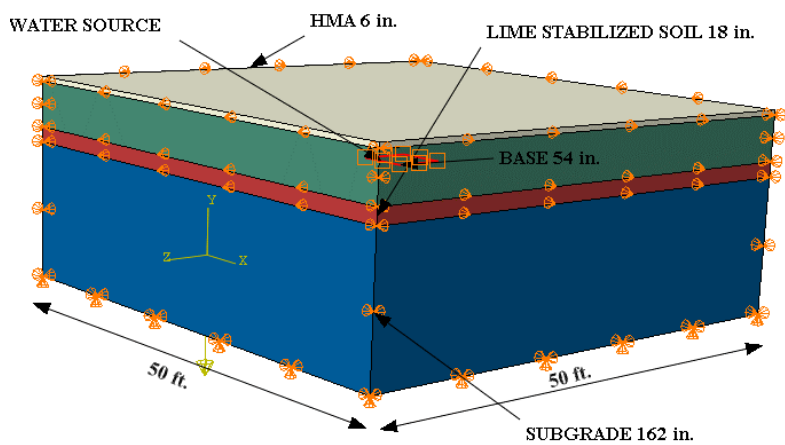
Figure 4.21   Isometric View of the Control Section (1 ft. = 0.305 m)
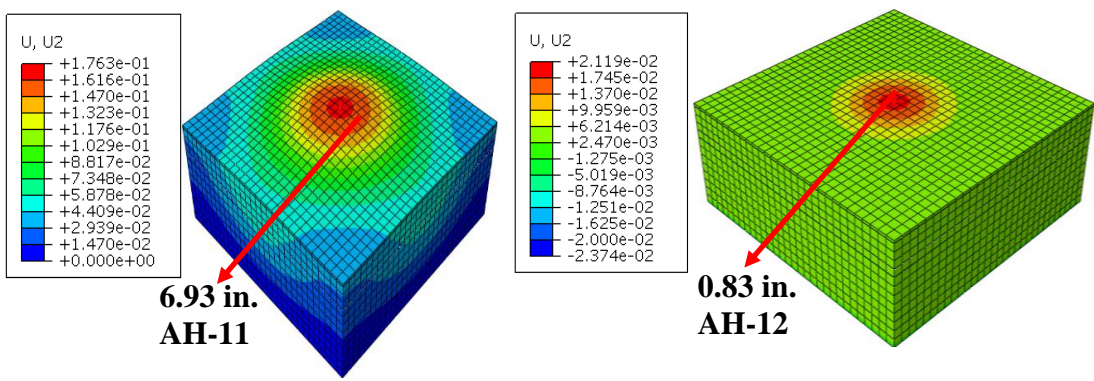
Figure 4.22   Displacement Contours for the Control Section (1 in. = 25.4 mm)

After successfully analyzing the pavement control section, the next task involved

incorporating design alternatives using geocell within a granular base layer.

4.7   Modify the Calibrated Numerical Model to Incorporate Geocell-
Reinforced System

4.7.1   Geocell Modeling

Geocells were modeled as three-dimensional shell element (due to its aspect ratio) with the dimensions of 6 in. $\times$ 6 in. $\times$ 0.06 in. (~152 mm $\times$~152 mm $\times$~1.5 mm). The shape of the cells was modeled as squares as per Leshchinsky (2011). Figure 4.23 shows a finite-element representation of the geocell layer that was modeled in this research. Each geocell layer was 6-in. (~152-mm) deep and consisted of several 6 in. (~152 mm) openings. These openings of the geocells were filled with base material, and the interaction between the base material and the geocell material caused the entire layer to behave as one stiff layer (see Figure 4.23b). The geocell was modeled with 4-noded reduced integration shell element (S4R).
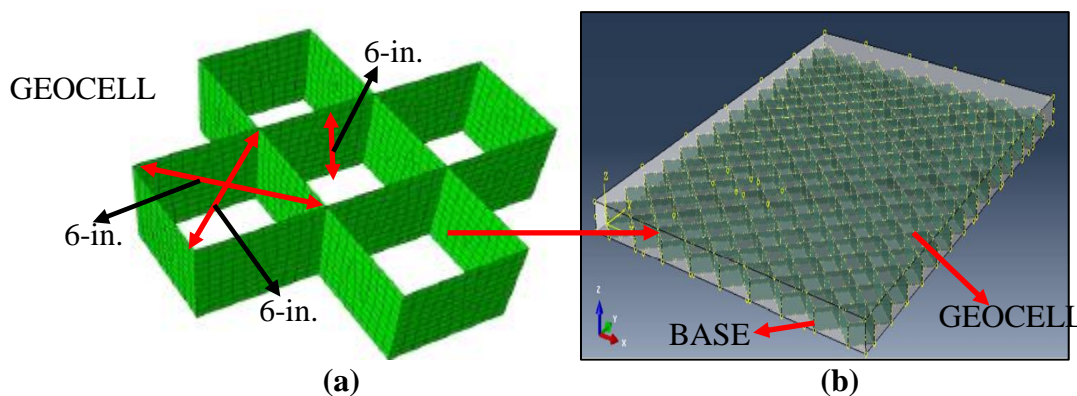
Figure 4.23   **(a) Element Representation of the Geocell Modeled in this Research Study, and (b) Embedded Geocells in the Base Layer (1 in. = 25.4 mm)**

4.8   Numerical Analysis Results

4.8.1   Effect of Geocell Stiffness and Geocell Reinforcement Configurations

Biabani et al. (2016) reported that the availability of varieties of polymeric material, such as High-Density Polyethylene (HDPE) or Novel Polymeric Alloy (NPA),

made it necessary to investigate the influence of geocell stiffness on the performance of a reinforced-subballast assembly. This was investigated by simulating geocell with a range of stiffness that varied from 43 ksi (0.3 GPa) to 725 ksi (5 GPa) to represent a variety of materials including HDPE, and NPA. The result shows that geocell with a relatively low stiffness performs very well compared to the geocell with a higher stiffness value (Biabani et al., 2016). According to Leshchinsky (2011), the effects of geocell stiffness were demonstrated by placing the model on a soft foundation (0.145 ksi or 1 MPa). Three embankment setups were run using geocell stiffness of 14.5 ksi to 29×10^3 ksi (0.1 GPa to 200 GPa) to demonstrate a variety of materials including HDPE, NPA, and structural steel. Use of HDPE, NPA, and steel in Test 2 and Test 3 displayed significant performance as the results show a significant reduction in settlement (75 % and 82 %, respectively) with the increasing geocell stiffness. Hence targeting several stiffness values would give insights into the geocell reinforced layer behavior with respect to reduction in differential heaving. The stiffness values evaluated were 290 ksi (2 GPa), 435 ksi (3 GPa), 580 ksi (4 GPa), 725 ksi (5 GPa).

Leshchinsky (2011) showed that geocell confinement effectively reduced the vertical settlement. In comparison to the control section, the geocell treated sections reduced vertical settlement by 69% and 72% for the single and double-layer reinforced sections, respectively. Saad et al. (2006) conducted a parametric study to investigate the three locations of geosynthetics reinforcement, namely the base–asphalt concrete interface, the base–subgrade interface, and inside the base layer at the height of 1/3 of its thickness from the bottom. The result showed that placing the geosynthetic reinforcement at the base–asphalt concrete interface led to the highest reduction of the fatigue strain

(46–48%). Placing two layers of geocells can create a relatively high modulus, confined granular layer, which acts as a continuous beam (Han et al., 2011). The hybrid geosynthetic solution (two layers geocell + a stiff biaxial geogrid) has been implemented by the Israeli Rail Authority (IRA) to restrain differential heave caused to rail track pavements by the uneven swelling of expansive soil subgrade for a decade (Keif, 2015).

Based on the literature, one and two layers of geocell composites were studied within the scope of this Master's thesis. The following geocell reinforcement configurations were analyzed using the numerical model.

I.   A single layer of geocell placed at the Base-Lime Stabilized Soil interface (GC-1).

II.   A single layer of geocell placed at the HMA-Base layer interface (GC-2).

III.   Two geocell layers: first at mid-depth of the Base layer; second at the Base-Lime Stabilized Soil interface (GC-3).

IV.   Two geocell layers: first at mid-depth of the Base layer; second at the HMA-Base layer interface (GC-4).

V.   Two geocell layers: first at the HMA-Base layer interface; second at the Base-Lime Stabilized Soil interface (GC-5).

VI.   Two geocell layers: Both layers stacked on top of one another and placed at the interface between Base and Lime Stabilized Soil layers (GC-6).

The rest of the modeling aspects including boundary conditions, meshing approach and initial conditions for these models remained the same as that for the control section. Figure 4.24 shows schematics of all the configurations listed above. Note that the black dotted lines in these figures indicate the location of the geocell.
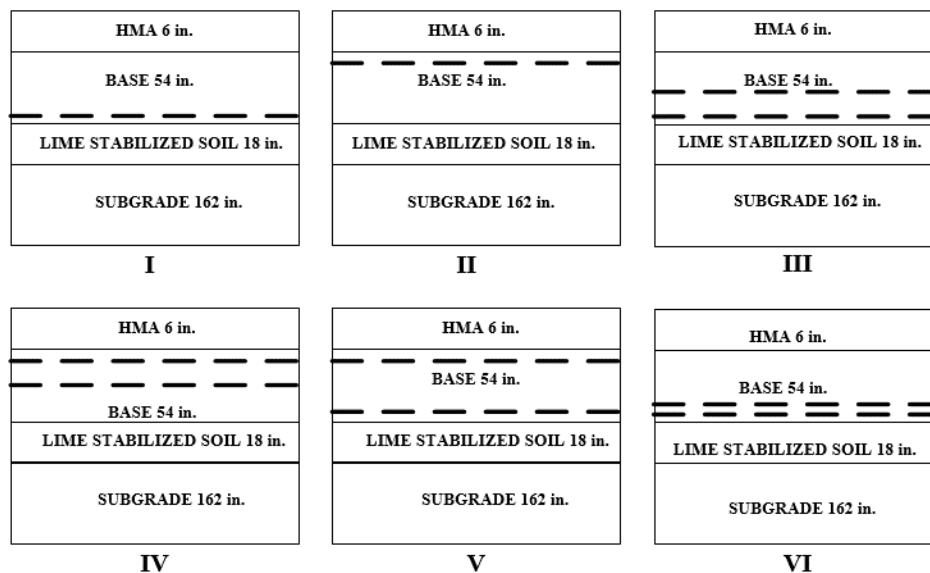
Figure 4.24   Schematic of all the Geocell Reinforcement Configurations (1 in. = 25.4 mm)

Figure 4.25 presents the isometric view of a pavement section comprising a geocell-stabilized base layer.
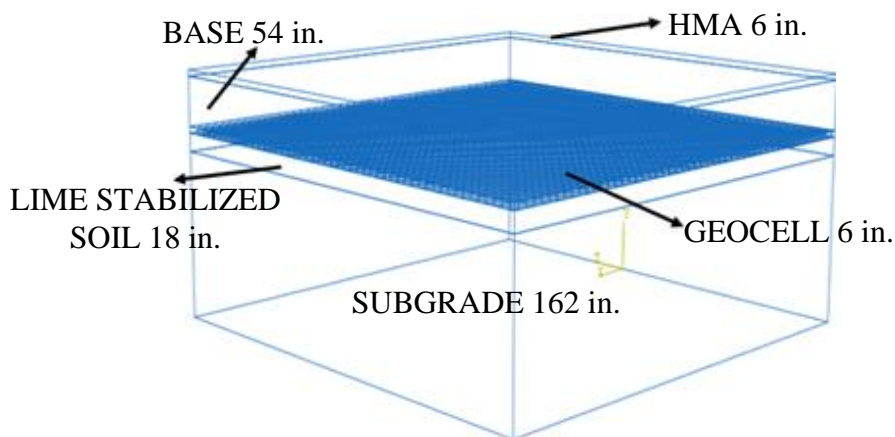
Figure 4.25   3D Isometric View of the Geocell Treated (GC-1) Pavement Section (1 in. = 25.4 mm)

Figure 4.26 shows vertical deformation contours for GC-1 configurations for geocell stiffness of 725 ksi (5 GPa). Similar deformation contours were generated for GC-2 through GC-6, and have been included in Appendix B. The maximum vertical displacement varied from 6.43 in. to 4 in. (~163 mm to ~102 mm) among the six geocell

treated sections (GC-1 to GC-6), in comparison to 6.93 in. (~176 mm) experienced by the

control section (see Figure 4.22). As the ultimate goal of the treatment is to reduce

differential heaving and not the maximum vertical displacement, the maximum and

minimum vertical displacement on the HMA surface were calculated at two reference

points as shown in Figure 4.26, and results are listed in Table 4.5.
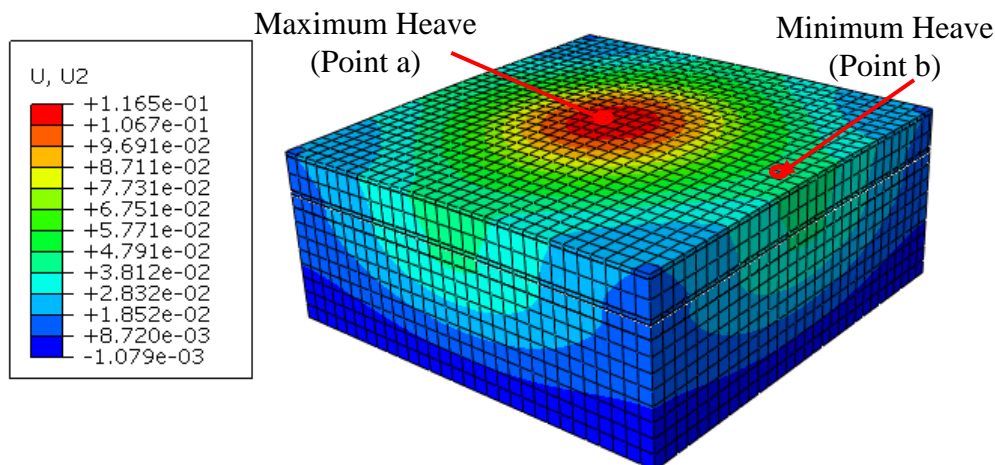
Figure 4.26   Displacement Contours for GC-1 Configuration

Table 4.5   Differential Heave for GC-1 Configuration (1 m = 39.37 in)

Modulus of Geocell, ksi (GPa)	Maximum Vertical Displacement in HMA, (m)	Minimum Vertical Displacement in HMA, (m)	Differential Heave, in. (m)
290 (2)	0.119	0.0526	0.067
435 (3)	0.118	0.0524	0.065
580 (4)	0.117	0.0524	0.064
725 (5)	0.116	0.0524	0.063

Differential heave was computed for all geocell treated sections, and these values

are plotted in Figure 4.27. It can be observed from this figure that the differential heave at

the HMA surface varied from 4.19 in. (~106 mm) to 1.91 in. (~48 mm) for different GC

combinations with varying stiffness for the geocell composite layer. The maximum

differential heave of pavement under geocell with varying stiffness is presented in Figure

4.27. As geocell stiffness increases, the differential heave of pavement decreases in every
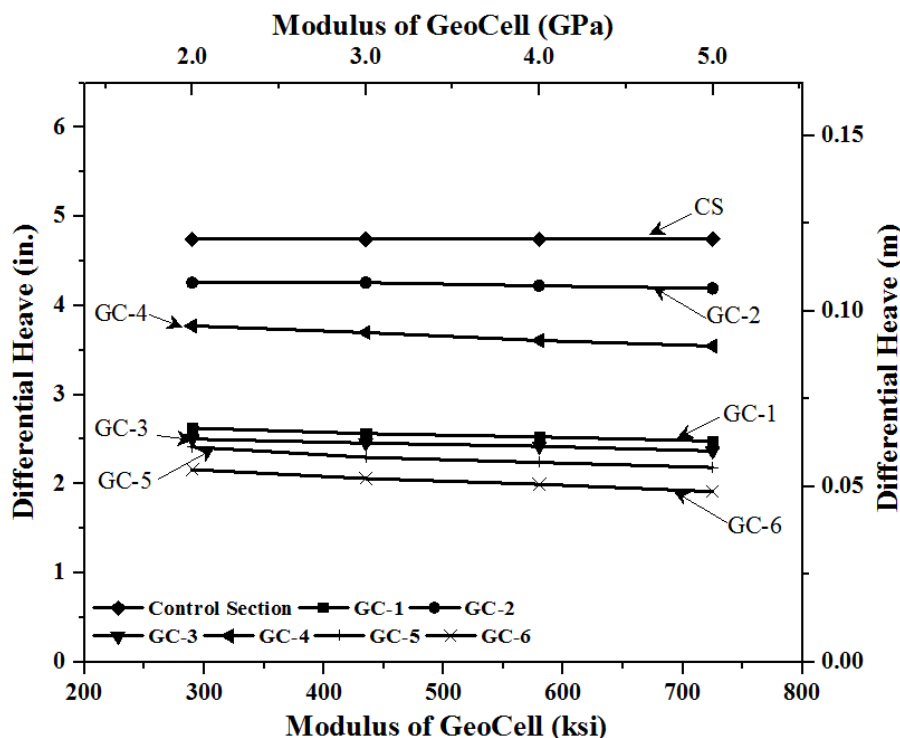
case, while unreinforced (control section) assembly exhibits the highest displacement.

Figure 4.27   Effect of Geocell Stiffness on the Pavement Differential Heave

Both the number of geocell layers and geocell location played significant roles in

reducing the differential heave. This may be explained by the confinement of geocell and

the fill materials. The vertical upward movement was resisted by confining mechanism of

fill materials and geocells, not by the stiff geocell layer. The location of the geocell layer

was optimal when they are closest to the expansive soil in the case of the single layer. It

was found that placing the double layers geocell-reinforcement at the base-lime stabilized

soil interface (GC-6) led to the highest reduction of the percent reduction in heave (54-

60%). The placement of single geocell layer is particularly effective; the highest percent

reduction in heave (44-50%) occurs when the geocell is placed at the base-lime stabilized

soil interface (GC-1). In addition to constructability issues and economics, a single layer

of geocell (GC-1) is the most effective alternative to minimize the differential heave at
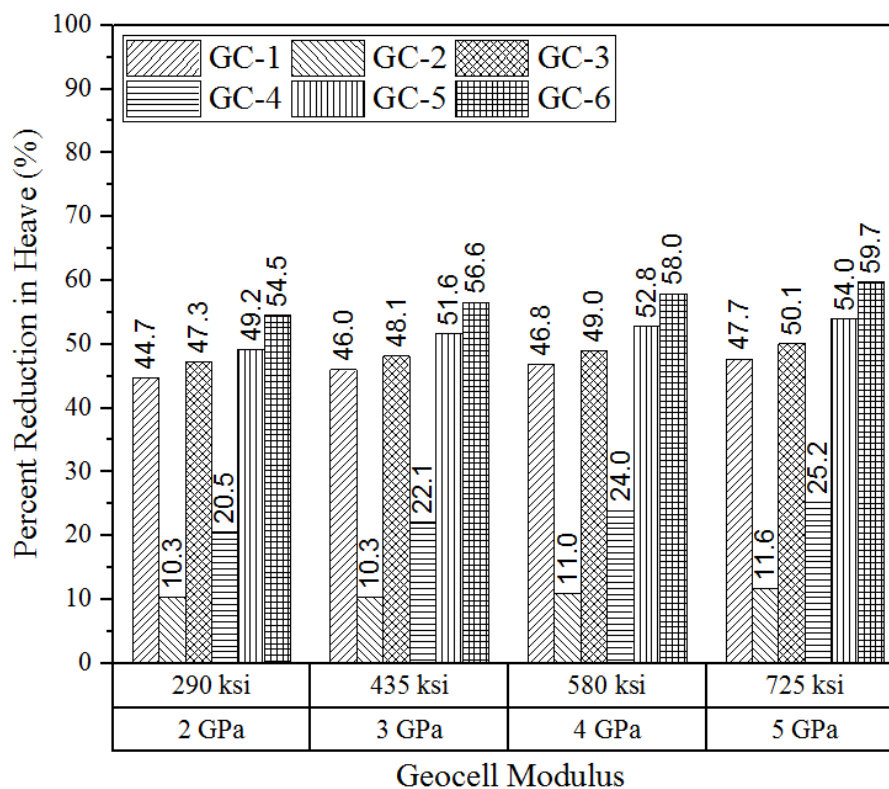
the pavement surface.

Figure 4.28   Percentage Reduction in Differential Heave with varying Geocell Stiffness

4.8.2   Effect of Geocell Height

Geocell height is defined as the depth of the geocell, and geocell width is the

opening size of the geocell. Although tall geocells seem to perform better in terms of

structural capacity, compaction of infill material becomes more difficult (Pokharel,

2011). In the geocell height sensitivity analysis, the effect of geocell height was evaluated

by modeling geocells that are 4 in. (~100 mm), 6 in. (~152 mm), and 8 in. (~200 mm)

tall, respectively. Other parameters in the model were held constant, as shown in Table

4.6. A parametric study was conducted through the numerical modeling effort. The

differential heave was observed from numerical models corresponding to the different heights of geocell and most suitable design alternative was selected considering mechanistic response and ease of implementation.

Table 4.6   Parametric Study of the Pavement Layers (1 in. = 25.4 mm)

Pavement Layers/Geocell	Thickness (in.)
HMA	6
BASE	54
Lime Stabilized Soil	18
Subgrade	162
Geocell Height, H_{GC}	4,6,8

The maximum differential heave of pavements under geocell with varying heights are presented in Figure 4.29. As geocell hight increases, the differential heave of pavement decreases in every case, while control section shows the highest differential heave. It can be observed from this figure that the differential heave at the HMA surface varied from 2.64 in. (~67 mm) to 2.28 in. (~58 mm) for different geocell heights with stiffness for the geocell fixed at 290 ksi (2 GPa).
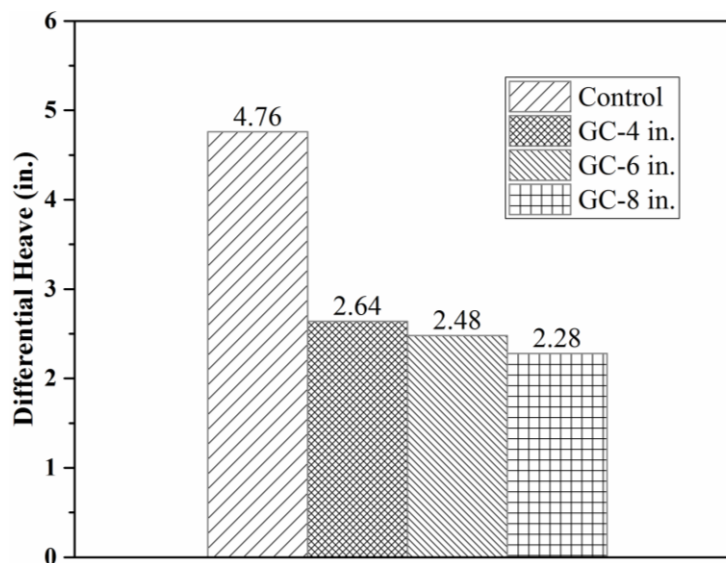
Figure 4.29   Effect of Geocell Heights on the Pavement Differential Heave (1 in. = 25.4 mm)

Figure 4.30 reveals that the percentage reduction of heave in comparison to control section ranged from 45% to 52% for different geocell heights. It was observed that GC-8 in. (~200 mm) exhibited the best performance among the three height of geocell treated sections. However, the difference in heave reduction percentage between GC-4 in. (~100 mm) and GC-8 in. (~200 mm) was only 7% at the same location. Although, GC-8 in. (~200 mm) performs better but from an economic point of view and compaction of infill materials in the field, GC-4 in. (~100 mm) is the best option to mitigate the differential heave at the pavement surface.
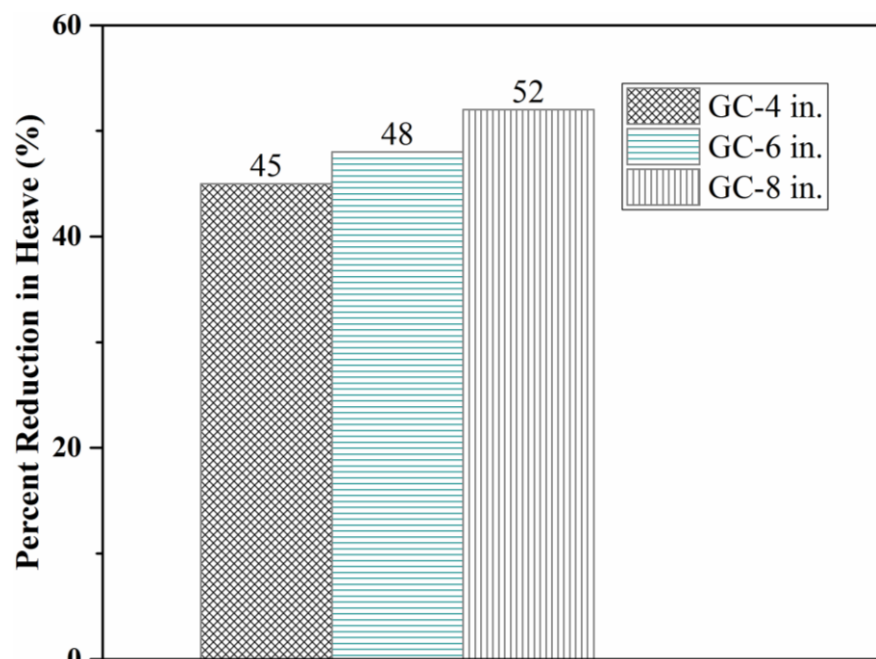
Figure 4.30   Percentage Reduction in Differential Heave with varying Geocell Heights (1 in. = 25.4 mm)

4.9   Inferences Based on Numerical Analysis Results

The following conclusions can be drawn from this study:

1.   The differential heave of the pavement can be reduced by increasing geocell stiffness. The differential heave at the HMA surface varied from 4.19 in. (~106 mm) to 1.91 in. (~48 mm) for different GC combinations with varying stiffness for the geocell composite layer. Results also indicate that geocell with a relatively low stiffness, E = 290 ksi (2 GPa) performs very well compared to the geocell with a higher stiffness, E = 725 ksi (5 GPa).

2.   The number of geocell layers and location of the geocell within the base layer played significant roles in reducing the differential heave. The percentage reduction of heave in comparison to control section ranged from 10% to 60% for different reinforcement combinations. It was observed that GC-6 exhibited the best performance among the six geocell treated sections. Results from the numerical modeling effort

established that placing two layers of geocell within the unbound granular base layer led to the highest reduction (~60%) in the differential heave. Placing a single layer of geocell, on the other hand, reduced the differential heave magnitude by approximately 50%. A single layer of geocell (GC-1) was therefore recommended for implementation to achieve the optimal balance between pavement performance and construction costs.

3.   The differential heave decreases with an increase in the height of geocell, and the differential heave at the HMA surface varied from 2.64 in. (~67 mm) to 2.28 in. (~58 mm) for different geocell height combinations with stiffness for the geocell fixed at 290 ksi (2GPa). It was observed that GC-8 in. (~200 mm) exhibited the best performance among the three different height of geocell treated sections.

4.10   Summary

This chapter presented findings the from finite-element simulation of pavement section comprising a geocell-stabilized base layer. Subsequently, the numerical modeling effort that includes the model geometry, material properties, element size and meshing approach, boundary and initial conditions were presented. Results obtained from the numerical models were presented in this chapter along with discussions.

The next chapter (Chapter 5) of this document will present the conclusions of the research works done within the scope of this Master's Thesis.

CHAPTER 5: SUMMARY, CONCLUSIONS, AND RECOMMENDATIONS FOR FUTURE RESEARCH

5.1   Research Framework

In this chapter, at first, a brief summary of the research tasks performed under the scope of this Master's thesis effort has been presented, along with important findings. Inferences have been drawn from the research findings to arrive at conclusions concerning the research questions and hypotheses. Finally, recommendations have been made for future research tasks that would lead to further understanding of the problem at hand.

The main objective of this research effort was to identify the primary mechanism contributing to differential heaving problems along with a section of U.S. highway 95 near the Idaho-Oregon border and to evaluate the effectiveness of geocells as a candidate remedial measure. For this purpose, twelve boreholes were drilled at strategically selected locations along the pavement section, and soil samples were collected for extensive laboratory characterization. Numerical modeling efforts focused on evaluating the effectiveness of geocell reinforcement for reducing expansive soil-related differential heave in pavements. All research objectives were fully accomplished; important findings from the research tasks are summarized in the following section.

1.   Moisture content tests on soil samples collected from different depths underneath the problematic pavement section indicated that the moisture movement within the soil was probably not governed by the suction mechanism as the ground water

table (GWT) was consistently at depths greater than 26 ft. (~793 cm) from the pavement surface.

2.   Atterberg limit tests indicated that the soil layers corresponding to seven of ten boreholes were likely to be expansive at depths greater than 6 ft. (~183 cm) from the pavement surface. Accordingly, shallow-stabilization alternatives were ruled out due to constructability concerns.

3.   Liquidity Index (LI) calculations indicated that the active-zone extended to a depth of at least 11 ft. (~335 cm) from the pavement surface, soil layers as deep as 11 ft. (~353 cm) from the pavement surface can undergo volume changes due to moisture fluctuation. Preventing moisture fluctuations at such depths through the installation of moisture barriers is not practical.

4.   The potential vertical rise (PVR) values for five of the ten boreholes (AH-1, AH-3, AH-5, AH-7, and AH-8) were greater than 1 in. (2.54 cm), which is often the threshold value used for deciding when a permanent section needs to be rehabilited. This established that rehabilitation is required for most of the pavement section. Investigation of pavement roughness profiles using international roughness index (IRI) values corroborated trends predicted from the PVR calculations.

5.   Cation exchange capacity (CEC) and specific surface area (SSA) tests results a demonstrated strong evidence regarding the presence of high amounts of Montmorillonite in the soil samples that can lead to significant volume changes.

6.   Results from 1D swell tests indicated that four of the boreholes (AH-1, AH-2, AH-3, and AH-7) exhibited swelling-pressure values greater than overburden pressures.

7.   Soluble sulfate content tests indicated that soils from several boreholes were susceptible to high levels of sulfate attack upon chemical stabilization using Calcium-based additives. Accordingly, cement or lime stabilization may not be feasible for those particular pavement sections.

8.   Numerical modeling of geocell-reinforced pavement sections showed that placing two layers of geocell within the unbound granular base layer led to the highest reduction (~60%) in the differential heave.

9.   Placing a single layer of geocell, on the other hand, reduced the differential heave magnitude by approximately 50%. A single layer of geocell was recommended for implementation to achieve the optimal balance between pavement performance and construction costs.

5.2   Recommendations for Future Research

Based on findings from this research study, the following recommendations are made for future research efforts.

1.   Construction and testing of a laboratory-scale box test to evaluate the suitability of geocells as a candidate remedial measure to mitigate expansive soil-related differential heave in pavements;

2.   Instrumentation of the problematic pavement section and/or the laboratory-scale box test to measure the swell pressures associated with volume change in the expansive-soil layer;

3.   Installation of moisture probes in the field to identify the spatial and temporal extent and magnitude of moisture fluctuation;

4. Falling-weight deflectometer (FWD) testing of pavement sections comprising geocell-reinforced base layers to obtain realistic estimates of the reinforced layer modulus values.

REFERENCES

AASHTO T 265 (2004). Laboratory determination of moisture contents of soils. AASHTO T265-93, Washington, D.C.

AAR/TTCI (2012). AAR/TTCI Research proves confinement system a superior geosynthetic for track stabilization. Pueblo, Colorado. http://www.prestogeo.com/wp-content/uploads/2016/10/GWRR-AAR-TTCI-Research.pdf

ASTM, D. 4318–93 (1994). Standard test method for the liquid limit, plastic limit and plasticity index of soils. Annual Book of ASTM Standards 4 (1994): 551-561.

ASTM D 4546-03 (2004) Standard test methods for one-dimensional swell or settlement potential of cohesive soils, American Society for Testing and Materials. Philadelphia, PA: American Society for Testing and Materials.

ASTM D5298-10 (2010), Standard test method for measurement of soil potential (suction) using filter paper, ASTM International, West Conshohocken, PA

ASTM D 4439-04 (2004). Standard terminology for geosynthetics. ASTM, Philadelphia.

Ahlberg, B., Lupi, W., Parks, N., Patel, N., Shah, A. (2015). Hybrid geotextile design for CCR materials in landfill drainage and closure systems, World of Coal Ash Conference, May 5-7, 2015, Nashville, TN.

Aitchison, G.D. (1973). The quantitative description of the stress-deformation behavior of expansive soils – preface to set of papers. Proceedings of the 3rd International Conference on Expansive Soils, 79 – 82. (Vol. 81, No. 658, pp. 17-19).

Alexiades, C. A., and Jackson, C. A. (1966). Quantitative clay mineralogical analysis of soils and sediments. Clays Clay Miner., 14(1), 35–42.

Altmeyer, W. T. (1955). Discussion of engineering properties of expansive clays. In Proc. ASCE (Vol. 81, No. 658, pp. 17-19).

Army TM 5-818-7. (1983). Army technical manual on the foundation in expansive soils. Department of Army, September 1983. http://armypubs.army.mil/eng/DR_pubs/dr_a/pdf/tm5_818_7.pdf

Al-Qadi, I. L., Brandon, T. L., & Bhutta, S. A. (1997). Geosynthetics stabilized flexible pavements (No. Volume 2).

Al-Qadi, I., Dessouky, S., Kwon, J., & Tutumluer, E. (2008). Geogrid in flexible pavements: validated mechanism. Transportation Research Record: Journal of the Transportation Research Board, (2045), 102-109.

Bathurst, R.J., and Jarrett, P.M. (1988). Large-scale model tests of geocomposite mattresses over peat subgrades. Transportation Research Record, No.. 1188, Transportation Research Board, Record, Washington, D.C., pp. 28-36.

Barksdale, R. D., Brown, S. F., & Chan, F. (1989). Potential benefits of geosynthetics in flexible pavement systems (No. 315).

Berg, R. R., Christopher, B. R., & Perkins, S. (2000). Geosynthetic reinforcement of the aggregate base/subbase courses of pavement structures (No. GMA White Paper II).

Biabani, M. M., Indraratna, B., & Ngo, N. T. (2016). Modelling of geocell-reinforced subballast subjected to cyclic loading. Geotextiles and Geomembranes.

Bortz, B. S. (2015). Geocellular confinement systems in low-volume paved roads (Doctoral dissertation, Kansas State University).

Browning, G. (1999). Evaluation of soil moisture barrier. FHWA/MS-DOT-RD-99-21 & 23; Final Report.

Bulut, R., Lytton, R. L., & Wray, W. K. (2001). Soil suction measurements by filterfPaper. expansive clay soils and vegetative influence on shallow foundations,

ASCE Geotechnical Special Publication No. 115 (eds. C. Vipulanandan, M. B. Addison, & M. Hasen), Houston, Texas, pp. 243-261.

Camberato, J.J. (2001). Cation exchange capacity http://virtual.clemson.edu/groups/turfornamental/tmi/fertlime/Cation%20exchang e %20capacity. Pdf.

Carter, D. L., Mortland, M. M., and Kemper, W. D. (1986). Specific surface methods of soils analysis. Part 1: Physical and mineralogical methods, 2nd Ed., A. Klute, ed., Soil Science Society of America (SSSA), Madison, WI.

Cerato, A. B., and Lutenegger, A. J. (2002). Determination of surface area of fine-grained soils by the ethylene glycol monoethyl ether (EGME) method. Geotech. Test. J., 25(3), 315–321.

Chapman, H. D. (1965). Cation-exchange capacity methods of soil analysis—Chemical and microbiological properties, C. A. Black,ed., SSSA, Madison, WI, 891–901.

Chen, F.H. (1988). Foundations on expansive soils. Elsevier Science Publishing Co., Inc., Amsterdam

Chittoori, B. C. S., (2008). Clay mineralogy effects on long-term performance of chemically treated expansive clays. Dissertation submitted to The University of Texas at Arlington.

Christopher, B. R. (2010). Geogrids in roadway and pavement systems. NAUE GmbH & Co. KG, and Global Synthetics Pty Ltd.

Croft, J.B. (1967). The Influence of soil mineralogical composition on cement stabilization. Geotechnique, vol. 17, London, England, pp.119–135.

Das, B.M. (1999). Principles of foundation engineering. 4th, PWS Publishing Company.

Dash, S.K., Rajagopal, K., and Krishnaswamy, N.R. (2001). Strip footing on geocell-reinforced sand beds with additional planar reinforcement. Geotextiles and Geomembranes,Vol. 19, No.8, pp. 529-538.

Dash, S. K., Reddy, P. D. T., & Raghukanth, S. T. G. (2008). Subgrade modulus of geocell-reinforced sand foundations. Proceedings of the Institution of Civil Engineers-Ground Improvement, 161(2), 79-87.

Djellali, A., Ounis, A., & Saghafi, B. (2012). The behavior of flexible pavements on expansive soils. International Journal of Transportation Engineering, 1(1), 1-14.

Estabragh, A. R. , Pereshkafti, M. R.S, Parsaei, B. & Javadi, A. A. (2013). Stabilized expansive soil behavior during wetting and drying, International Journal of Pavement Engineering, 14:4, 418-427, DOI: 10.1080/10298436.2012.746688. http://dx.doi.org/10.1080/10298436.2012.746688

Felt, E. J. (1953). Influence of vegetation on soil moisture contents and resulting soil volume changes. In Proceedings of 3rd Conference on SMFE, Zurich (Vol. 1).

Gay, D. A., & Lytton, R. L. (1988). Moisture barrier effects on pavement roughness. in measured performance of shallow foundations (pp. 88-107). ASCE

Gay, D.A. (1994). Development of a predictive model for pavement roughness on expansive clay, Doctoral Dissertation, Texas A&M University, College Station, Texas.

Gromko, G. J. (1974). Review of expansive soils: 5F, 6T, 52R. J. Geotech. Engng. Div, V100, GT6, 1974, P667–687. In International Journal of Rock Mechanics and Mining Sciences & Geomechanics Abstracts (Vol. 11, No. 10, p. 198). Pergamon.

Han, J., Yang, X., Leshchinsky, D., and Parsons, R. (2008). The behavior of geocell-reinforced sand under a vertical load. Transportation Research Record, Vol. 2045, Transportation Research Board, Record, Washington, D.C., pp. 95-101.

Han, J., Pokharel, S. K., Yang, X., Manandhar, C., Leshchinsky, D., Halahmi, I., & Parsons, R. L. (2011). Performance of geocell-reinforced RAP bases over weak subgrade under full-scale moving wheel loads. Journal of Materials in Civil Engineering, 23(11), 1525-1534.

Hardcastle, J. H. (2003). Evaluation and treatment of expansive volcanic soils US-95, Owyhee County, Idaho. Boise, ID, University of Idaho.

Hayes, F.C. (2007). Test methods for water-soluble sulfate in soils. Research & Development Information, PCA R&D Serial No. 3016

Hodgson, M., & DUDENEY, A. W. L. (1984). Estimation of clay proportions in mixtures by X-ray diffraction and computerized chemical mass balance. CLAYS CLAY MINER. Clays Clay Miner., 32(1), 19.

Holtz, W.G. & Gibbs, H.J., (1956). Engineering properties of expansive clays. Transaction of ASCE, Vol. 121, 641-667.

Jones, D.E., and Holtz, W.G. (1973). Expansive soils – the hidden disaster. Civil Eng., ASCE, New York, NY pp 87-89, Aug. 1973.

Johnson, D., Patrick, D. M., Division, S. M. (1975). A review of engineering experiences with expansive soils in highway subgrades. Report No. FHWA-RD-75-48

Johnson, L. J., Chu, C. H., & Hussey, G. A. (1985). Quantitative clay mineral analysis using simultaneous linear equations. Clays Clay Miner, 33(2), 107-117.

Jayatilaka, R., GAY, D., Lytton, R. L., & Wray, W. K. (1993). The effectiveness of controlling pavement roughness due to expansive clays with vertical moisture barriers. final report (no. FWA/tx-92/1165-2f).

Jayatilaka, R., & Lytton, R. L. (1997). Prediction of expansive clay roughness in pavements with vertical moisture barriers (No. FHWA/TX-98/187-28F,).

Jayatilaka, R. (1999). A model to predict expansive clay roughness in pavements with vertical moisture barriers. Doctoral Dissertation, Texas A&M University, College Station, Texas.

Keif, O. (2015). The hybrid geosynthetic solution for rail track on expansive clay, Geosynthetics Conference, Feb 15-18, 2015, Portland, Oregon.

Kim, J., and Hjelmstad, K. (2009). Three-dimensional finite element analysis of multi-layered systems: Comprehensive nonlinear analysis of rigid airport pavement systems. Federal Aviation Administration DOT 95-C-001, COE Rep. No. 10, Univ. of Illinois at Urbana-Champaign, Urbana, Ill.

Kwon. J (2007). Development of a mechanistic model for geogrid reinforced flexible pavement.Ph.D. Thesis, Department of Civil and Environmental Engineering, the University of Illinois at Urbana-Champaign.

Koerner, R.M. (2005). Designing with Geosynthetics. Fifth Edition, Prentice Hall, New Jersey.

Kuo, C., Huang, C. (2006). Three-dimensional pavement analysis with nonlinear subgrade materials. Journal of Materials in Civil Engineering, v 18, n 4, August, p 537-544.

Lambe, T. W. (1960). The character and identification of expansive soil, Soil PVC meter. Federal Housing Administration, Technical Studies Program, FHA 701.

Leshchinsky, B. A. (2011). Enhancing ballast performance using geocell confinement. In Geo-Frontiers 2011: Advances in Geotechnical Eng. (pp. 4693-4702).

Little, D. N., Males, E. H., Prusinski, J.R. and Stewart, B. (2000). Cementitious stabilization. 79th Millennium Rep. Series, Transportation Research Board.

Lytton, R.L. (1977). The characterization of expansive soils in engineering. Presentation at the Symposium on Water Movement and Equilibria in Swelling Soils, American Geophysical Union, San Francisco, California.

Lytton (2004). Introduction, design procedure for pavements on expansive soils. Report No. FHWA/TX-05/0-4518-1, Texas Department of Transportation,

Mackiewicz, S. M., & Ferguson, E. G. (2005). Stabilization of soil with self-cementing coal ashes. World, 1–7.

Malhotra, M., & Naval, S. (2013). Stabilization of expansive soils using low-cost materials, 2(11), 181–184.

Manosuthikij, T. (2008). Studies on volume change movements in high PI clays for better design of low volume pavements (Doctoral dissertation, The University of Texas at Arlington).

McDowell, C. (1956). The interrelationship of load, volume change, and layer thickness of soils to the behavior of engineering structures. Proc. Highway Research Board, No.35, 754-770Research Board, No. 35, 754-770.

Mitchell, P.W. and Avalle, D.L. (1984). A technique to predict expansive soil movements. Proceedings, 5th International Conference on Expansive Soils, Adelaide, South Australia.

Mitchell, J.K. & Soga, K. (2013). Fundamentals of soil behavior. John Wiley & Sons, Inc. New York.

Murthy, V.N.S., (2010). Soil mechanics and foundation engineering. CBS Publishers and Distributors Pvt., Ltd., New Delhi, India.

Nelson, J.D. & Miller, D.J.(1992). Expansive soils: problems and practice in foundation and pavement engineering. John Wiley & Sons, Inc. New York.

Nottingham, K. N. (1985 & 1986). The swelling soils-Oregon line to elephant butte.In Intra-Departmental Correspondence to District 3 Materials Engineer, Idaho Transportation Department, p. 23.

O'Neill, M. W., and Poormoayed, N. (1980). Methodology for foundations on expansive clays. Journal of the Geotechnical Engineering Division, American Society of Civil Engineers, Vol. 106, No. GT12, 1345-1367.

Palmeira, E. (2009). Geosynthetics in road engineering. Internation Geosynthetics Society.

Petry, T. M., & Armstrong, J. C. (1989). Stabilization of expansive clay soils.Transportation Research Record, (1219).

Pokharel, S., Han, J., Manandhar, C., Yang, X., Leshchinsky, D., Halami, I. and Parsons, R. (2011). Accelerated pavement testing of geocell-reinforced unpaved roads over weak subgrade. J.of the Trans. Research Board, No. 2204, Low-Volume Roads. Vol. 2, 67-75.

Puppala, A. J., Viyanant, C., Kruzic, A. P., and Perrin, L.(2002). Evaluation of a modified soluble sulfate determination method for fine-grained cohesive soils, GeotechnicalTesting Journal, GTJODJ, Vol. 25, No. 1, pp.85-94

Punthutaecha, K., Puppala, A. J., Vanapalli, S. K., & Inyang, H. (2006). Volume change behaviors of expansive soils stabilized with recycled ashes and fibers. Journal of materials in Civil Engineering, 18(2), 295-306.

Ramana Murty, V. (1998). Study on swell pressure and the method of controlling swell of expansive soil,Ph.D. Thesis, University of Kakatiya, Warangal.

Randall, K. K., Laird, D. A., and Nater, E. A., (1994). Comparison of four elemental mass balance methods for clay mineral quantification. Clays and Clay Minerals, v 42, p 437- 443.

Rao, M. R., Rao, a. S., & Babu, D. R. (2008). Efficacy of lime-stabilised fly ash in expansive soils. Proceedings of the ICE - Ground Improvement, 161(February), 23–29. http://doi.org/10.1680/grim.2008.161.1.23

Rhoodi, G., & Zornberg, J. (2012). Effect of geosynthetic reinforcements on mitigation of environmentally induced cracks in pavement. Austin: The Univeristy of Texas at Austin.

Saad, B., Mitri, H., & Poorooshasb, H. (2006). 3D FE analysis of flexible pavement with geosynthetic reinforcement. Journal of transportation Engineering, 132(5), 402-415.

Sayers, M. W. (1986). The international road roughness experiment: establishing correlation and a calibration standard for measurements.

Seed, H. B., & Lundgren, R. (1962). Prediction of swelling potential for compacted clays. Journal of the soil mechanics and foundations division, 88(3), 53-88.

Sitharam, T.G, Sireesh, S., and Dash, S.K. (2005). Model studies of a circular footing supported on geocell-reinforced clay. Canadian Geotechnical Journal, Vol. 42, No. 2, pp. 693-703.

Simulia (2016). Abaqus analysis user's manual. Dassault Systemes.

Snethen, D. R., Townsend, F. C., Johnson, L. D., Patrick, D. M., & Vedros, P. J. (1975). A review of engineering experiences with expansive soils in highwa subgrades. Interim Report Army Engineer Waterways Experiment Station, Vicksburg, MS., 1.

Snethen, D. R., Johnson, L. D., & Patrick, D. M. (1977). An evaluation of expedient. methodology for identification of potentially expansive soils (No. FHWA-RD-77-94 Interim Rpt.).

Steinberg, M.L. (1992). Vertical moisture barrier update. Transportation Research Record 1362. pp.111-117.

TxDOT (Texas Department of Transportation) (1999) Tex- 124-E: Test procedure for determining potential vertical rise. TxDOT, Austin, TX, USA, Designation: Tex-124-E, p. 11.

Thomas, P. J. (1998). Quantifying properties and variability of expansive soils in selected map units (Doctoral dissertation, Virginia Polytechnic Institute, and State University).

Vanapalli, S. K., & Lu, L. (2012). A state-of-the-art review of 1-D heave prediction methods for expansive soils. International Journal of Geotechnical Engineering, 6, 15–41. http://doi.org/10.3328/IJGE.2012.06.01.15-41

Vanapalli, S. K., & Adem, H. H. (2013). A simple modeling approach for estimation of soil deformation behavior of expansive soils using the modulus of elasticity as a tool, Poromechanics, ASCE 2013, 1057-1066

Wanstreet, P. (2007). Finite element analysis of slope stability. West Virginia University.

Webster, S.L., and Alford, S.J. (1977). Investigation of construction concepts for pavement across soft ground, Report S-77-1. Soils and Pavements Laboratory, U.S. Army Engineer Waterways Experiment Station, Vicksburg, MS.

Wray, W. K., (1995). So your home is built on expansive soils: a discussion of how expensive soils affect buildings. American Society of Civil Engineers, New York.

Yang, X. (2010). Numerical analyses of geocell-reinforced granular soils under static and repeated loads. Ph.D., University of Kansas, United States.

Yukselen, Y., & Kaya, A. (2006). Prediction of cation exchange capacity from soil index properties. Clay Minerals, 41(4), 827-837.

Zornberg, J. G., & Gupta, R. (2009). Reinforcement of pavements over expansive clay subgrades. In Proceedings of the 17th International Conference on Soil Mechanics and Geotechnical Engineering (Vol. 1, pp. 765-768).

Zhao, M. H., Zhang, L., Zou, X. J., & Zhao, H. (2009). Research progress in two-direction reinforced composite foundation formed by geocell reinforced mattress and gravel piles. China Journal of Highway and Transport, 1, 002.

APPENDIX A

Appendix A: Literature Review and Project Background


```
                          ┌─────────┐
                          │  START  │
                          └────┬────┘
                               │
                               ▼
                 ┌──────────────────────────┐
                 │   CONDUCT ROUTINE         │
                 │   CLASSIFICATION TESTS    │
                 │   AND MESSURE SOIL        │
                 │   SUCTION. DEFINE SWELL   │
                 │   POTENTIAL               │
                 └──────────────────────────┘
```

POTENTIAL SWELL > 0.5 %

NO

COMPLETE DESIGN USING BASIC STRENGTH PARAMETRS. VOLUME CHANGE WILL BE MINIMAL AND NORMAL CONSTRUCTION WILL MINIMIZE THE LIMITED PROBLEMS

ALL LOCATIONS WHICH EXIHIBIT MARGINAL POTENTIAL SWELL WILL REQUIRE TESTING AND AN ESTIMATE OF VOLUME CHANGE IF CHANGES IN CHARACTERISTIC PROPERTIES ARE ANTICIPATED DECISION SHOULD CONSIDER PAST EXPERIENCE WITH THE SOIL, IF AVAILABLE

MARGINAL

YES

FOR MARGINAL AND HIGH POTENTIAL SWELL SOILS ADDITIONAL TESTING TO ESTIMATE ANTICIPATED VOLUME CHANGE IS NECESSARY

HIGH

ALL LOCATIONS WHICH EXIHIBIT HIGH POTENTIAL SWELL WILL BE SAMPLED (UNDISTURBED), TESTED, AND AN ESTIMATE MADE OF ANTICIPATED VOLUME CHANGE

END

Figure A 1   Recommended Decision Process for Identifying and Qualitatively Classifying Potentially Expansive Soils (From Snethen et al., 1977)

AH-1

DATE DRILLED: 6/1/2015

SHEET 1 of 1

DISTRICT 3

KEY NUMBER 19112   PROJECT NUMBER A019(112)   PROJECT NAME US-95, Elephant Butte Swelling Clay

COUNTY Owyhee   GROUNDWATER ENCOUNTER No Water Encountered

DRILLER/CONTRACTOR Kelley Dick   LOGGED BY Keith Nottingham   GEOLOGIST Keith Nottingham

DRILLING METHOD Hollow Stem Auger   LOCATION NBL of 3 Lanes

COLLAR ELEV. 2994.4'   HOLE SIZE 9"   ROUTE / SEGMENT / MILEPOST US-95 / 001540 / 17.008

GPS COORDINATES LAT: 43.446582°   / Long: -116.859679°   STATION / OFFSET 3.5 ' LT of right shoulder stripe

ELEV. (ft)	DEPTH (ft)	TYPE - No.	RECOVERY %	BLOW COUNTS	LITHOLOGY	MATERIAL DESCRIPTION (Stratification lines represent approximate boundaries between materials.)	LL (%)	PI (%)	Depth	TESTS AND REMARKS
						Asphalt (1.06')			1.1	Layers same as AH-1A Solid Stem auger to 7.0' no samples
						(GW) Brown 3/4" Aggregate Base			2.0	
						(GM) Brown Silty Gravel with Sand				
2990	5					(ML) Light Brown Lime Treated Sub Grade			4.6	
						(MH) Light Brown Sandy Elastic Silt (Mostly Dry)			6.1	
						7.0' Start Continuous Sampling				7.0' - 9.5' Recovery = 36%
2985	10						118	53		9.3' - 9.5' Moisture = 36.5% 16-3DI-0017 11-P 9.3' - 9.5' (MH) Fines = 53.6% 9.5' - 12.5' Recovery = 100%
						White / Tan Selenite Crystals				
2980	15									
2975	20									
						Silt is hard and dry in sampler shoe				
2970	25		100	4-6-8 (14)		Compact Elastic Silt, Slightly Moist			26.0	SPT 24.5' - 26.0'

Bottom of hole at 26.0 feet.

Figure A 2   Example Borelog Generated During the Drilling Operation-Courtesy-ITD

APPENDIX B

: Laboratory Tests Results and Numerical Analysis Profiles

Moisture Content Tests

Table B 1   Summary of Moisture Content (1 ft. = 30.5 cm)

S. No.	Sample Depth (ft.)	Moisture Content (%)	S. No.	Sample Depth (ft.)	Moisture Content (%)
AH-2					
1	3.6-3.8	18	5	8.4-9.5	22
2	3.8-3.9	5	6	10.9-13.2	35
3	3.9-5.2	24	7	15.9-18.2	41
4	5.9-8.2	32	8	18.4-20.4	28
AH-3					
1	2.0-5.0	10	4	15.0-17.5	58
2	5.0-9.7	75	5	17.5-19.8	61
3	10.0-14.7	54			
AH-4					
1	2.0-3.0	5	5	9.8-10.0	26
2	3.0-4.0	15	6	10.0-10.3	25
3	6.5-8.3	24	7	10.8-11.7	20
4	8.5-9.8	24			
AH-5					
1	8.8-9.3	54	4	14.5-16.3	34
2	9.5-11.8	46	5	16.5-17.7	35
3	12.0-13.8	60			
AH-6					
1	4.1-4.3	4	5	6.0-8.3	38
2	4.3-4.8	42	6	8.5-9.6	49
3	4.8-5.5	45	7	9.8-10.2	43
4	5.5-5.6	35	8	10.4-10.8	41
AH-7					
1	5.0-7.5	51	4	15.5-16.2	65

S. No.	Sample Depth (ft.)	Moisture Content (%)	S. No.	Sample Depth (ft.)	Moisture Content (%)
2	7.5-9.8	43	5	16.2-17.0	64
3	12.5-13.8	62	-	-	-
AH-8					
1	2.0-3.0	5	5	10.5-12.5	62
2	3.8-4.5	58	6	15.8-16.3	62
3	6.4-7.3	56	7	18.0-18.7	66
4	8.3-9.7	61	8	18.7-19.5	64
AH-9					
1	5.5-6.0	16	3	8.5-10.1	25
2	6.0-6.6	16			
AH-10					
1	1.5-1.9	4	4	3.0-4.0	25
2	1.9-2.4	3	5	4.0-4.5	13
3	2.4-3.0	8	6	4.5-5.2	5

Atterberg Limits Tests Data

Table B 2   **Summary of Atterberg limits for 10 Boreholes (1 ft. = 30.5 cm)**

S. No.	Sample Depth (ft.)	Liquid Limit (%)	Plastic Limit (%)	Plasticity Index (%)
AH-2				
1	3.6-3.8	47.2	33	14.2
2	3.8-3.9	47.2	33	14.2
3	3.9-5.2	47.2	33	14.2
4	5.9-8.2	46	35	11
5	8.4-9.5	47	30	17
6	10.9-13.2	80	40	40
7	15.9-18.2	95	45	49.8
8	18.4-20.4	98	51	47
9	21.0-22.0	94	47	47

S. No.	Sample Depth (ft.)	Liquid Limit (%)	Plastic Limit (%)	Plasticity Index (%)
AH-3				
1	2.0-5.0	42	29	13
2	5.0-9.7	96	61	35
3	10.0-14.7	116	55	61
4	15.0-17.5	116	58	58
5	17.5-19.8	133	63	70
AH-4				
1	2.0-3.0	30	23	7
2	3.0-4.0	37	26	11
3	6.5-8.3	29	25	4
4	8.5-9.8	47	24	23
5	9.8-10.0	40	28	12
6	10.0-10.3	38	29	9
7	10.8-11.7	37	28	9
AH-5				
1	8.8-9.3	164	54	110
2	9.5-11.8	130	46	84
3	12.0-13.8	94	53	41
4	14.5-16.3	86	44	42
5	16.5-17.7	94	58	36
AH-6				
1	4.1-4.3	58	43	15
2	4.3-4.8	58	43	15
3	4.8-5.5	58	43	15
4	5.5-5.6	58	43	15
5	6.0-8.3	62	38	23.9
6	8.5-9.6	88	49	39
7	9.8-10.2	86	56	30

S. No.	Sample Depth (ft.)	Liquid Limit (%)	Plastic Limit (%)	Plasticity Index (%)
8	10.4-10.8	88	58	30
9	13.4-14.1	70	37	33
10	14.1-14.7	70	37	33
AH-7				
1	5.0-7.5	49	31	18
2	7.5-9.8	96	45	51
3	12.5-13.8	132	53	79
4	15.5-16.2	134	71	63
5	16.2-17.0	135	71	64
AH-8				
1	2.0-3.0	42	25	17
2	3.8-4.5	42	25	17
3	6.4-7.3	114	32	82
4	8.3-9.7	80	60	20
5	10.5-12.5	87	63	24
6	15.8-16.3	100	71	29
7	18.0-18.7	124	69	55
8	18.7-19.5	124	69	55
AH-9				
1	5.5-6.0	28	22	6
2	6.0-6.6	29	23	6
3	8.5-10.1	38	32	6
AH-10				
1	1.5-1.9	36	21	15
2	1.9-2.4	36	21	15
3	2.4-3.0	36	21	15
4	3.0-4.0	42	27	15
5	4.0-4.5	42	27	15
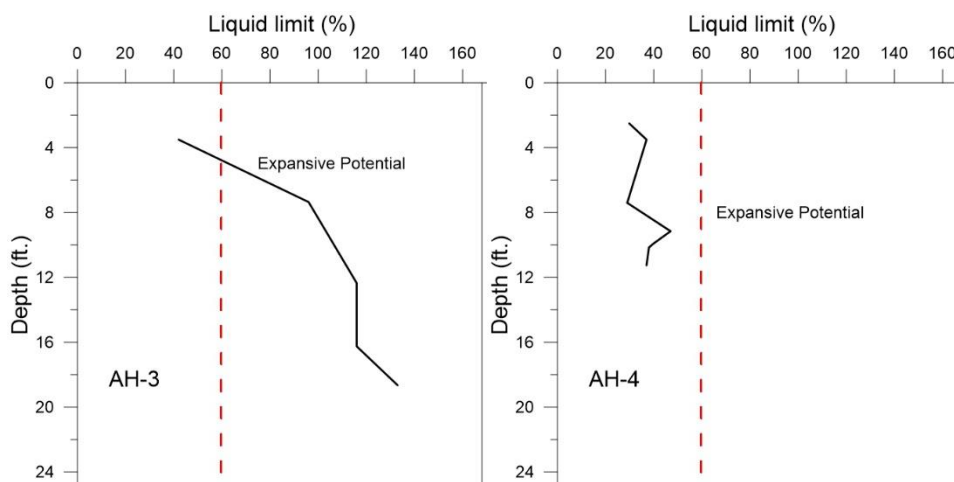
Figure B 1   Liquid Limit vs. Depth for Boreholes AH-3 and AH-4 (1 ft. = 30.5 cm)
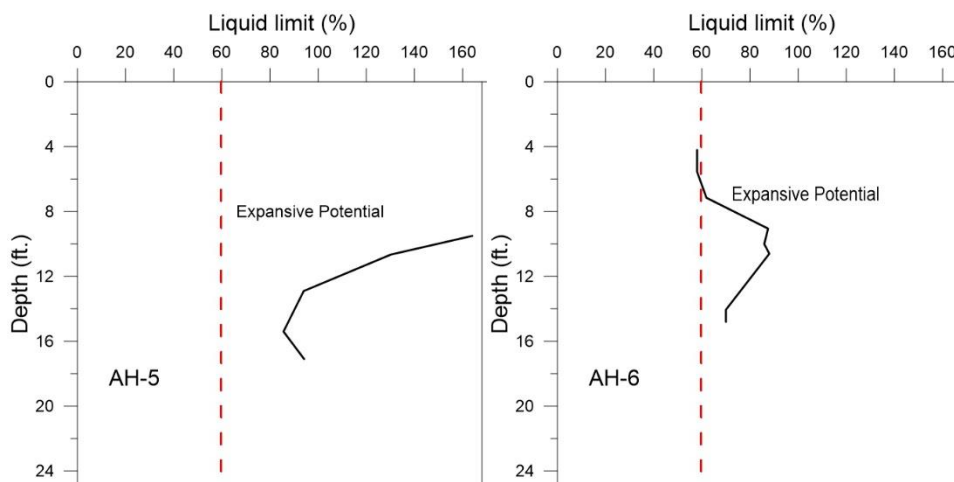
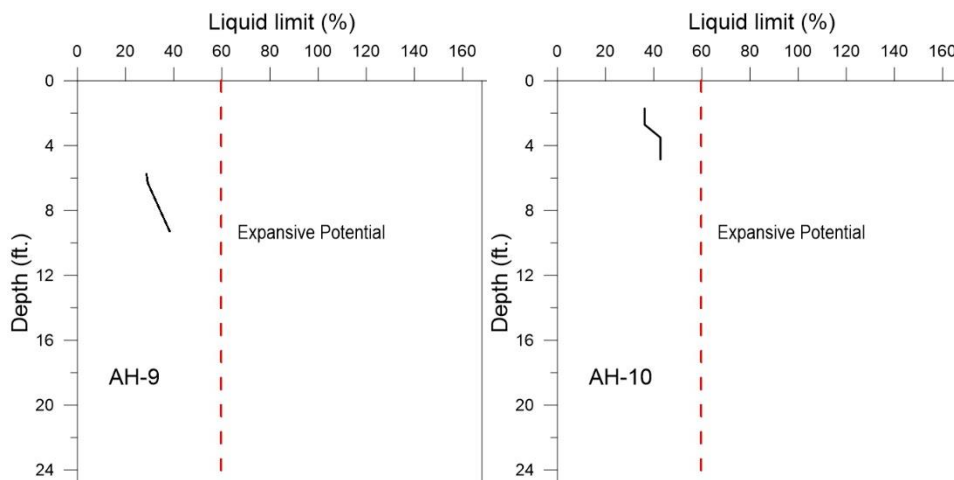**Figure B 2   Liquid Limit vs. Depth for Boreholes AH-5 and AH-6 (1 ft. = 30.5 cm)**
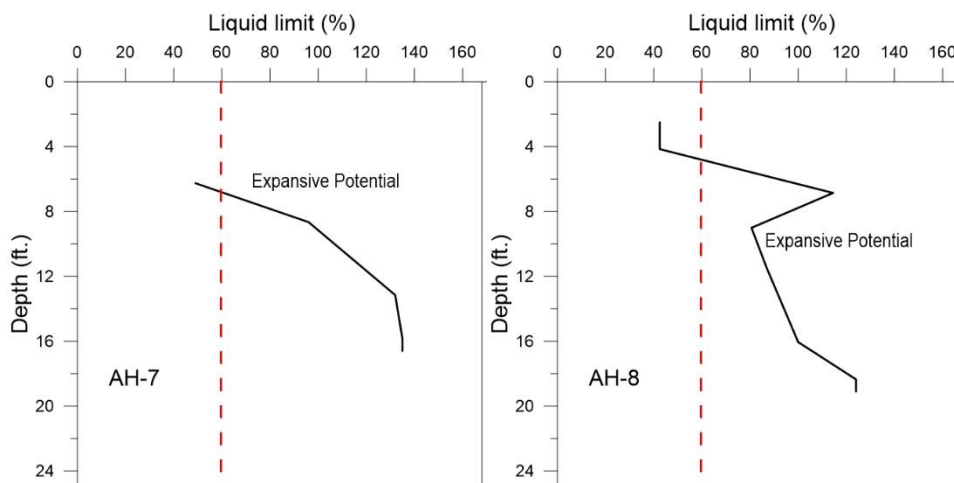
Figure B 3   Liquid Limit vs. Depth for Boreholes AH-7 and AH-8 (1 ft. = 30.5 cm)

Figure B 4   Liquid Limit vs. Depth for Boreholes AH-9 and AH-10 (1 ft. = 30.5 cm)

Liquidity Index Results
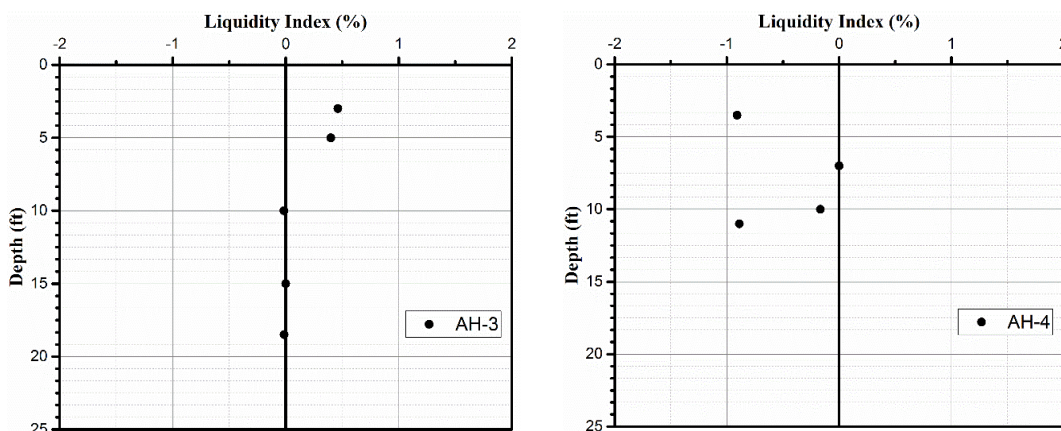
Figure B 5   Liquidity Index vs Depth for Boreholes AH-3 (left) and AH-4 (right) (1 ft. = 30.5 cm)
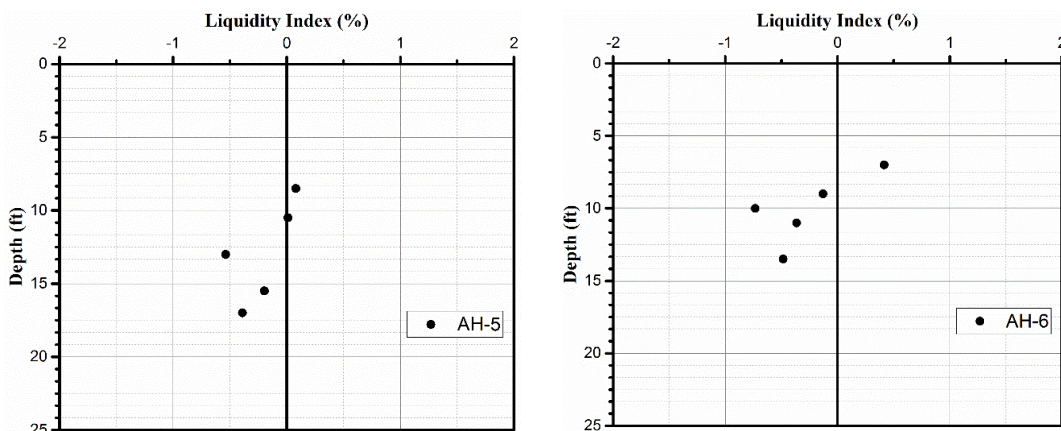
Figure B 6   **Liquidity Index vs Depth for Boreholes AH-5 (left) and AH-6 (right)**
(1 ft. = 30.5 cm)
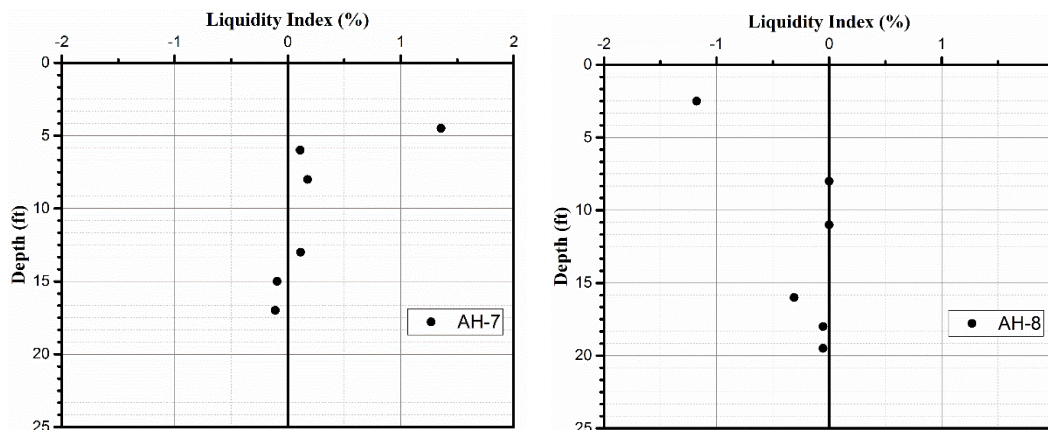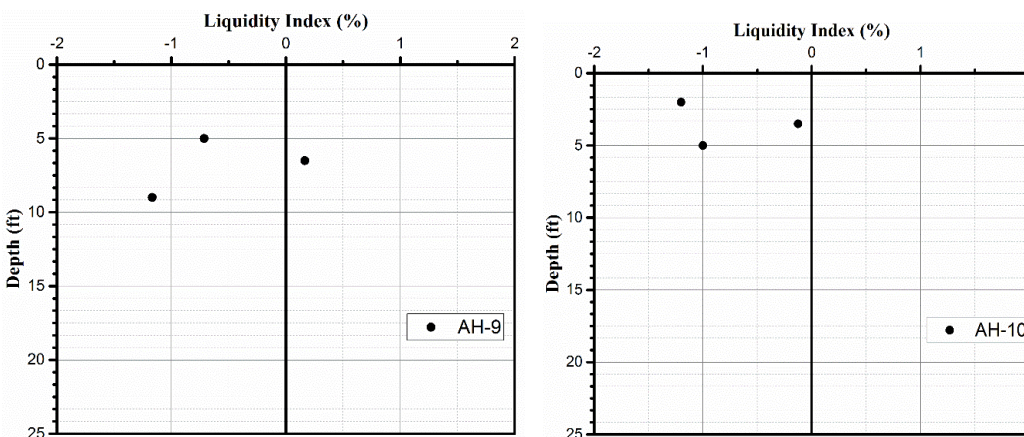

Figure B 7   **Liquidity Index vs Depth for Boreholes AH-7 (left) and AH-8 (right) (1 ft. = 30.5 cm)**

Figure B 8   **Liquidity Index vs Depth for Boreholes AH-1 (left) and AH-2 (right) (1 ft. = 30.5 cm)**

Potential Vertical Rise (PVR) Calculations

Table B 3   Summary of PVR values for AH-1

PVR Data BH

Depth to Bottom of Layer [ft]	Average Load [psi]	Liquid Limit (LL)	Dry 0.2LL+9	Wet 0.47LL+2	Percent Moisture	Dry Avg Wet	Percent -No.40	Plasticity Index (PI)	Percent Volume Swell	Percent Free Swell	PVR [in] Top of Layer	PVR [in] Bottom of Layer	Differential Swell [in]	Modified -No.40 Factor	Modified Density Factor	PVR in Layers [in]	Total PVR [in]
0.0	0.0	-	-	-	-	-	-	-	-	-	-	-	-	-	-	-	5.34
2.0	1.0	60	21.0	30.2	7.1	Dry	36.0	25	6.4	9.4	0.00	0.37	0.37	0.36	1.00	0.13	5.20
4.0	3.0	60	21.0	30.2	8.0	Dry	36.0	25	6.4	9.4	0.37	0.91	0.54	0.36	1.00	0.19	5.01
6.0	5.0	60	21.0	30.2	69.8	Wet	36.0	25	2.5	5.3	0.33	0.38	0.06	0.36	1.00	0.02	4.99
8.0	7.0	89	26.8	43.8	69.8	Wet	96.0	35	4.7	7.6	1.02	1.17	0.15	0.96	1.00	0.14	4.84
10.0	9.0	89	26.8	43.8	71.0	Wet	96.0	35	4.7	7.6	1.17	1.27	0.09	0.96	1.00	0.09	4.76
12.0	11.0	148	38.6	71.6	73.0	Wet	96.0	94	29.3	34.0	9.28	10.83	1.55	0.96	1.00	1.49	3.27
14.0	13.0	148	38.6	71.6	71.0	Wet	96.0	94	29.3	34.0	10.83	12.23	1.40	0.96	1.00	1.34	1.92
16.0	15.0	139	36.8	67.3	68.9	Wet	96.0	80	23.3	27.6	9.61	10.49	0.88	0.96	1.00	0.85	1.08
18.0	17.0	138	36.6	66.9	63.0	Wet	96.0	75	21.2	25.3	8.92	9.52	0.60	0.96	1.00	0.58	0.50
20.0	19.0	138	36.6	66.9	63.0	Wet	96.0	75	21.2	25.3	9.52	10.04	0.52	0.96	1.00	0.50	0.00

|	
Fields are chart inputs	Fields are final answers per layer

Final Total PVR for the borehole

Note: PVR calculations are based on future pavement grade being the same as present grade. Bold numbers are interpolated and extrapolated values.

International Roughness Index (IRI)

Table B 4   Total Summary of IRI values for the 10 boreholes (South Bound)

Borehole Number	Path website		Spreadsheet	
	Left IRI	**Right IRI**	**Left IRI**	**Right IRI**
AH-1	405	455	197	177
AH-2	410	450	197	177
AH-3	240	270	172	156
AH-4	455	265	172	156
AH-5	430	500	266	263
AH-6	500	500	266	263
AH-7	345	485	199	172
AH-8	400	440	199	172
AH-9	150	155	61	70
AH-10	90	110	94	78
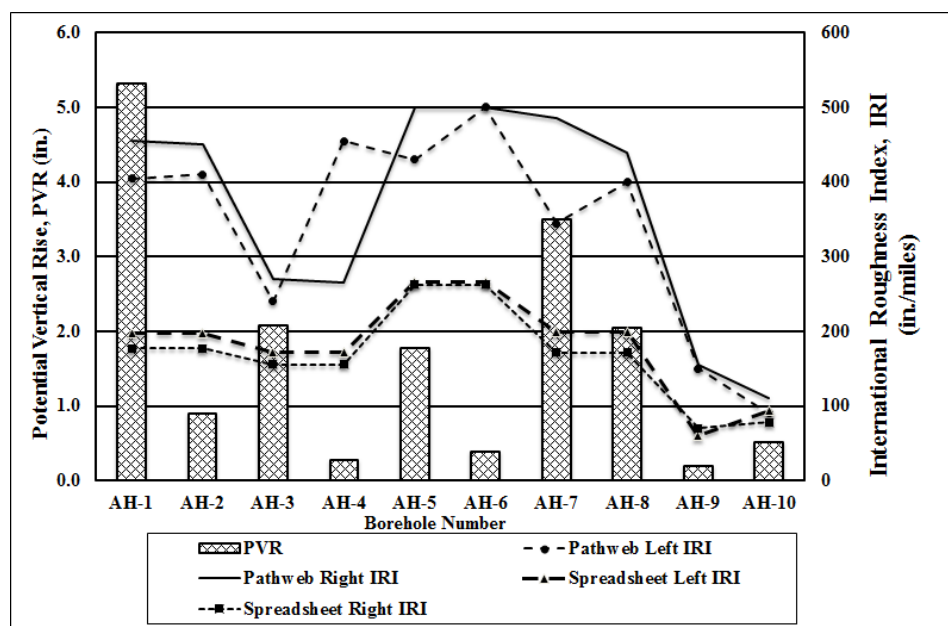
Figure B 9   Plot of Potential Vertical Rise (PVR) and International Roughness Index (IRI) Trends along the Problematic Section of US-95 being Investigated (South Bound; 1in. = 2.54 cm)

Specific Surface Area (SSA) and Cation Exchange Capacity (CEC) Tests
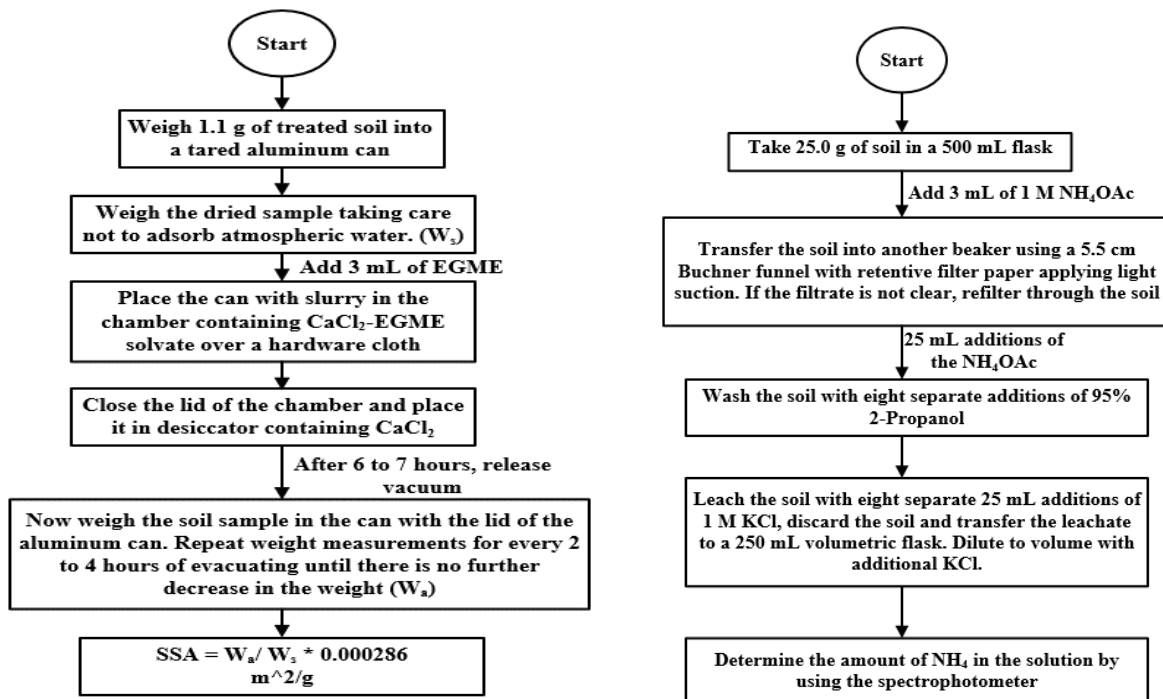
Figure B 10   Flowchart Showing the Procedure Followed to Determine Specific Surface Area, and Cation Exchange Capacity

Table B 5 Summary of SSA and CEC for AH-1 (1 ft. = 30.5 cm; 1 m²/g = 1.42×
10⁻⁶ ft²/lb; 1 meq/100g = 1meq/0.22 lb)

S. No.	Sample Depth (ft.)	Liquid Limit (%)	SSA (m²/g)	CEC (meq/100g) Measured	CEC (meq/100 g) Predicted	%MM in fines fraction (-#200) of the soil
AH-1						
1	1.0-2.0	60	53	411	10	4
2	2.5-4.0	60	43	435	6	2
3	4.7-5.5	60	457	622	172	78
4	6.1-6.3	89	512	875	184	86
5	9.5-11.8	148	517	905	167	82
6	14.5-16.8	139	530	950	175	85
7	19.5-21.8	138	467	950	150	74
AH-2						
1	3.9-5.2	47.2	218	35.7	80	35
2	5.9-8.2	46	278	34.8	105	47
3	8.4-9.5	47	274	35.5	103	46
4	10.9-13.2	80	381	68.7	135	63
5	15.9-18.2	94.8	162	92.4	42	21
6	18.4-20.4	98	241	98.5	73	35
AH-3						
1	5.0-9.7	96	384	94.6	131	62
2	10.0-14.7	116	212	141.2	55	28
3	15.0-17.5	116	509	141.2	174	83
4	17.5-19.8	133	573	198.3	194	93
AH-4						
1	2.0-3.0	29.8	114	25.2	44	18
2	3.0-4.0	37	168	29.1	64	27
3	6.5-8.3	29	133	24.8	52	21
4	8.5-9.8	47	216	35.5	80	35

S. No.	Sample Depth (ft.)	Liquid Limit (%)	SSA (m²/g)	CEC (meq/100g) Measured	CEC (meq/100 g) Predicted	%MM in fines fraction (-#200) of the soil
5	9.8-10.0	40	255	30.9	98	43
6	10.0-10.3	38	288	29.7	111	49
7	10.8-11.7	37	297	29.1	115	51
AH-5						
1	8.8-9.3	164	450	368.7	135	68
2	9.5-11.8	130.2	384	187.5	120	59
3	12.0-13.8	93.98	474	90.9	168	79
4	14.5-16.3	85.6	440	76.9	157	73
5	16.5-17.7	94.2	516	91.3	184	86
AH-6						
1	4.8-5.5	58	271	44.3	98	44
2	6.0-8.3	61.9	338	47.8	124	57
3	8.5-9.6	87.5	555	79.8	202	94
4	9.8-10.2	85.9	572	77.3	209	98
5	10.410.8	88	489	80.6	175	82
6	13.414.1	70	352	56.3	127	58
AH-7						
1	5.0-7.5	49	253	37	94	42
2	7.5-9.8	96	360	94.6	121	57
3	15.516.2	134.8	465	205.6	150	74
4	16.217.0	134.8	465	205.6	150	74
AH-8						
1	2.0-3.0	42.5	66	32.5	21	8
2	3.8-4.5	42.5	386	32.5	149	67
3	6.4-7.3	114.5	369	137	119	57
4	8.3-9.7	80.6	376	69.5	133	62

S. No.	Sample Depth (ft.)	Liquid Limit (%)	SSA (m²/g)	CEC (meq/100g) Measured	CEC (meq/100 g) Predicted	%MM in fines fraction (-#200) of the soil
5	10.5-12.5	87	408	79	143	67
6	15.8-16.3	100	486	102.5	170	80
7	18.0-8.7	124	524	165.7	178	85
AH-9						
1	5.5-6.0	28.7	179	24.6	71	30
2	6.0-6.6	29.2	111	24.9	44	18
3	8.5-10.1	38.38	177	29.9	67	29
AH-10						
1	4.0-4.5	42.8	124	32.7	44	19

Soluble Sulfate Content Tests

Initial 10g of soil → Adding 100 ml of distilled water → Shake the mixed solution for 30 minutes by using Eberbach Shaker → Centrifuge the solution at 14,000 rpm for 30 minutes → Dilute the filtrate to 200 mL by adding distilled water

Resulting Precipitate After Filtration of Precipitate Solution ← Heating of sample and Addition of BaCl₂ solution ← Bring the pH of the dilutant close to the range of 5 to 7 by adding HCl
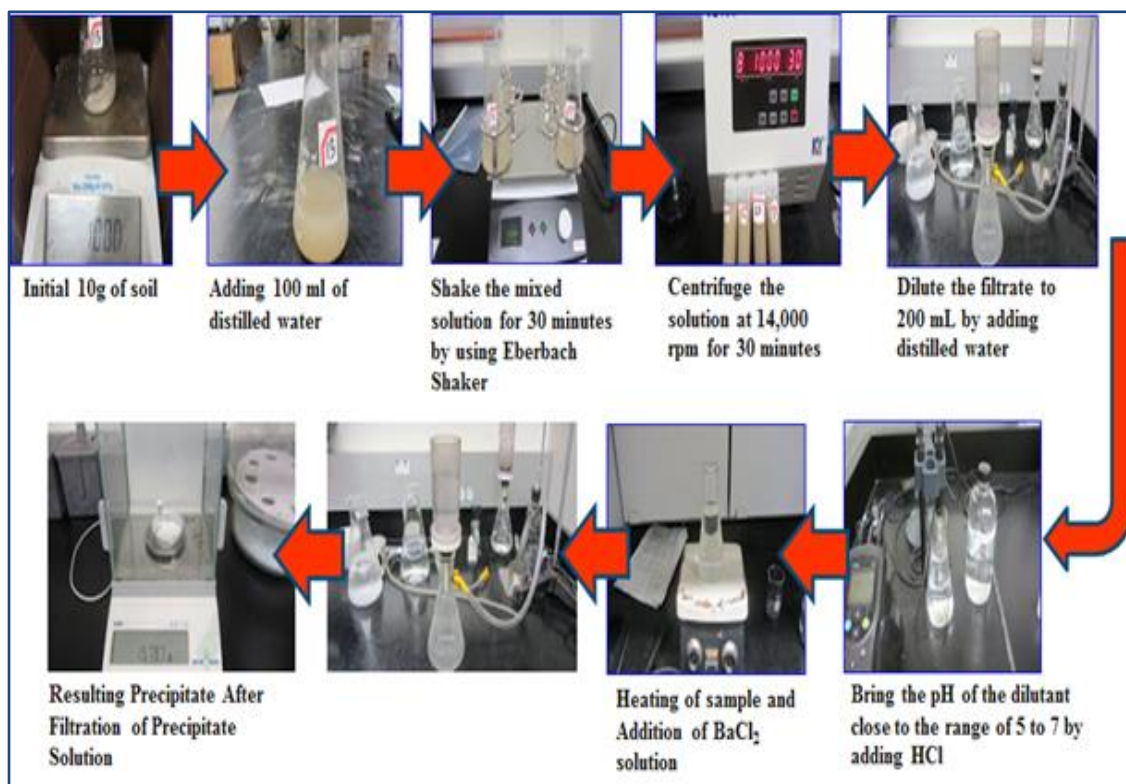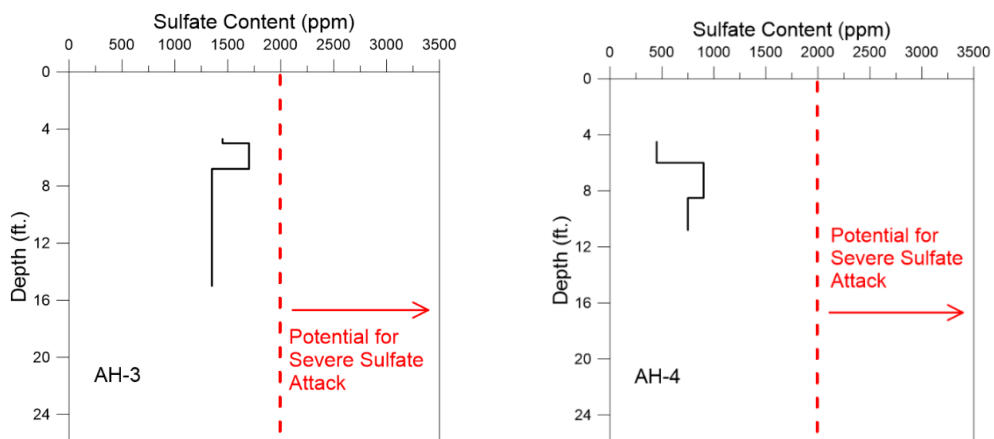
Figure B 11   Photographic Representation of Sulfate Test Procedure

**Table B 6   Summary of Soluble sulfate test data (1 ft. = 30.5 cm)**

| S. No.	Sample Depth (ft.)	Soluble sulfate content (ppm) in samples	S. No.	Sample Depth (ft.)	Soluble sulfate content (ppm) in samples
AH-2					
1	5.7-5.9	3238	4	15.9-18.2	3366
2	8.4-9.5	3366	5	18.4-20.4	3366
3	10.9-13.2	3366	-	-	-
AH-3					
1	4.7-5.0	1450	3	14.7-15	1350
2	6.0-6.8	1700	4	17.5-19.8	1350
AH-4					
1	4.0.5-6	450	3	10.3-10.8	750
2	8.3-8.5	900	4	10.8-11.7	750
AH-5					
1	9.3-9.5	2750	3	16.5-17.7	2900
2	14.3-14.5	2900			
AH-6					
1	1.1-1.5	600	3	10.4-10.8	1100
2	9.6-9.8	1100	4	14.1-14.7	1100
AH-7					
1	4.0-5.5.0	2600	3	12.5-13.8	3350
2	9.8-10.0	3350	4	13.8-14.0	3100
AH-8					
1	3.8-4.5	2200	5	10.5-12.5	2450
2	5.0.5-6	2500	6	14.4-15.6	2450
3	8.1-8.3	2450	7	18.7-19.5	2450
AH-9					
1	3.0-3.7	953	3	2	6.6-6.8
AH-10					
1	7.0-7.5	450	2	11.1-11.5	700

Figure B 12   Sulfate content vs. Depth for boreholes AH-3 and AH-4 (1 ft. = 30.5 cm)
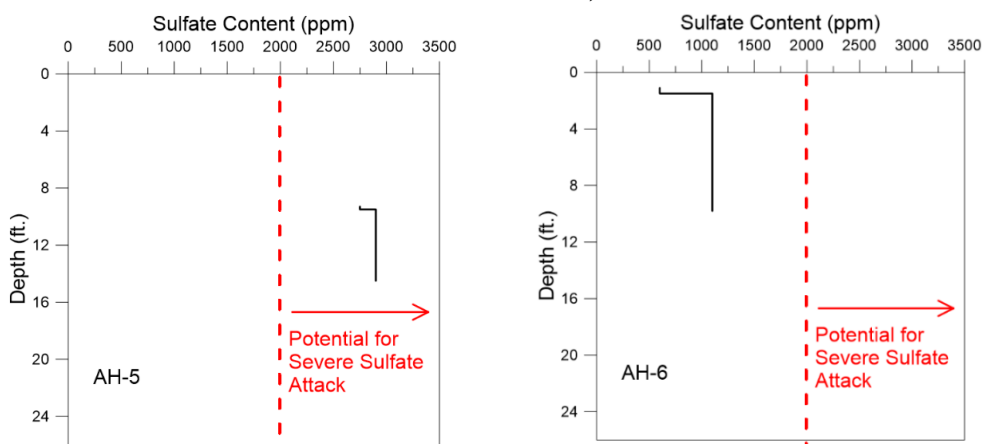
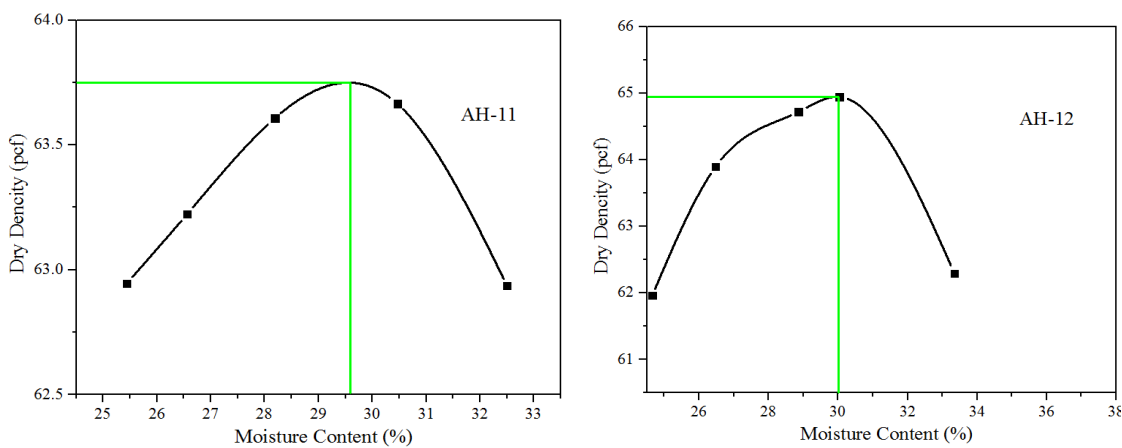**Figure B 13   Sulfate content vs. Depth for borehole AH-5 and AH-6 (1 ft. = 30.5 cm)**
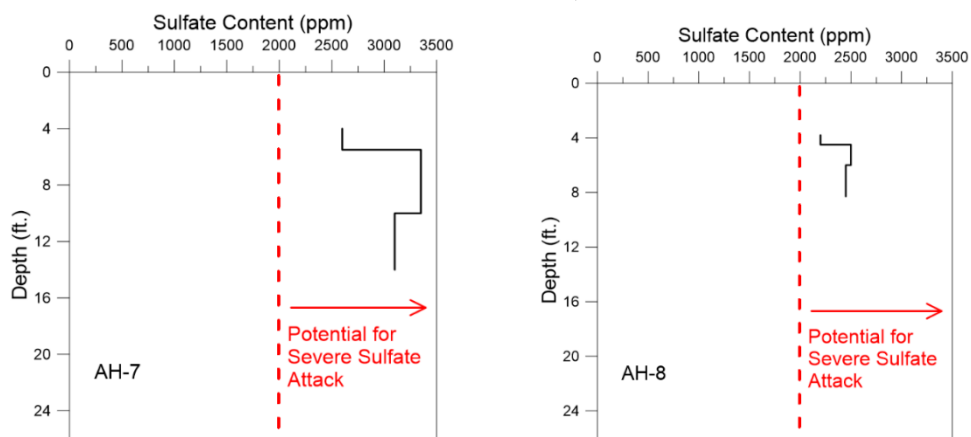
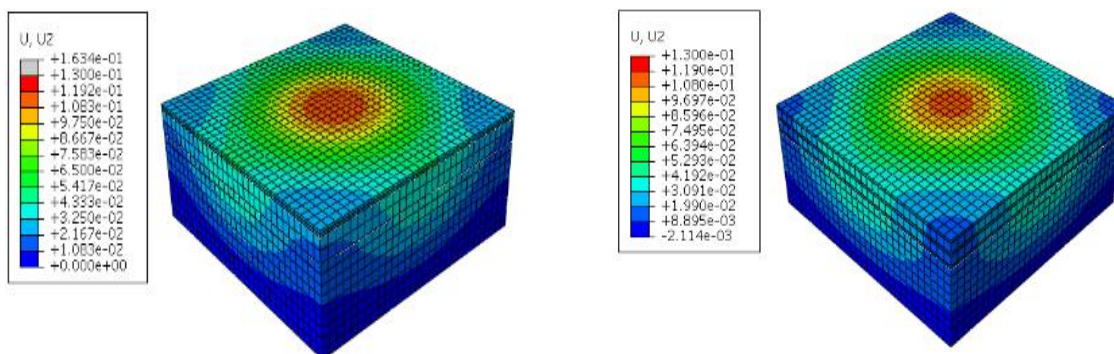**Figure B 14** **Sulfate content vs. Depth for borehole AH-7 and AH-8 (1 ft. = 30.5 cm)**
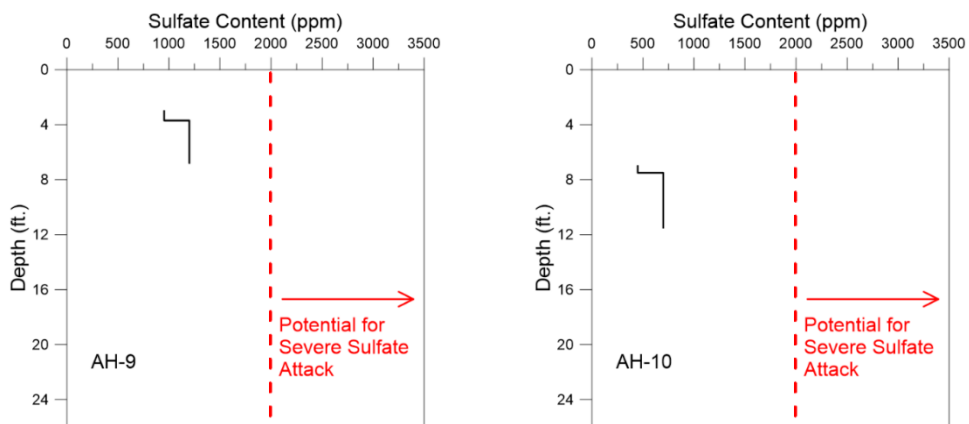
Figure B 15 **Sulfate content vs. Depth for borehole AH-9 and AH-10 (1 ft. = 30.5 cm)**
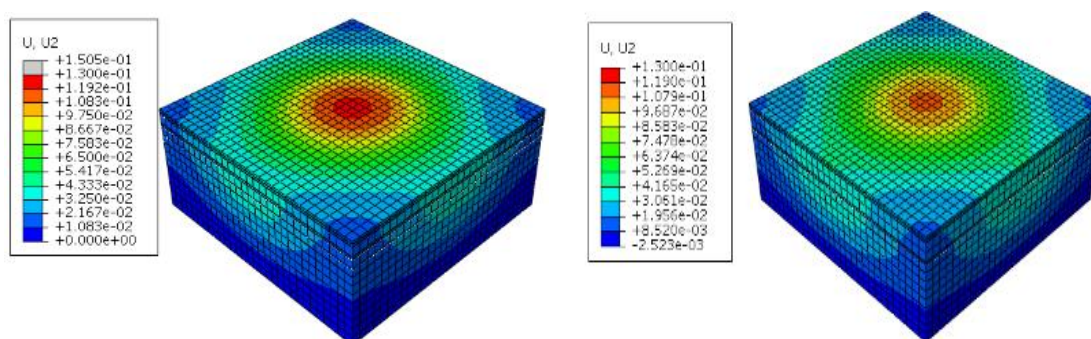
Standard Compaction Tests

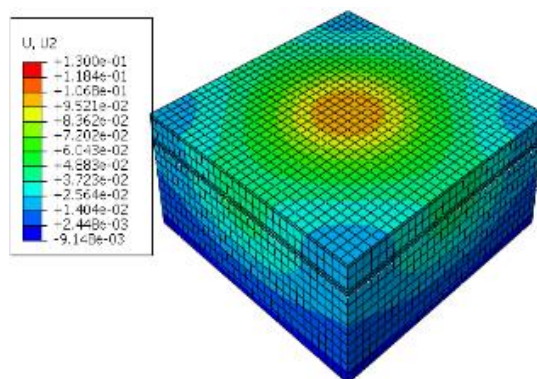**Figure B 16** **Moisture Density Relation Curve for Boreholes AH-11 & AH-12**

Numerical Analysis Profiles

Figure B 17   Displacement Contours for GC-2 and GC-3 Configuration

Figure B 18   Displacement Contours for GC-4 and GC-5 Configuration

Figure B 19   Displacement Contours for GC-6 Configuration